

LAMINAR GROUND WATER FLOW THROUGH STOCHASTIC CHANNEL NETWORKS IN ROCK

THÈSE N° 2736 (2003)

PRÉSENTÉE À LA FACULTÉ ENVIRONNEMENT NATUREL, ARCHITECTURAL ET CONSTRUIT

SECTION DE GÉNIE CIVIL

ÉCOLE POLYTECHNIQUE FÉDÉRALE DE LAUSANNE

POUR L'OBTENTION DU GRADE DE DOCTEUR ÈS SCIENCE

PAR

Patrick BRUINES

ingénieur, Technische Universiteit Delft, Pays-Bas
et de nationalité néerlandaise

acceptée sur proposition du jury:

Prof. P. Egger, directeur de thèse
Dr P. Blümling, rapporteur
Prof. Y. Ohnishi, rapporteur
Prof. A. Schleiss, rapporteur
Dr W. Steiner, rapporteur

Lausanne, EPFL
2003

Acknowledgement

I wish to thank the three academic advisors involved in my thesis over the past four years: Prof. D.D. Genske, for giving me the opportunity to start this research project; Prof. Y. Ohnishi, for allowing me to continue it; and Prof. P. Egger, who made it possible to bring this research to a successful conclusion.

Prof. A. Schleiss, Dr. W. Steiner and Dr. P. Blümling, members of the examination committee, have provided me with valuable input for improving this thesis.

At the commencement of this study Prof. G. Ben Arous and Dr. J. Cerny of the mathematics department of the EPFL, were essential in providing important programming skills to the Critical Path Analysis computer program.

In addition I would like to thank my colleagues and friends from the EPFL and Kyoto University, Japan for their continued support and friendship.

Financial support for this research came from the Swiss National Science Foundation and the Swiss Academy of Engineering Sciences.



Summary

The flow through fractured rock is of great importance for many civil engineering projects, for example, when considering the safe storage of nuclear waste or the stability and profitability of dams, tunnels and slopes. How the fluid actually flows through a fractured rockmass is still a matter of vivid discussion within the hydrogeologic community. Various approaches to calculate the flow through a fractured rockmass exist. Which approach is best depends on the rockmass properties and the size of the rockmass under investigation.

This study presents a new model which assumes that groundwater flow will take place preferably at the intersection of fractures.

Study of the scientific literature showed that flow through intersections of fractures exists and can play a major role in flow through a fractured rockmass.

Fieldwork has been conducted at outcrops close to Granada, Spain. At these outcrops fossilized flow paths have been observed at the intersections of fractures. During this fieldwork, fracture data have been gathered, which could be used to reconstruct the fracture geometry.

As part of this research a mathematical model has been developed to simulate flow along the intersections of fractures, neglecting flow within the fractures or through the rock matrix. To this end a computer program, CPA, developed for a different purpose, has been modified and completed in order to generate a stochastic tubular network of fracture intersections and calculate flow rates through this network. The new version of the CPA code has been applied to a number of problems to test the correctness of the model and investigate the effects of the different input parameters. The application part of this study can be roughly divided into: network generation, sensitivity analysis, and the comparison with a model, Joint-OKY, that assumes flow to take place through the fractures.

The field data gathered during fieldwork in Spain have been used to confirm the geometric modelling capabilities of the CPA program. A comparison between the network model generated by CPA and the observations in the field showed good agreement. The use of an eigenvec-

tor approach to represent fracture orientation distribution has proven to be a good and simple method.

To better understand the influence of various input parameters in the CPA model, sensitivity analyses were performed on the models generated by the CPA code. The following parameters have been investigated: fracture density, size of the model area, fracture size and anisotropy of conductivity.

Finally a comparison between the CPA code and the Joint-OKY code, which assumes flow to take place within the plane of the fractures, has been made. This comparison showed that a model assuming flow within the fractures is more conductive.

Further studies are needed to better include the transport of contaminants in the current CPA program.

Zusammenfassung

Die Durchströmung von zerklüftetem Gestein ist von grosser Bedeutung bei vielen Ingenieurvorhaben wie zum Beispiel bei der Erstellung von Lagerstätten nuklearer Abfälle sowie der Stabilitätsbetrachtung von Dämmen, Tunneln und Hängen. Wie die Flüssigkeit jedoch tatsächlich durch zerklüftetes Gestein fliesst, wird in den Kreisen der Hydrogeologie noch immer lebhaft diskutiert. Es bestehen verschiedene Ansätze, um die Strömung durch zerklüftete Medien zu berechnen. Welcher am besten zutrifft, hängt von den Gesteinseigenschaften und der Grösse der Gesteinsmasse ab, welche untersucht wird.

Diese Studie präsentiert ein neues Modell, welches davon ausgeht, dass Grundwasser präferenziell den Schnittlinien der Klüfte entlang strömt.

Eine Literaturstudie ergab, dass Strömung entlang der Schnittlinien der Klüfte existiert und eine wichtige Rolle spielen kann bei der Durchströmung zerklüfteter Medien.

In der Nähe von Granada, Spanien, wurde eine Feldforschung an Aufschlüssen durchgeführt. An diesen Aufschlüssen wurden an den Schnittlinien von Klüften fossile Fliesspfade wahrgenommen. Während dieser Feldforschung wurden Kluftdaten aufgezeichnet, die es ermöglichten, die Kluftgeometrie zu rekonstruieren.

Teil dieser Forschung war die Entwicklung eines mathematischen Modells, um Strömung an den Schnittlinien der Klüfte zu simulieren, wobei die Durchströmung sowohl der Klüfte als auch des porösen Gesteins ignoriert wurde.

Das für einen anderen Zweck entwickelte CPA-Computerprogramm wurde abgeändert und erweitert, um stochastisch ein Röhrennetzwerk aus den Schnittlinien der Klüfte zu generieren und die Durchflussmenge durch das Netzwerk zu berechnen. Das CPA-Programm wurde in einer Reihe von Testrechnungen angewendet, um die Richtigkeit des Modells festzustellen und die Effekte der verschiedenen Eingangsparameter zu untersuchen. Die Versuchsreihe kann dabei unterteilt werden in: Netzwerkgenerierung, Empfindlichkeitsanalyse und einen Vergleich mit einem Programm (Joint-OKY), welches von der Annahme der Strömung durch die Klüfte ausgeht.

Die gesammelten Felddaten aus Spanien wurden benutzt, um die Fähigkeiten der geometrischen Modellierung des CPA-Programmes zu überprüfen. Der Vergleich zwischen realem und generiertem Kluftgefüge zeigte eine gute Übereinstimmung. Die Benutzung von Eigenvektoren, um eine Kluftorientierungsverteilung darzustellen, hat sich als gut und einfach anwendbar erwiesen.

Um die Effekte von verschiedenen Eingangsparametern zu untersuchen, wurden Empfindlichkeitsanalysen an den vom CPA-Programm generierten Modellen durchgeführt. Dabei wurden die folgenden Parameter untersucht: Kluftdichte, Grösse des Modellvolumens, Kluftgrösse und Anisotropie der Konduktivität.

Zum Schluss wurde ein Vergleich zwischen CPA und Joint-OKY durchgeführt, welcher ergab, dass ein Modell, welches von der Annahme, dass Strömung durch die Klüfte stattfindet, ausgeht, eine höhere Konnektivität und folglich eine grössere Durchlässigkeit aufweist.

Weitere Studien müssen durchgeführt werden, um Schadstofftransporte besser in das derzeitige CPA-Programm zu integrieren.

Table of Contents

Acknowledgement	I
Summary	III
Zusammenfassung	V
Table of Contents	VII
List of figures	XI
List of tables	XV
Symbols	XVII
1 Introduction	1
2 State of the art	5
2.1 Porous media	7
2.2 Single fracture	12
2.3 Double porosity	15
2.4 Network models	16
2.4.1 Stochastic fracture development	16
2.4.2 In-fracture flow	18
2.4.3 Fracture intersection flow	19
2.4.4 Development of channels at fracture intersections	23
3 Scope of this thesis	31
4 Tools	35
4.1 Data gathering	35
4.2 Models	38
4.2.1 CPA	38
4.2.2 Joint-Okky	45
4.2.3 Combination of models	47
5 Application	49
5.1 Example of data gathering	49

5.2 Application of the Critical Path Analysis program	53
5.2.1 Network generation	55
5.2.2 Sensitivity analysis with changing fracture density	60
5.2.3 Sensitivity analysis with changing modelling domain size	65
5.2.4 Sensitivity analysis to the randomness of geometry and conductivity distribution	69
5.2.5 Sensitivity analysis of an orthogonal system with changing fracture density	71
5.2.6 Sensitivity analysis of an orthogonal system with changing fracture sizes	73
5.2.7 Sensitivity analysis of an orthogonal system with changing conductivities	75
5.3 Combination of the CPA and the Joint-OKY programs	77
6 Conclusions	81
7 Recommendations	85
References	87
A Filling the field data gap in fractured aquifer interpretation	93
A.1 Introduction	93
A.2 Data requirements	94
A.2.1 Flow	94
A.2.2 Transport	95
A.3 Outcrop data application	95
A.3.1 Fracture orientation	95
A.3.2 Fracture density / spacing	96
A.3.3 Fracture aperture	97
A.3.4 Roughness	98
A.3.5 Channelling	98
A.3.6 Fracture length	98
A.3.7 Fracture connectivity	99
A.3.8 State of stress	100
A.3.9 Fracture skin	101
A.4 Conclusions	102
A.5 References	102
B Description and manual of the CPA program	107
C Spain field work	111
C.1 Geography of the area	111
C.2 Terms of reference	112

C.3 Available information	113
C.4 Landscape and general geology	113
C.4.1 Landscape	113
C.4.2 General geology of the area.	114
C.5 Survey techniques	116
C.5.1 Fracture survey techniques	116
C.5.2 Channels survey techniques	116
C.5.3 Laboratory work	116
C.6 Fracture survey	117
C.7 Data processing	122
C.8 Conclusions	127
Curriculum vitae	129



List of figures

2.1	Location of the problem domain in the: (a) very-near-field, (b) near-field, (c) far-field, (d) very-far-field.	6
2.2	Different flow regimes considering fracture roughness and Reynolds number (from Kolditz, 1997).	13
2.3	In-fracture tubular network model. To simplify calculations, the fractures are idealized by tubular structures that connect the centre of a fracture with the centres of the intersections.	19
2.4	Layout and dimensions of the test site for the 3-D migration experiment at the Stripa mine (from Abelin et al., 1988)..	20
2.5	Natural water inflow rates at the Stripa mine (from Abelin et al., 1988).	20
2.6	Fracture characteristics compared with water inflow rates at the 3-D migration experiment at the Stripa mine show that water inflow rates seem to be more related to the number of fracture intersections per area, than the fracture length per area (from Abelin et al., 1988).	21
2.7	Fracture channel as found during tomographic flow test experiment (Shimo and Iihoshi, 1995).	22
2.8	Photo of the abutting fracture tested at JNC in Tokai-mura, Japan.	22
2.9	Schematic drawing of spheroidal weathering, where the numbers 1, 2 and 3 indicate the different stages of weathering from freshly fractured rock to the formation of rounded boulders.	25
2.10	Picture of an outcrop at the quarry for the Kansai international airport, showing weathering phenomena in a sedimentary rock that can lead to flow at fracture intersections. The picture shows the intersection of the bedding plane (perpendicular to the axis of view) and two perpendicular joints.	25
2.11	Displacement of fracture walls lead to in-fracture flow channelling	26
2.12	Displacement of blocks can lead to the development of fracture channels at the intersection of fractures. Please note that the edges of the blocks can be subject to stress concen-	

	trations, which contribute to a faster disintegration of the rock at those locations.	27
2.13	Channel development in folding structures.	27
2.14	In an unfractured rock, several offset, parallel fractures can develop under an angle with the shear direction (riedel shears). Additional shear movement will result in more dilation and opening of these fractures. Such features are often filled with minerals and preserved as en-echelon veins.	28
2.15	When two developing parallel fractures approach each other, the fracture tips will be deviated towards the other fracture (a) until a connection is made. This structure is called a jog (b). More shear can result in the creation of additional porosity at this jog structure (c).	29
4.1	Breithaupt compass used for fieldwork.	36
4.2	Fracture terminations: A butting, B lind, C rossing and D iffuse.	36
4.3	Automotive feeler gauge designed to measure the gap of a spark-plug is used to measure fracture aperture.	37
4.4	Carpenter's contour gauge.	38
4.5	Flow chart of the CPA program. Behind each module the developer of that particular part of the code is mentioned between brackets.	40
4.6	Before start of the intersection procedure a box will be placed around the fracture for easy comparison. In this case only for two intersection routine is started out of the six possible combinations.	42
4.7	Artificial fractures used to generate boundary nodes necessary for flow rate calculations in three dimensions.	43
4.8	Possible intersection options for a channel intersecting a cylinder are no intersection, one intersection point, or two intersection points.	43
4.9	Idealization of in-fracture flow as modelled in Joint-OKY. The flowpaths connect the centres of the fractures to the centre of the fracture intersections.	46
4.10	Intersections of fractures with the boundary faces in the Joint-OKY program.	46
5.1	Upper photograph shows an outcrop at the Sierra Elvira.	50
5.2	Lower photograph show a close-up of a discoloration feature.	50
5.3	Flow rates through a cube are calculated using a fractured rockmass with unit dimensions (1x1x1). The flow rate is calculated in the three directions.	54
5.4	Radial flow rates are calculated by flow through a cylinder with an outer diameter of 1 and an inner diameter of 0.2 and simulates flow towards a borehole during groundwater	

testing or flow towards a shaft.	54
5.5 A realisation generated with CPA using the directional data from the Spain fieldwork. The view is from above. The different fracture sets can be distinguished.	56
5.6 Model fracture intersections constructed with the data from Spain fieldwork. Only channels that are connected to other channels are shown.	57
5.7 Backbone of the channel network. To obtain the backbone two artificial nodes are inserted and connected to the boundary nodes. All channels that are not connected with these two nodes are then deleted.	58
5.8 Fastest flowpath. By repetitive addition of the most conductive tubes a single channel is determined that represents the fastest flowpath.	58
5.9 Photo of an outcrop in the investigated area near Granada, Spain.	59
5.10 Virtual cut through model, parallel to the outcrop shown in previous Figure 5.9.	59
5.11 Stereo-graphic projection of all fractures generated of a realization using the orientational data from the Spain outcrops.	60
5.12 Semi-logarithmic plot of the number of nodes, number of tubes and the files sizes. An exponential increase of the tubular network can be observed.	61
5.13 Ratio of the number of tubes and the number of nodes plotted against the number of fractures. An increase of fractures leads to a better connected systems with less nodes located at dead ends.	62
5.14 Semi-logarithmic plot of total flow rate against the number of fractures.	63
5.15 Ratio of radial flow rate and parallel flow rate for total flow rate (solid points) and the flow rate of the fastest path (open points).	64
5.16 Showing the sizes of the different equivalent cubes used in the calculations.	66
5.17 Average flow rates of the parallel flow simulations.	67
5.18 Average flow rates of the radial flow simulations.	67
5.19 Coefficient of variation of flow rates against model size.	68
5.20 Flow rates calculated with the same networks but with different realizations of the same conductivity distribution function, as indicated by the random numbers, result in a certain amount of scatter (horizontal). Flow rates of different network geometries will however result in more scatter (vertical).	70
5.21 Schematic drawing of the models <i>or111</i> , <i>or112</i> , <i>or121</i> , <i>or211</i>	71
5.22 Histogram of the calculated flow rate frequency in a direction perpendicular to the enlarged fracture set and distribution curve fitted through the data.	74

5.23	Comparison of networks generated by CPA (left) and Joint-OKY (right) using the same fracture model parameters (or111) as an input.	78
A.1	Anisotropy of the Edwards aquifer [adapted from 7]. Rose diagrams of length weighted orientation are illustrated from regional scale lineament map as well as fracture mapping at two location with exposed creek beds. Using anisotropy predicted from the outcrop, predictions of flow direction correspond well to dye trace experiments (solid line). Without the fracture data, the predicted dye direction would be east to Southeast instead of to the Northeast. (Groundwater elevation in feet)	96
A.2	Left - Fractures generated in a 100-m by 100-m region from the Fanay-Augères. Right - A 70-m by 70-m section of the generated fracture network, only the connecting fractures are shown [from 27].	100
A.3	Shale from a quarry near Mintaro, South Australia showing fracture skin. This iron-rich fracture skin occurred along a bedding plane fracture and indicates that flow occurred between asperities in the bedding plane in a combination "pillar" flow. Fractures occurring perpendicular to bedding demonstrated a planar flow with highly uniform iron coatings.	101
B.1	Two dimensional regular lattice generated within the CPA program	108
B.2	Three dimensional regular lattice generated within the CPA program	108
C.1	Location of the fieldwork area.	112
C.2	Excerpt of the geological map of the Granada area.	112
C.3	Sketch of outcrop 1.	117
C.4	Sketch of outcrop 2.	118
C.5	Photo of tube. This tube is located south of outcrop 2, the diameter of the tube is about 20 cm. The rough surface (popcorn) indicates precipitation of calcite in the unsaturated zone.	119
C.6	Photo of wet spots. Water seeps from a bedding plane and from some spots where the fractures are not directly visible.	119
C.7	Photo of a stylolitic surface, which indicates the direction of stress.	120
C.8	Sketch of outcrop 3.	121
C.9	Composite photo of outcrop 4	122

List of tables

5.1	Directional statistics of the outcrops 1, 2 and 3.....	51
5.2	Statistics of the fracture spacing [m].	52
5.3	Termination statistics	53
5.4	Average number of nodes, number of tubes and file size of ten model-realizations with different fracture densities.	61
5.5	The average results of the ten model-realizations for the different fracture density models. Recorded is the total flow rate and the flow rate of the fastest path.	62
5.6	Conversion table showing the equivalent model length for the number of fractures added to the unit cube.....	66
5.7	Average flow rate calculations of ten model-realizations for models with different fracture densities in orthogonal fracture sets.....	72
5.8	Average flow rate calculation results of ten model-realizations with a single fracture set with enlarged fractures. The underlined flow rates are directed perpendicular to the enlarged fracture set.....	74
5.9	Average total flow rate calculation results of ten model-realizations with variable channel conductivities. The underlined flow rates point to similar result in the same set of models. The bold flow rates indicate similar values for the radial flow, but widely varying values of the flow rate in the x-direction.....	76
5.10	Comparison of the average and the coefficient of variation of the flow rates of ten model-realizations of the <i>orIIIc</i> model using the fracture intersection and the in-fracture approach.....	78
B.1	Format of the parameter file with explanation	109
C.1	Directional statistics of the outcrops 1, 2, and 3.	123
C.2	Fracture spacing distribution data (in metres).	124
C.3	Termination statistics.....	125



Symbols

A	cross-sectional area	m^2
A_{fr}	area of a fracture	m^2
b	aperture of a fracture	m
C_i	concentration of component i	kg/m^3
\bar{c}	concentration in fracture	kg/m^3
c_{sfr}	mass of contaminant adsorbed on the solid wall	kg/m^3
c_{spb}	mass adsorbed in porous rock	kg/m^3
C_{tube}	tube (or channel) conductivity as used in CPA	m^3/s
d	tube diameter	m
D_d	diffusion coefficient through liquid	m^2/s
D_d'	diffusion coefficient through porous rock	m^2/s
D_h	hydrodynamic dispersion	m^2/s
D_L	longitudinal diffusion coefficient	m^2/s
D_{mp}	molecular diffusion in porous rock	kg/m^3s
d_m	mean grain size	m
$f_{fr \rightarrow s}$	rate of adsorption from fluid to rockwall	kg/m^2s
g	gravitational acceleration	m/s^2
h_L	hydraulic head	m
i	hydraulic gradient	-
J_i	mass flux of component i	kg/m^2s

K	hydraulic conductivity	m/s
K_d	distribution coefficient between solid and fluid	m ³ /kg
$K_{dfr \rightarrow s}$	partitioning coefficient	-
K_{fr}	hydraulic conductivity in the fracture	m/s
K_{spb}	partitioning coefficient in porous rock	-
k	intrinsic permeability	m ²
l	length of channel	m
L	length	m
L_{fr}	fracture trace length	m
L_e	length of the flow path	m
n	porosity	-
n_e	effective porosity	-
n_{fr}	number of fractures	-
$p(x)$	probability function	-
Q	volumetric flow rate	m ³ /s
q_c	leakage into porous rock	kg/m ³ s
R_f	retardation factor	-
r	rate of decay	kg/m ³ s
T_{fr}	transmissivity of the fracture	m ² /s
t	time	s
V	measuring volume	m ³
v_z	velocity in fracture	m/s
v_x	linear groundwater velocity	m/s
γ	unit weight	N/m ³
λ	coefficient of radioactive decay	s ⁻¹
μ	dynamic viscosity	kg/ms
ρ	density	kg/m ³

ρ_s	density of the solids	kg/m ³
σ_L^2	variance of longitudinal diffusion coefficient	m ²
τ	tortuosity	-
ϕ_{pb}	porosity of porous rock	-



1

Introduction

A typical flow problem in a fractured rockmass. Nuclear energy is currently used all over the world. Nuclear energy does not pollute the air, does not charge the atmosphere with carbon dioxide, and the availability of fuel material is virtually without limit. The radioactive waste is however, an extreme health and security hazard. It is therefore of utmost importance to safely store these wastes. The deep underground is currently being considered by many countries for the storage of nuclear wastes. Most concepts include an engineered barrier system and a geological barrier. The engineered barrier might fail after a certain period, in which case the geological barrier, i.e. the rockmass, has to prevent the contaminants from reaching the biosphere. The choice of a good location is difficult, but is preferably deep, and located in low permeable rock. Many research sites are located in igneous rocks. These rocks have an extremely low matrix permeability but often include secondary permeability features, such as joints, faults and channels, that will conduct most of the flow. The understanding of this secondary permeability will be of great importance for the safety of the storage of nuclear waste installations.

Understanding this type of flow is not only of importance for nuclear waste storage, but also for geothermal heat projects, the fate of contaminants in the shallow fractured subsurface and for the stability and economy of civil engineering structures such as tunnels, dams and slopes.

Fracture channels. Field evidence shows that flow is often concentrated to flow paths in a fractured rock environment. These flowpaths can occur within the plane of a fracture or at the intersection of fractures. Fieldwork conducted as part of this project in the south of Spain near the town of Granada revealed outcrops that clearly showed fossilized flow paths, showing preferential orientations. These outcrops suggested that most flow took place along intersections of fractures. Studies at the Stripa mine, in Sweden, showed that there is a positive correlation

between the water inflow and the number of fracture intersections in an observation gallery (Abelin et al., 1988), a correlation much stronger than the one with the intersecting fracture length. Similar observations have been made at the Forsmark and Kymmen tunnels in Sweden (Neretnieks, 1994). With this, and other evidence, including observations made in the field as part of this research project in Granada (Spain) in mind, it has been decided to construct a computer program that would allow the creation and investigation of a network that would be defined entirely by the intersections of fractures.

Definition of terms. Some terms used in this thesis can be ambiguous in their meaning and are therefore defined to prevent confusion.

Fracture. The definition of Long et al. (1996) will be used throughout this thesis. They define fractures as mechanical breaks in rock involving discontinuities in displacement across surfaces or narrow zones. This is a term for generic discontinuities used by different scientists. Different types of fractures exist with different geometric, mechanical and hydraulic properties. Fractures can be geologically divided into three main groups: dilating, shearing and closing fractures. These are commonly referred to as joints, faults and pressure solution surfaces respectively. For fracture flow only joints and faults are of importance. In engineering fracture mechanics a slightly different classification is used, a joint, which develops by dilation only, is referred to as a mode I fracture. A fault can be either a mode II or a mode III fracture depending whether the shearing occurred in the direction perpendicular to the fracture propagation front or parallel to it. Combinations of different fracture types or modes exist and displacement, geometry, and internal structure of such fractures will be different from the ideal cases. The same will apply when the joints are altered or (partially) filled.

Channels and Tubes. Long et al. (1996: 273) make a clear distinction between two important processes: Fracture channels and channelized transport (or flow). A fracture channel is defined as a long narrow region of enlarged aperture formed at the intersection of two fractures or by processes such as shearing. It is mentioned that transport along enlarged intersections could be significantly greater than transport along grooves on fracture planes. Channelized flow results from the non-uniform velocity in a variable-aperture fracture. Fracture channels are fixed in orientation and position, whereas pathways of least resistance vary according to the flow direc-

tions. The terms channel and channelling are used in both cases. In this thesis the aforementioned definitions will be used. A tube is the idealization of a channel as used in the model and is assigned a conductivity.

Stochastic. A stochastic channel network is a network of conductive features that has been stochastically defined. The location and properties of the tubes are not known but are generated using statistical data.

Outline. The contents of the next chapters in this thesis is as follows:

Chapter 2 gives a review of the related literature on the state of the art of modelling in fluid flow and contaminant transport in fractured rockmass. For this purpose the concept of the Representative Elementary Volume is used to guide through this chapter.

Chapter 3 formulates the issues to which this thesis endeavours to contribute. It also states the assumptions made, the theoretical base of the modelling strategy used and indicates the limits of this study.

Chapter 4 deals with the methodologies and procedures used in this thesis. It explains which data have been gathered during the field work campaign, the different parts of the computer code developed for this research as well as the functioning of the computer code developed at Kyoto University that has been used as a reference model.

Chapter 5 presents the findings of the research. The observations from the fieldwork are presented first, followed by the application of these findings into the developed code to check the geometric correctness of the CPA program. The following section is then dedicated to investigating the sensitivity of the code to the various input parameters and finally a comparison with the code of Kyoto University is made.

Chapter 6 contains the conclusions of this thesis.

Chapter 7 presents recommendations for a possible continuation of this research.

2

State of the art

In this chapter an introduction about the state of the art in fracture flow modelling is presented. In order to keep a consistent structure of this chapter the approach of Bear and Berkowitz (1987) will be used to distinguish four different zones of flow and contaminant transport in a fractured porous media (see Figure 2.1).

- very-near-field,
- near-field,
- far-field, and
- very-far-field.

These different zones depend on the characteristics of the fractured rock mass but also on the size of the area of interest for the flow and contamination transport problem to be solved.

To make a distinction between these different cases the concept of a Representative Elementary Volume (REV) has been proposed. An REV contains a persistent solid phase or solid matrix, and void space, which are both distributed throughout the REV. An REV should however also be small enough to accurately describe what happens at that point and its close vicinity. The size of the REV is such that the distribution of void space and solid matrix is statistically meaningful. In more practical terms this means:

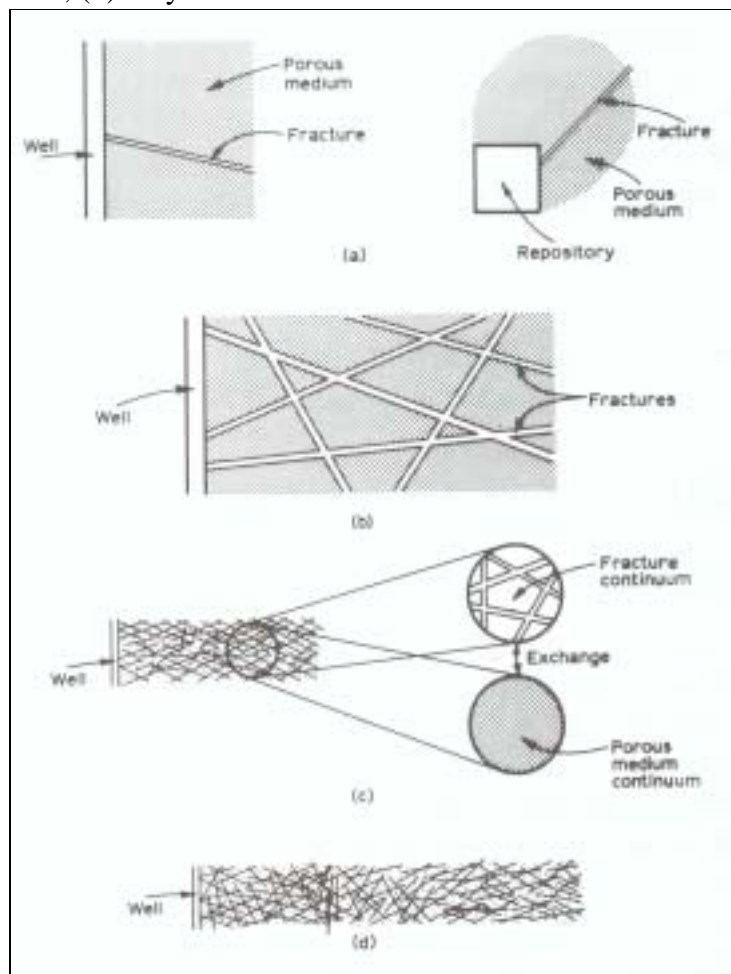
- The volume of the REV should be uniform in magnitude and shape throughout the domain.
- The averaged values should be independent of size, shape and orientation of the Representative Elementary Volume.
- The size of an REV must be much larger than the scale of the “microscopic” inhomogeneities, e.g. the diameter of pores in case of porous rock, or the fracture spacing in case of a fractured rockmass.

- The REV must be much smaller than the size of the “macroscopic” heterogeneities, e.g. facies changes over distance in the case of porous rocks, or lithology related fracture density changes in case of fractured rock.
- Finally the size of the REV must be much smaller than size of the problem domain.

In the case of an unfractured porous rock a REV can be determined in most cases. In the case of a fractured rockmass however often an REV cannot be determined. The near-field and very-near-field zones correspond with this latter situation. The far and very-far-field zones correspond to the cases in which an REV can be determined for the considered domain.

Please note that for determining the appropriate strategy the size of the problem domain is determining, not the size of the entire domain, e.g. a large fractured aquifer can be described using an equivalent porous media approach, but to describe the development of a contaminant plume a double porosity approach is used since the problem domain does not allow for an equivalent porous media approach.

Figure 2.1 Location of the problem domain in the: (a) very-near-field, (b) near-field, (c) far-field, (d) very-far-field.



In the **very-near-field** a single or a few well defined fractures will be determining the behaviour of the system. In this case it might be feasible to thoroughly investigate the fracture and construct a deterministic model for fluid flow and contaminant transport through these fractures.

In the **near-field** zone a relatively small number of fractures are considered. The location and shape in the model will have to be known. The definition of fractures, however, does not have to be deterministic, but can be described using statistics, resulting in models that are random realizations of the real system.

In the **far-field** a double continuum approach can be used. The fracture network and the porous medium are treated as two continua interacting with each other. The fracture network can also be separated in more than one continuum to reflect the different processes that lead to the development of the fracture network.

In the **very-far-field** zone the system can be regarded as an equivalent porous medium. Please note that a very-far-field situation only applies when a large amount of fractures are included in the problem domain, so that an REV is present.

In the following sections the different approaches to modelling flow and transport through fractured rockmasses will be described in more detail. Departing slightly from the order described above, the porous medium approach, which is appropriate for porous rocks as well as for the far-field situation in a fractured aquifer, will be first presented in Section 2.1. This section also includes an introduction to some general terms used in fluid flow and contaminant transport. Section 2.2 presents basic issues in the fracture flow approach, as is appropriate in the very-near-field situation. In section 2.3 the two approaches mentioned in 2.1 and 2.2 are combined to the double porosity approach as used in a far-field situation. In section 2.4 fracture network modelling is introduced. Since this thesis deals mainly with network modelling this section will be treated in more detail. The generation of the network, and the difference between in-fracture network models and fracture intersection models will be explained. At the end of each section the advantages and disadvantages of the approach are pointed out.

2.1 Porous media

All rock types have some sort of porosity. Porosity ranges from around 50% in the case of loosely packed sand and gravel to less than 0.1% in some igneous rocks. Flow can only take place through connected pores. Equation 2.1 shows the equation of flow through porous media,

first described by Darcy, a French engineer working on the public water supply of Dijon (Darcy 1856).

$$Q = KiA \quad (2.1)$$

Q = Volumetric flow rate [m^3/s]; K = hydraulic conductivity [m/s]; i = hydraulic gradient [-];

A = Cross-sectional area [m^2]

The hydraulic conductivity K in a purely porous medium depends on the properties of the groundmass, and the properties of the fluid.

$$K = \frac{\rho g}{\mu} k \quad (2.2)$$

K = hydraulic conductivity [m/s]; ρ = density [kg/m^3]; g = gravitational acceleration [m/s^2];

μ = dynamic viscosity [kg/ms]; k = intrinsic permeability [m^2]

The permeability of a porous medium can be determined from testing of a rock sample or estimated by investigating the grain size distribution and cementation. In the case of an equivalent porous medium, pumping tests are indispensable. For fractured aquifers usually Lugeon tests are performed. However an entire array of other pumping tests exist. For an exhaustive description the reader is referred to Domenico and Schwartz (1990). The hydraulic conductivities of porous rocks range from 3×10^{-4} - 3×10^{-2} m/s for gravels to 3×10^{-14} - 2×10^{-10} m/s for unfractured igneous and metamorphic rocks.

Contaminant transport in a rockmass includes the following mechanisms that occur irrespective of the type of rockmass, but differently elaborated in each:

- **advection**, which is purely governed by the fluid flow,
- **dispersion**, where we have to distinguish at least three different types,
- **diffusion**, the spreading of contaminants due to molecular motion,
- **sorption**, interaction between contaminants in the fluid and other phases (colloids, fracture skin, intact rock) which might result in retardation, and
- **decay**, be it radioactive or biological.

A good description of these phenomena for porous media can be found in Domenico and Schwartz (1990) of which follows a short resume.

Advection. Contaminants are carried along with the fluid. It is therefore necessary to know the flow rate first. Advective transport is described by equation 2.3.

$$J_i = v_x C_i n_e = K C_i \quad (2.3)$$

J_i = mass flux of component i per unit area per unit time [$\text{kg}/\text{m}^2\text{s}$];

v_x = linear groundwater velocity [m/s]; C_i = concentration of component i [kg/m^3];

n_e = effective porosity [-]

Dispersion. A porous material is built up of individual solid phase particles. Flow has to take place around these particles. Due to velocity differences within and between the different “microscopic” flow paths (e.g. pores, fractures, channels), dispersal of contaminants results. Longitudinal and transverse dispersion can be distinguished. Dispersion is described by the diffusion coefficient:

$$D_L = \frac{\sigma_L^2}{2t} \quad (2.4)$$

where D_L = longitudinal diffusion coefficient [m^2/s]; σ_L^2 = the variance [m^2] as can be deduced from a break through curve; t = time [s].

The amount of dispersion depends on the medium under investigation. There are however different scales of heterogeneity. The network of tubes or fractures, or flow within the tubes or fracture (Taylor, 1953), will create a type of dispersion on a much larger scale than the grains in sandstone. An increasingly larger contaminant plume would therefore encounter increasingly larger heterogeneities. This will result in an apparent linear increase of the longitudinal dispersivity with increasing observation scale (Dominico and Schwartz, 1990). This behaviour is similar to that of the REV discussed before. To get reliable data on dispersion, tracer tests are indispensable.

Diffusion. A contaminant due to its Brownian motion will spread through a material. In most cases diffusion is assumed Fickian. This means that the chemical mass flux is proportional to the concentration gradient and depends on the diffusion coefficient.

$$J_i = -D_d \nabla C_i \quad (2.5)$$

J_i = mass flux [$\text{kg}/\text{m}^2\text{s}$]; D_d = diffusion coefficient [m^2/s]; C_i = concentration [kg/m^3];

∇ = gradient operator [s^{-1}].

The diffusion coefficient only depends on the chemical and the medium. In most cases diffusion through the minerals can be neglected so that diffusion will only take place through the fluid. Lower porosity or higher tortuosity will thus result in slower diffusion through the rockmass. To take this into account a D_d' can be defined that includes also the properties of the rock:

$$D_d' = \frac{n}{\tau} D_d, \text{ where } \tau = \left(\frac{L}{L_e}\right)^2 \quad (2.6)$$

n = porosity [-]; τ = tortuosity [-]; L = the length of the sample [m];

L_e = length of the flow path [m]

In the case of a fractured rock mass therefore a distinction between matrix diffusion and fracture diffusion has to be made. Dead end porosity that does not contribute to the flow can be important for diffusion. Matrix diffusion can be severely inhibited by certain types of fracture skins (Moench 1984, Robinson et al. 1998).

Mechanical dispersion and diffusion are often combined into a single term called hydrodynamic dispersion. Using the Peclet number, the ratio between the advective and diffusive transport, it is possible to determine which mode of transport prevails.

$$N_{Peclet} = \frac{v d_m}{D_d} \quad (2.7)$$

v = linear groundwater velocity [m/s]; d_m = mean grain size [m];

D_d = diffusion coefficient [m²/s]

In the case of high Peclet numbers, the longitudinal dispersion will be much higher than the transverse dispersion, whereas at low Peclet numbers the diffusion gains importance.

Sorption. Sorption is a generic term for adsorption (adherence to a surface), absorption (inclusion into a material), and desorption (detaching or leaving the material). By sorbing onto the solid phases, the contaminants are temporarily removed from the flow, contaminants will therefore be retarded. The only exception is when sorption takes place preferentially on colloids in the fluid, in these cases the breakthrough can be faster than the non sorbing solute (Grindrod, 1993).

The effects of sorption are usually included as a retardation coefficient in the transport equation. The retardation can be determined using sorbing and conservative tracers during tracer tests. The retardation factor is described as follows:

$$R_f = \left[1 + \frac{(1-n)}{n} \rho_s K_d \right] \quad (2.8)$$

R_f = retardation factor [-]; n = porosity [-]; ρ_s = density of the solids [kg/m³]; K_d = distribution coefficient between solid and fluid [m³/kg]. This relation assumes the linear Freundlich isotherm. (Domenico and Schwartz, 1990: 640)

Decay. To describe decay, a distinction has to be made, between radioactive and biological decay. Radioactive decay depends only on time and not on concentration or rock properties and is therefore relatively straight forward (equation 2.9). Biological decay however, is extremely complicated. The organisms involved, need certain redox and pH conditions, as well as nutrients, carburants, and do not necessarily show first order decay rates. The organisms might for instance slow down metabolism or even perish at elevated contaminant concentrations. Organisms can also influence the hydraulic properties of the rockmass. In the case of first order decay, the following equation applies:

$$r = \frac{d}{dt}(nC) = -\lambda nC \quad (2.9)$$

where r = rate of decay [kg/m³s]; λ = decay constant [s⁻¹]

General transport equation for porous media. All these elements combine into the following general transport equation for one-dimensional transport. (Domenico and Schwartz, 1990)

$$\frac{\partial C}{\partial t} + \frac{v_x \partial C}{R_f \partial x} - \frac{D_x d^2 C}{R_f dx^2} + \lambda C = 0 \quad (2.10)$$

It can be solved numerically and adjusted, simplified or refined according to the problem to be solved.

The flow and transport of contaminants in porous media is well described in the engineering literature (e.g. Domenico and Schwartz, 1990; Freeze and Cherry, 1979; Bear, 1988). The advantage of a porous or an equivalent porous media approach is therefore that many tools for testing and modelling have been developed, are easy to use, and are readily available for many

different situations. The challenge in using this approach in a fractured aquifer situation lies in the difficulties to determine the necessary parameters needed to solve such problems.

The major disadvantage is that an REV must exist. An assumption that can only rarely be accepted in a fractured aquifer. The homogeneity that is needed is only seldom present as we will see in the next section.

2.2 Single fracture

In order to understand flow through a fractured media it is of the utmost importance to understand fluid flow and contaminant transport through a single fracture. Domenico and Schwartz (1990) gives a range between 8×10^{-9} - 3×10^{-4} m/s as a typical range of hydraulic conductivity values for fractured igneous and metamorphic rock, which is five or six orders of magnitude more conductive than the intact equivalent. A similar difference can be observed between karstic rock and intact carbonate rocks. Flow through a fracture depends mainly on the geometry of the fracture. The most important geometric parameter of a fracture is its aperture. The aperture in natural rock however is not constant due to the roughness of the fracture. A fracture will not always remain the same. Due to changing stresses, groundwater movement, weathering, chemical reaction and erosion, fractures can be filled-in, or washed open, fracture walls can be coated with minerals, and the fracture wall properties can be altered.

The most simple representation of a fracture however is that of two smooth parallel plates with a fixed aperture (b). In that case the hydraulic conductivity in the fracture (K_{fr}) can be described as (Snow, 1968):

$$K_{fr} = \frac{\rho g}{\mu} k_{fr} = \frac{\rho g b^2}{\mu 12} \quad (2.11)$$

or in terms of transmissivity of the fracture:

$$T_{fr} = K_{fr} b = \frac{\rho g b^3}{\mu 12} \quad (2.12)$$

The terms transmissivity and hydraulic conductivity are often used interchangeably. Equation 2.12 is commonly referred to as the cubic law. A small change in fracture aperture has a large effect on conductivity and directly shows one of the major difficulties in fracture flow. A fracture aperture that can be measured is always affected by stress relief and weathering at the outcrop level, or stress redistribution in boreholes or tunnels. The shape of the aperture distribution

will however remain the same (Barton and Hsieh, 1989). The hydraulic aperture is in general smaller than the mechanical aperture and is preferably determined using pumping tests. One of the biggest challenges lies in obtaining a correct hydraulic aperture in the field.

The cubic law assumes perfectly smooth parallel plates and laminar flow. In the field this is not the case, although Witherspoon et al. (1980) demonstrated that, even with irregular fractures, the cubic law still holds. Other relations are needed when surfaces become increasingly irregular, or the assumption of laminar flow no longer applies. Lomize (1951) and Louis (1974) propose formulas to deal with fracture flow through rough fractures in both laminar and turbulent flow situations. Figure 2.2 shows the different flow regimes for given fracture roughness and Reynolds numbers. For a comprehensive summary of the applicable formulae for each area see Kolditz (1997).

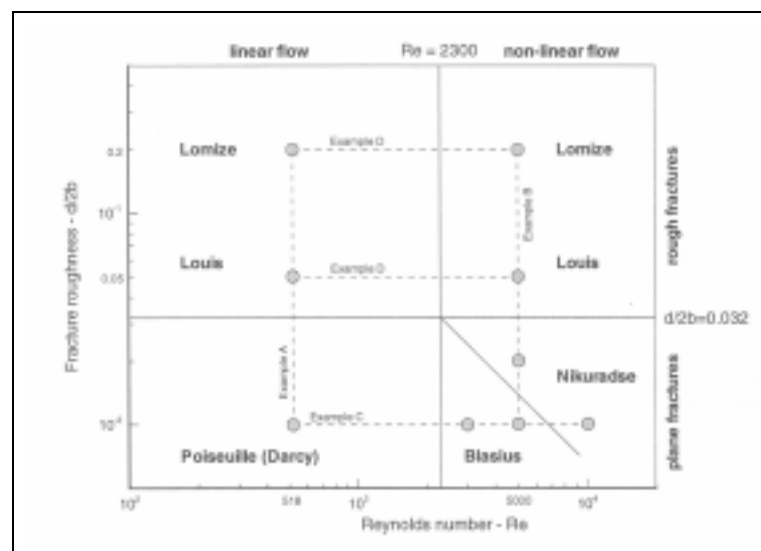


Figure 2.2 Different flow regimes considering fracture roughness and Reynolds number (from Kolditz, 1997).

Rough fractures also result in channelling of the flow within a fracture. A comprehensive review of the research conducted to this type of channelized flow within fracture planes, can be found in Tsang and Neretnieks (1998). Tsang et al. (1991) and Moreno et al. (1990) for instance, showed by calculating flow in a variable aperture model, that channels with increased flow developed. At this point a distinction has to be made between the different types of channels. Long et al. (1996) make a clear distinction between two important processes: Fracture channels and channelized transport or channelized flow.

- A fracture channel is defined as a long narrow region of enlarged aperture formed at the intersection of two fractures or by processes such as shearing.
- Channellized flow results from the non-uniform velocity in a variable-aperture fracture, which is probably applicable to the flow through all fractures.

Fracture channels are fixed in orientation and position, whereas pathways of least resistance vary according to the flow directions. In the literature the terms channel and channelling are used interchangeably. In this thesis the definitions by Long et al. (1996) will be used.

To describe contaminant transport in a single fracture, a distinction has to be made between the fracture and the adjacent porous media. Depending on the assumptions made, different authors derive different formulae. As an example the mass balance equations as solved by Tang et al. (1981) are shown here (see also Bear et al., 1993 for more details). This solution includes advection, hydrodynamic dispersion within the fracture and diffusion into the porous rockwall, as well as adsorption on the fracture wall and radioactive decay. The mass balance equation for the fracture is:

$$\frac{\partial}{\partial t}(\tau) + v_z \frac{\partial}{\partial X}(\tau) - D_h \frac{d^2}{dz^2}(\tau) + q_c + \frac{2}{b} f_{fr \rightarrow s} + \lambda \tau = 0 \quad (2.13)$$

where τ = concentration in the fracture [kg/m^3]; v_z = velocity in fracture [m/s]; D_h = hydrodynamic dispersion [m^2/s]; q_c = leakage into porous rock [$\text{kg}/\text{m}^3\text{s}$]; $f_{fr \rightarrow s}$ = rate of adsorption from fluid to rockwall [$\text{kg}/\text{m}^2\text{s}$]; λ = coefficient of radioactive decay [s^{-1}].

The mass balance equation of the fracture wall is:

$$\frac{\partial c_{sfr}}{\partial t} = \frac{2}{b} f_{fr \rightarrow s} - \lambda c_{sfr} \quad (2.14)$$

with:

$$c_{sfr} = K_{dfr \rightarrow s} \tau \quad (2.15)$$

where c_{sfr} is the mass of contaminant adsorbed on the solid wall [kg/m^3] and $K_{dfr \rightarrow s}$ the partitioning coefficient [-] assuming a linear equilibrium isotherm.

The mass balance for the porous rock is:

$$\frac{\partial c}{\partial t} - D_{mp} \left(\frac{\partial^2 c}{\partial y^2} + \frac{\partial^2 c}{\partial z^2} \right) + \lambda c + \frac{f_{f \rightarrow s}}{\phi_{pb}} \tau = 0 \quad (2.16)$$

with

$$\phi \frac{\partial c_{spb}}{\partial t} = f_{f \rightarrow s} - \phi_{pb} \lambda c_{spb} \quad (2.17)$$

and

$$c_{spb} = K_{dpb} c \quad (2.18)$$

Where D_{mp} = molecular diffusion in the porous rock [$\text{kg}/\text{m}^3\text{s}$]; ϕ_{pb} = porosity of the porous rock [-]; c_{spb} = mass adsorbed in the porous rock [kg/m^3] and K_{spb} = partitioning coefficient in the porous rock [-]. By inserting the equations belonging to the solid fracture wall or porous rock mass into the mass balance equations for the fracture, the entire system can be solved.

This solution is one of many and is shown to demonstrate the principles, it can be simplified by neglecting certain parts, (e.g. impermeable rockwalls by assuming no porosity, no decay) or expanded (e.g. adding a fracture skin, non-linear sorbtion assumption, decay series). The different mechanisms of transport in the mass balance equations for transport in fractures and for porous media are the same, so is the essence of the equations with the only difference of added boundary conditions at the interfaces of fracture-rockwall and rockwall-porous rock.

2.3 Double porosity

In a far-field situation a fractured porous rockmass can be treated as an equivalent porous media. There is however a significant difference between normal porous rockmass and a fractured porous rockmass. Most of the porosity will be located in the pores of the rock matrix. Flow however, will take place mainly in the fractures. It is therefore advantageous to consider such a problem as two overlapping media. The first medium will account for most of the storage, whereas the other mainly conducts the fluid. These two media are then coupled to result in one system. Different double porosity models have been developed. For a more detailed description of such models the reader is referred to the well known models by Barenblatt et al. (1960), Warren and Root (1963) and Streltsova (1976). Additionally the model by Moench (1984) is mentioned which also accounts for the effect of fracture skins.

The problem of double porosity models is that a sufficiently large Representative Elementary Volume (REV) must be available. In practice this means a regular fracture pattern. In a hierarchy of fractures, where just a small part of the fractures are responsible for the main part of the flow, such a REV will not be available.

2.4 Network models

In the near-field case more than one fracture is included in the problem domain, however not enough to justify an equivalent porous medium approach. In this case the problem can be seen as a network of conductive features. Since the exact location of all fractures is almost never known, a stochastic description of the conductive elements is preferably used.

In subsection 2.4.1 the state of the art in stochastic modelling of the fractures for network development is described. According to the conceptual model of the flow through a fractured medium, two approaches will be described. The in-fracture flow approach will be described in subsection 2.4.2 and the fracture intersection approach in subsection 2.4.3.

2.4.1 Stochastic fracture development

For each fracture network flow model, fractures have to be generated first. Due to the normally large numbers of fractures and unknown exact location of fractures in a problem domain, a statistical description of the fracture sets is usually used. The parameters of importance are the number of fracture sets, the number of fractures per set, the location of the fractures, the orientation of the fractures, the size of the fractures and the shape of the fractures. Most of these data can be obtained from site investigation.

Fracture sets. In a rock mass fractures occur in sets. Fractures in the same set are generally formed at the same time, by the same process. Fractures in the same fracture set usually have similar properties. It is therefore of great importance to be aware of the different fracture sets before measuring the data in the field. This can be difficult, especially in complicated geologies with multiple tectonic events. For practical reasons, fracture sets that are similarly orientated are often grouped. In many field campaigns however, fractures have been collected without regard to which fracture set they belonged. In a later stage it can be almost impossible to assign each fracture to a fracture set correctly.

Number of fractures. Different ways exist to measure the amount of fractures. Linear fracture density, i.e. the number of fractures per length, are most easily obtained. Linear fracture density should be measured perpendicular to each fracture set. If this is not possible, such as in most boreholes, a correction needs to be made. An other approach is to measure the trace length of

all fractures intersecting a plane resulting in a planar density, finally the total fracture area per volume can be measured.

$$Density_{linear} = \frac{n_{fr}}{L} \quad (2.19)$$

where n_{fr} = nr. of fractures [-], L = measuring length [m].

$$Density_{planar} = \frac{\sum L_{fr}}{A} \quad (2.20)$$

where L_{fr} = fracture trace length [m], A = measuring area [m²].

$$Density_{volumetric} = \frac{\sum A_{fr}}{V} \quad (2.21)$$

where A_{fr} = area of a fracture [m²], V = measuring volume [m³]

Knowledge of the fracture density does however not mean that the number of fractures in a volume is known, which depends also on the shape and size of the fractures.

Orientation of the fracture sets. There are different ways to describe the spread of fracture orientations within fracture sets. An often used distribution is the Fisher distribution, also used are the Bingham distribution, the bivariate Fisher distribution, the bivariate Bingham distribution, and the bivariate normal distribution. For a description of these distributions see Yu (2000).

These distributions have the disadvantage that they describe only a special shape of distribution and usually a statistically relevant selection can not be made. An eigenvector/eigenvalue approach can describe spherical, oval, girdle and totally random distributions using the same method.

To visualize the physical significance of the eigenvector/eigenvalue approach assume a unit mass at every point at which a directional vector cuts through a unit sphere. If the sphere is to be rotated around a random axis, a specific energy is needed to start the rotation. This energy requirement is proportional to the inertia of the sphere. In most cases there will be one axis with maximal inertia, one with the smallest inertia and an axis perpendicular to both. These axes are orthogonal. The directions of these axes are identical with the eigenvectors of the inertia tensor matrix. The eigenvalues give the shape of the tensor. From the eigenvalues and their ratios we can draw conclusions about the type of distributions. For further explanations of the concept and

detailed calculation procedures of eigenvectors and eigenvalues the reader is referred to Wallbrecher (1986).

Location of fractures. The distribution of the location of fractures is in general assumed to be Poissonian for modelling purposes, i.e. the fracture centre location is randomly located in space. In many existing models this approach has been used (e.g. Cacas et al., 1990; Yu, 2000). Many outcrops however suggest that the fracture centre locations are not randomly distributed, but fractures seem to be clustered, especially in intrusive igneous rocks (Pollard and Aydin, 1988). The network model Fracman by Golder Associates has many options to model distributions that are not Poissonian distributions. At Kyoto University the author has been involved in research of the construction of clustered models using a parent-daughter model (Long and Billaux, 1987), which has resulted in a bachelors thesis by Chiba (2002). Other interesting studies to determine fracture clustering parameters from tunnel and borehole data is currently ongoing at the Japanese Nuclear Cycle Development Institute (Choi et al., 1999).

Fracture size and shapes. Fractures formed in an intact rock will propagate in the form of an ellipse (Pollard and Aydin, 1988). When other fractures are encountered, fractures can stop, cross or continue in different directions. What the exact shape of a fracture is in reality, however, is hard to obtain. Therefore, from lack of better understanding, a circular fracture is often assumed (e.g. Cacas et al., 1990; Yu, 2000). Fractures can be approximated by polygons. The size of the fractures is almost impossible to obtain, since the outcrop shows only the fracture trace. There is a relationship between the size, shape of the fractures and the density of the fracture network. Larger fractures will lead to higher fracture densities, an increase in the number of fractures will have the same effect. Since fracture density is often measured in a borehole or in the best case on an outcrop, the exact geometry is not clear.

2.4.2 In-fracture flow

Most researchers in the field of network flow have looked at the case of flow taking place within the fracture planes (e.g. Cacas et al. 1990; Billaux, 1990; Yu, 2000, FracMan technology group, 2002; Nordqvist et al., 1992). These models generate a discrete fracture network model by approximately the same procedure. The intersections of all fractures are determined. Each fracture intersection will form a line in three-dimensional space. Usually the centre of this line is

calculated and linked to the fracture centres of the fractures forming the intersection, in that way generating a three dimensional network of conductive features (Figure 2.3). The fracture can also be further discretized. This is computationally intensive, but might give better results when modelling contaminant transport and thereby preventing the development of unnatural flow paths, where each flow feature first has to go through the fracture centre before connecting to an other fracture.

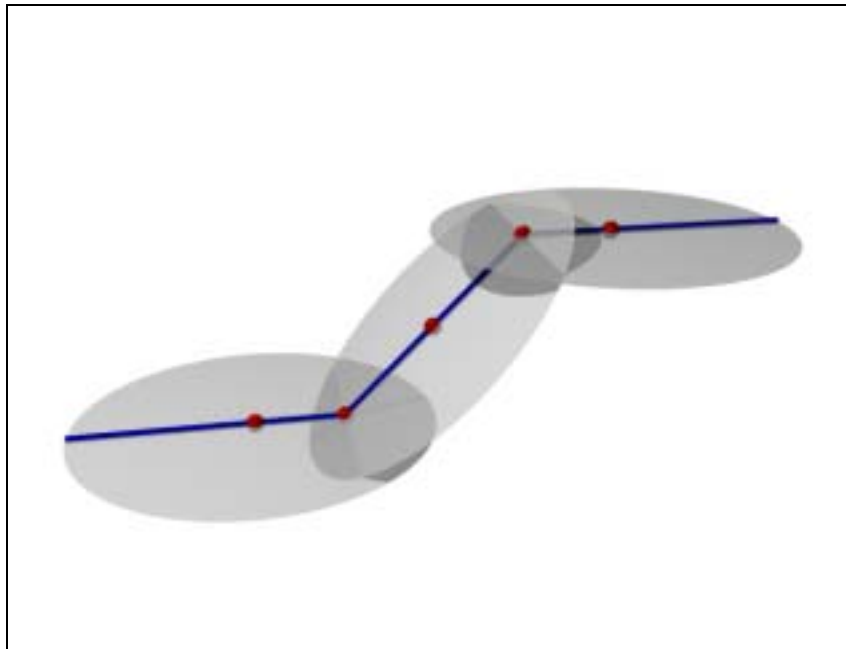


Figure 2.3 In-fracture tubular network model. To simplify calculations, the fractures are idealized by tubular structures that connect the centre of a fracture with the centres of the intersections.

2.4.3 Fracture intersection flow

A central part of this thesis is the development of a fracture network model that assumes flow to take place at the intersection of fractures. In the literature many authors have mentioned flow at the intersection of fractures (Abelin et al., 1988; Neretnieks, 1994, Shimo and Iihoshi, 1995; Sugimura et al., 1999). During the 3-dimensional migration experiment at the Stripa mine in Sweden, which is one of the most detailed experiments of its kind ever carried out, a clear correlation between the number of intersections per area and the amount of inflow into the test gallery has been shown (Abelin et al., 1988). A much higher correlation than that with the total fracture length per area (Figures 2.4 - 2.6) Similar features have been observed at Forsmark and

Kymmen tunnel in Sweden (Neretnieks, 1994). Moreno and Nieretnieks (1993) have developed a channel network model that also includes as well in-fracture flow channels as fracture intersections. Additional information on their model can be found in Gylling (1997).

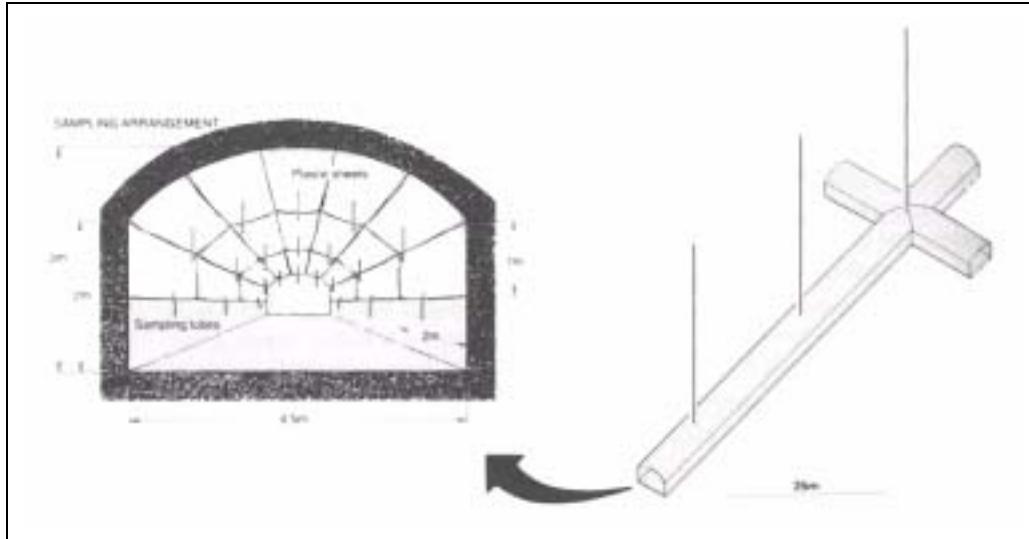


Figure 2.4 Layout and dimensions of the test site for the 3-D migration experiment at the Stripa mine (from Abelin et al., 1988).

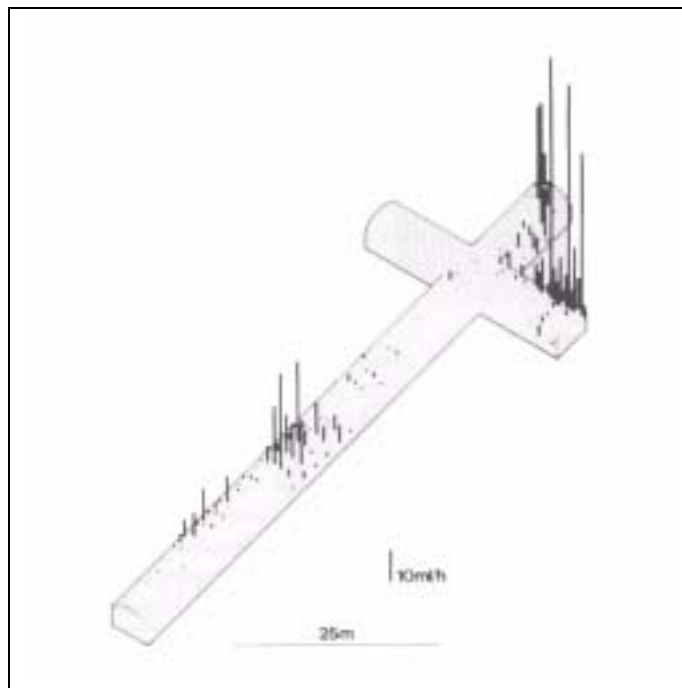


Figure 2.5 Natural water inflow rates at the Stripa mine (from Abelin et al., 1988).

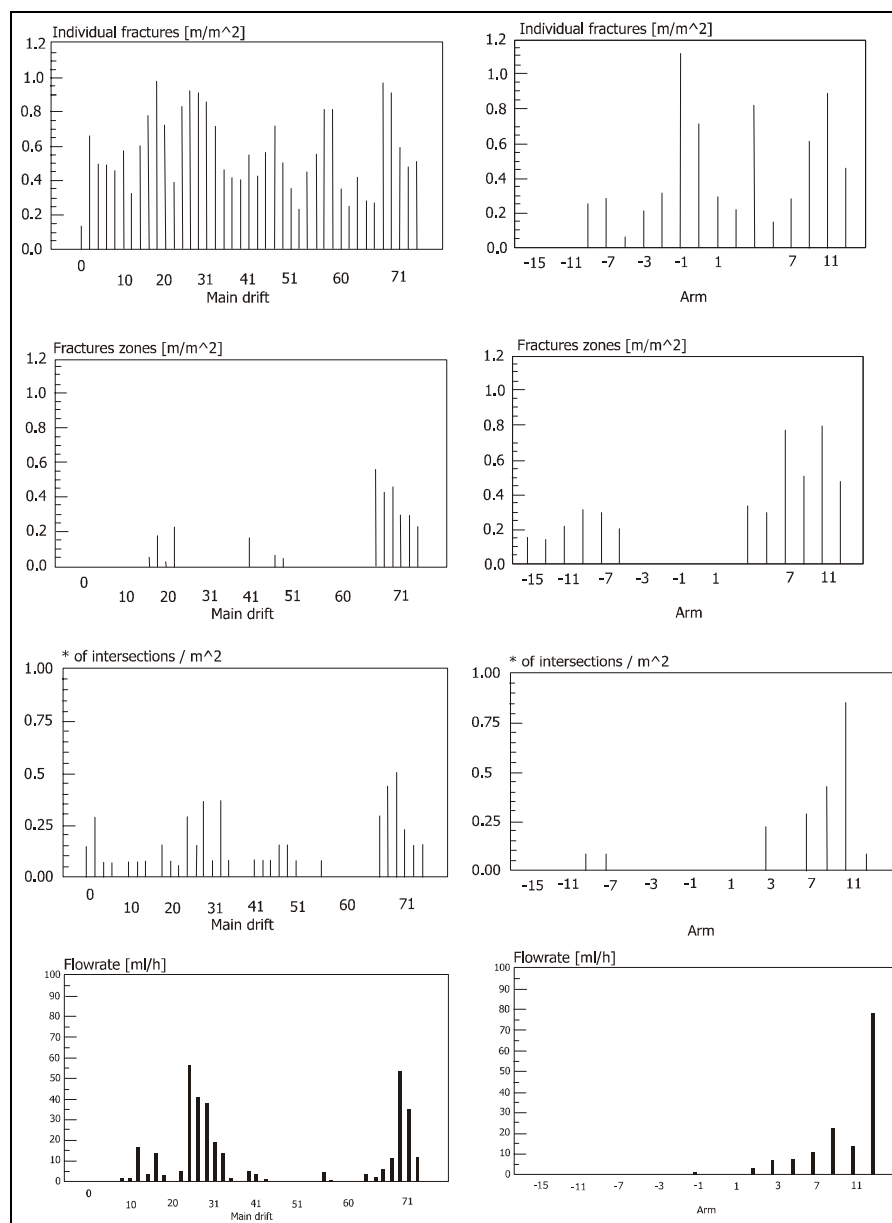


Figure 2.6 Fracture characteristics compared with water inflow rates at the 3-D migration experiment at the Stripa mine show that water inflow rates seem to be more related to the number of fracture intersections per area, than the fracture length per area (from Abelin et al., 1988).

Shimo and Iihoshi (1995), in an other unique experiment, have also shown the existence of a significant flow path located at the intersection of two fractures. In their experiment they have performed a tomographic flow experiment through a 30 cm cube of chert. At each face, 25 inflow areas were created that could be used to pump water in or out. Exactly at the intersection of two prominent fractures, a high flow conduit has been detected (Figure 2.7).

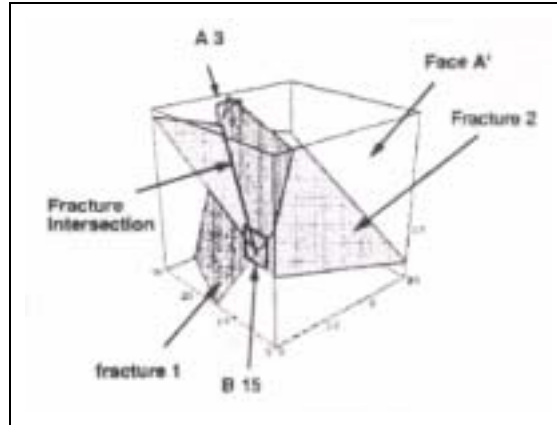


Figure 2.7 Fracture channel as found during tomographic flow test experiment (Shimo and Iihoshi, 1995).

A similar testing apparatus is currently under development at the Japanese Nuclear Cycle Development Institute (JNC). This apparatus has been designed for rock samples up to 1 cubic meter. Until now however, no intact rock sample of such a size could be obtained. Currently 50cm cubes are being prepared for testing. The preliminary tests carried out on a rock sample including two abutting fractures (Figure 2.8), showed a two times higher conductivity at the intersection of the two fractures than through the fractures (Sawada, personal contact 2002).



Figure 2.8 Photo of the abutting fracture tested at JNC in Tokai-mura, Japan.

Jourde (1999) presents fracture intersections as important flow features in a carbonate geology and develops a tubular network model with tubes located at the intersection of discontinuities in stratified media. His work has been influenced by work of Bruel (1998) and by Drogue and Grillot (1976) that both state that preferred flow paths develop at the intersections of fractures, with a preference for the intersection of vertical joints and bedding planes in a carbonate geology. In an oversaturated environment, precipitation of minerals would preferably occur in the fractures focusing flow to the intersections.

Although many researchers have observed flow at the intersection of fractures, reasons as to the existence of such channels are scarce. In the following section possible explanations for the existence of channels where fractures meet are summarized.

2.4.4 Development of channels at fracture intersections

In general three different types of channel development can be distinguished:

- Dissolution
- Weathering
- Tectonics

Often channel development will be the result of a combination of these factors.

Dissolution. The development of channels by solution is a well known phenomenon, especially in limestone, dolomites and gypsum. But in principle, each rock mass containing minerals dissolves under the prevailing geochemical conditions. The principle of dissolution is that a solution flowing through a rock mass is undersaturated with respect to the minerals in the rock. Minerals will be dissolved and over time, the undersaturated solutions will reach saturation at which point further dissolution will stop. Undersaturated conditions can develop at each geochemical boundary. This can be a change of mineralogy, for instance at a fault where two different rocks are situated next to each other. In karstic rockmasses this geochemical boundary is usually at or near the surface, since meteoric water is generally undersaturated with respect to most minerals. Meteoric water infiltrating into the highly fractured and weathered surface will dissolve materials along the flow paths. By the action of dissolution these flow paths will increase in size, focusing more flow to these paths. Some of these flow paths can develop into enormous cave systems. The channels that develop by simple solution in carbonates will follow the paths of least resistance. These can be (but not necessarily) the intersections of discontinu-

ities. Many cave systems usually follow the fracture system. In the case of limestone, a covering soil layer can enhance the dissolving capacity of the solution by increasing CO₂ levels.

Another well known mechanism of dissolution is groundwater mixing. Two groundwaters of different composition that are both saturated for a certain mineral can be undersaturated for the same mineral when mixed. This type of dissolution is common in carbonatic aquifers close to the sea. In these regions sea water mixes with groundwater of terrestrial origin. The increased dissolution at groundwater level, can often be observed in cave systems, and can also be regarded as a mixing zone between air and water. For the mixing type of dissolution, intersection flow is more likely. When fractures carrying different solutions meet at the intersection of discontinuities, mixing, and therefore dissolution, takes place. The tube that develops, will initially not be orientated in the direction of flow, but perpendicular to it. Similar phenomena may take place when deep groundwater surges up and mixes with shallow water. The opposite might also happen. When groundwater surges up, a drop in pressure and decrease in temperature, might result in precipitation of minerals, forming a vein, for example enriched in gold.

Weathering. Spheroidal weathering, a phenomenon, often associated with granite, is the weathering of rocks starting from the joints. The results are rounded boulders. The initially angular blocks round off because weathering is more effective at corners, where the area of "attack" is larger in comparison to the volume. The following figure schematically shows the progressive development of this phenomenon (Figure 2.9).

Like dissolution, weathering is most active in the shallow subsurface, where rock, water and air can interact freely. It can however, take place at any geochemical boundary. This process can lead to the formation of channels at the intersection of fractures. Although generally associated with granite, the process can be observed in other rock types. An example is the photo from the quarry in the south of the Osaka prefecture (Japan) used for the construction of the second runway of the Kansai International Airport (Figure 2.10).

Weathering is a complex geochemical process. Common degradation products of many weathering reactions are clay and iron oxides and hydroxides. These materials can be washed into openings and clog any preferential paths as often seen in calcareous dissolution features that are filled with residual soil, but can also emphasize the importance of the largest flow features that will clog last.

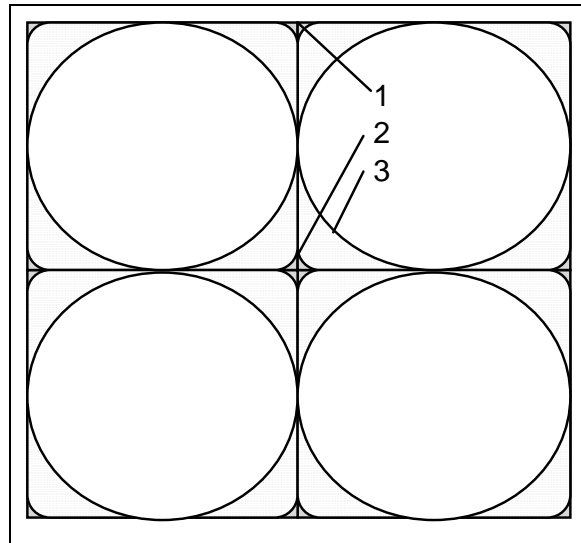


Figure 2.9 Schematic drawing of spheroidal weathering, where the numbers 1, 2 and 3 indicate the different stages of weathering from freshly fractured rock to the formation of rounded boulders.



Figure 2.10 Picture of an outcrop at the quarry for the Kansai international airport, showing weathering phenomena in a sedimentary rock that can lead to flow at fracture intersections. The picture shows the intersection of the bedding plane (perpendicular to the axis of view) and two perpendicular joints.

Tectonics. Channels can develop in almost any tectonic regime. The major principle is dilation. We can distinguish the following three tectonic situations:

- Compression
- Shear
- Extension

Compression. In an ideal compressional situation no openings can form. Any existing opening should be closed by the pressure, where the smaller opening would close first, leaving only the largest channels open, resulting in a larger importance of in-fracture channelized flow as opposed to parallel plate type of fracture flow, at higher pressures. Due to the heterogeneous nature of rockmasses however (e.g. existing fracture sets, bedding), stress concentrations will always develop, resulting in shear movements leading to differential stresses in different directions, and on a large scale to folding, reverse and thrust faulting.

Existing joints will often displace in a compressional situation. This will lead to non fitting joint walls and therefore to in-fracture channelling (Figure 2.11).

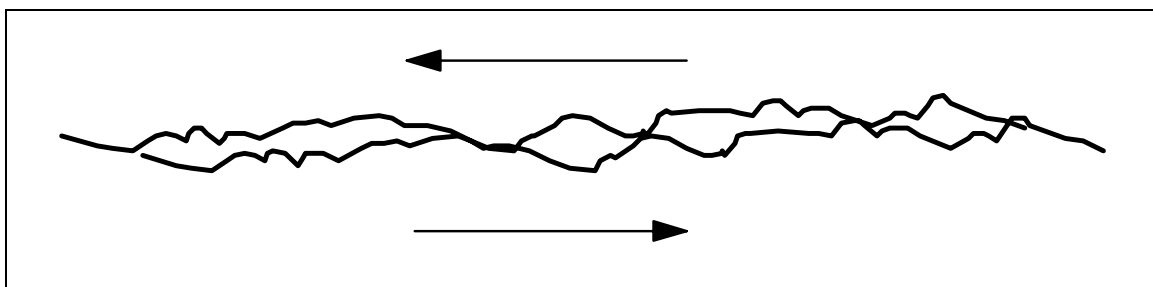


Figure 2.11 Displacement of fracture walls lead to in-fracture flow channelling

At faults the same processes will take place. Asperities can be broken off and alterations can take place resulting in a filled fracture that might be a hydraulic barrier instead of a conduit.

Development of channels at intersections of discontinuities is possible, as can be seen in Figure 2.12. During these slight movements one can imagine that the corners are more susceptible to breakage and therefore to accelerated weathering and dissolution. The sample currently under investigation at JNC might be an example of such a case (Figure 2.8).

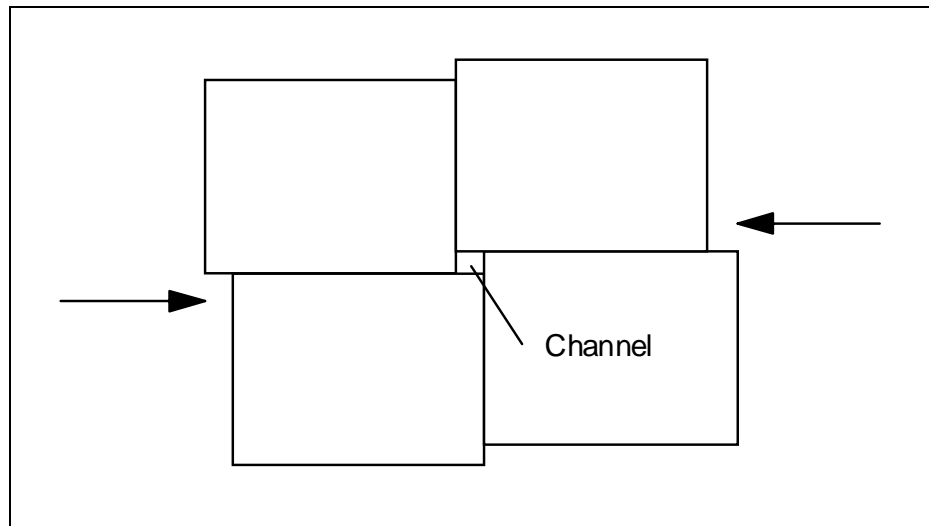


Figure 2.12 Displacement of blocks can lead to the development of fracture channels at the intersection of fractures. Please note that the edges of the blocks can be subject to stress concentrations, which contribute to a faster disintegration of the rock at those locations.

An other possibility is the development of channels in folding structures. During folding fractures can develop parallel to the folding plane. In the folds, extensional stresses can open up these fractures partially or open space can develop between different bedding planes (Figure 2.13).

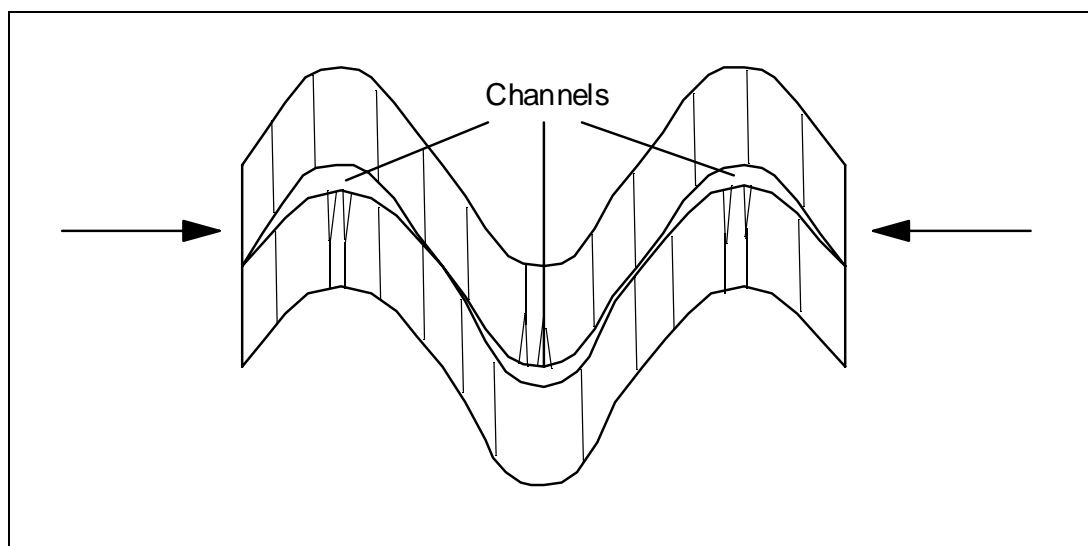


Figure 2.13 Channel development in folding structures.

The orientation of the channels are in each case in the direction of the intermediate stress component.

Shear. The mechanisms discussed in the compression section can also be interpreted as shear features, since they actually developed in shear in a compressional environment. Additional shear features are the development of en-echelon jointing and veins (Figure 2.14), and jogs (Figure 2.15). En-echelon joints accommodate shear without forming a continuous fracture. These structures are later often filled with minerals.

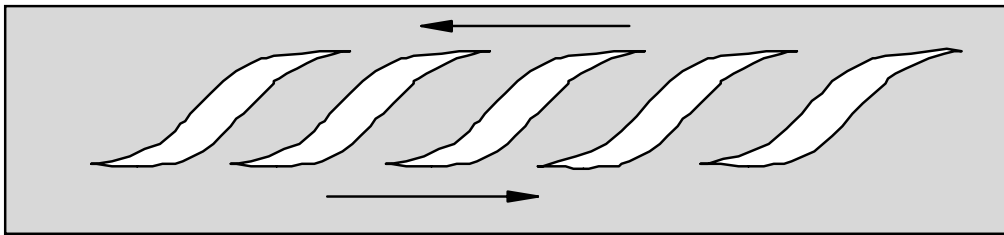


Figure 2.14 In an unfractured rock, several offset, parallel fractures can develop under an angle with the shear direction (Riedel shears). Additional shear movement will result in more dilation and opening of these fractures. Such features are often filled with minerals and preserved as en-echelon veins.

When two parallel fractures connect under shear, an area of enlarged permeability is formed, called a jog. At a small scale these jumps form channels, at the scale of faults, a large area which is extensively fractured, and increased in permeability, is formed (Watanabe, 1995). The Japanese Nuclear Cycle Development Institute (JNC) is currently investigating these jogs using data from the Kuji Underground Oil Storage Facility, Iwate prefecture in Japan (Choi et al., 1999).

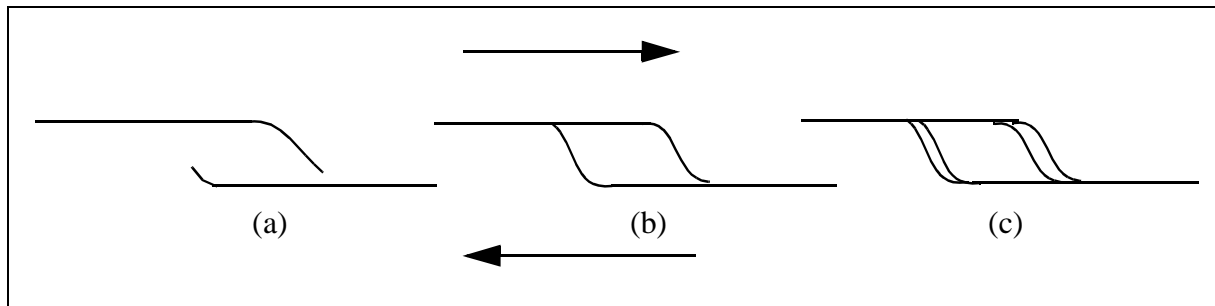


Figure 2.15 When two developing parallel fractures approach each other, the fracture tips will be deviated towards the other fracture (a) until a connection is made. This structure is called a jog (b). More shear can result in the creation of additional porosity at this jog structure (c).

In reports by the NAGRA (1985, 1994), the development of channel-like structures in kakirite, a cataclastic gouge material found in shear faults, is discussed. These channels are assumed to be long, non-crossing tubes through void space in the fractured material.

Extension. Extension will normally lead to an opening of fractures, and not necessarily to channels. These fractures can fill partially (see shear section) or certain paths can be enlarged, and both may result in fracture channels. Extension cracks also allow water to enter, which will speed up the weathering and dissolution, forming new channels. In certain cases, block rotation occurs during extension. In such a case channels also orientate in the direction parallel to the intermediate stress direction.

3

Scope of this thesis

Chapter two introduced to the current state of the art in flow and transport within fractured rock masses. It introduced the concept of a Representative Elementary Volume (REV) and went on to explain the basics of each methodology. In each of the approaches many open research questions remain. The focus of this thesis lies in network modelling, since the author is of the opinion that many groundwater problems, especially in the field of contaminant transport, are situated in a near-field situation. Observations during fieldwork in Spain, which was part of this research, suggest that flow channels develop at intersections of fractures. Similar observations have been made by other researchers. Some researchers have included fracture intersections as additional conductive features in their in-fracture flow models, which makes it difficult to distinguish the effect of each of the two phenomena. In this thesis, therefore, a model that includes only fracture intersections as conductive features is presented.

The most authoritative publication on research of fluid flow and rock fractures is the report by the Committee on fracture characterization and fluid flow (Long et al., 1996) of the (United States) National Research Council. In the last chapter of this report the committee points out what the needs are in the field of fractures and fluid flow and makes recommendations for future research. The report states that the exact nature of fluid flow in many patterns has still not been confirmed, and suggests further study to the processes that are responsible for producing distinctive fracture patterns in order to better understand the system of fracture flow. The research presented in this thesis starts from the observations of flow channels in the field. Taking into account the geological history of the site, a conceptual model is developed. The report of the committee also mentions that fracture genesis and geometry should be considered as a fully three-dimensional problem. Therefore a three-dimensional approach will be adopted in this thesis. Furthermore the report states that further research is needed to determine how the

geometry of a structure gives rise to preferential flow paths. In this thesis networks of preferential flow paths, assumed to develop at the intersections of fractures, are studied.

Physical model. The basis of this study is the assumption that intersections of discontinuities are zones of mechanical weakness and might therefore contribute considerably to the flow through a fractured rockmass. These ideas have been strengthened by observations in the field. Therefore a mathematical network model has been developed based on the following physical model:

In a fractured rockmass with a relatively low permeability of the intact rock, groundwater flows mainly through preferential paths. Part of these preferential paths will be situated at the intersection of different fractures. In this research, flow is assumed to take place only at these intersections. In a sufficiently fractured rockmass a network of interconnected tubes will develop. These tubes have different directions, lengths, cross areas which results in a different conductivity for each tube. Some tubes might even be closed.

Assumptions and delimitations. Although size, shape, location of fractures and resulting flow paths in rock masses are irregular, these parameters cannot, or only with great difficulty, be obtained and certain simplifications have to be made. In this study the shape of fractures will be assumed circular, fracture centres will be assumed randomly distributed in space and fracture sizes will be assumed uniformly distributed.

The following assumptions for flow through the network will be made:

- laminar flow
- fully saturated conditions
- single phase flow
- steady state

For further development of the models presented in this thesis, some of these assumptions can be studied further, because in real world situations some of these assumptions may not apply.

The fieldwork data has been used to check the geometry of the model with reality. Because of the lack of hydrogeologic data at the fieldwork site, a sensitivity analysis has been performed. These tests are not only of academic value but are designed to give answers to practical questions such as:

- If the fracture density is increased, how many possible tubes can develop at fracture intersections? (see section 5.2.2)
- How large a volume is needed to make sure flow rate calculations will be within a given error margin? (see section 5.2.3)
- Generating stochastic models results in a spread of the flow rates calculated. How much of this spread is due to the stochastic parameters that generate the fracture network? And how much due to the stochastic parameters used for assigning conductivities? (see section 5.2.4)
- What influence has a fracture set with a considerably larger fracture density on the flow rate in each direction? (see section 5.2.5)
- What is the influence of a fracture set with considerably larger fracture diameters? (see section 5.2.6)
- If tubes in one direction show much higher conductivities, how will it affect an overall flow rate in the same direction? (see section 5.2.7)
- For investigating the permeability of a rockmass single borehole tests, such as Lugeon tests, are easy and economical to conduct. What can the result of such a test tell about the rockmass if a tubular network is present? (see section 5.2.7)

4

Tools

In this chapter the methodology and procedure used in this study are described. Section 4.1 deals with the data collection procedures used to gather data in the field. Section 4.2 describes the computer models used for this study. Subsection 4.2.1 explains the working of the CPA program, in subsection 4.2.2 the functioning of the Joint-OKY code will be described, followed by subsection 4.2.3 that deals with the interface code developed to enable an exchange of data between CPA and Joint-OKY.

4.1 Data gathering

Observations at outcrops have lead to the formulation of the hypothesis that flow at the intersection of fractures takes place. Outcrops can be an efficient, reliable and economical source for fracture data and a help to define a physical model of the subsurface. How outcrops can help to define a physical model, which data can be obtained and how these data can be used, has been described in Bruines and Halihan (1999). A copy of this paper has been included in Appendix A.

Important data that can be obtained from an outcrop have been compiled in a data collection sheet in advance of the fieldwork that was part of this project in Granada, Spain. The developed data collection sheet includes parts of other researcher's data collection sheets (Priest, 1993; Halihan, personal communication; ITC/TUD, 1996). Good references on fracture data are La Pointe and Hudson (1985), Dershowitz and Einstein (1988) and Barton and Hsieh (1989). The general description of the outcrop and conditions at the site have been adapted from ITC/TUD (1996). The part on the fracture descriptions has been developed with scanline measurements and fracture flow problems in mind. The following data fields were included:

- Fracture number. Each fracture is numbered for identification.
- Location along scanline. To investigate fracture densities and possible clustering of fractures the location and therefore the distance between fractures need to be recorded.

- Dip direction and dip angle. Fractures are orientated in space. The orientations of fractures can explain part of the tectonic history at the site and possible anisotropic behaviour of fluid flow. For the fieldwork a compass of the Breithaupt company has been used (Figure 4.1).



Figure 4.1 Breithaupt compass used for fieldwork.

- Half lengths and total length. Half lengths are the lengths from the scanline to the terminations of the fracture on both sides of the scanline. Half lengths result in more data to be used to determine fracture length distributions. For more details on this approach see Priest (1993).
- Fracture termination. Fractures can terminate abutting to another fracture, blindly, crossing another fracture, or diffuse where a fracture is connected to another fracture by hair line fractures (Figure 4.2). In some cases the termination of a fracture is not visible. terminations give clues about the tectonic history and anisotropy of the system.

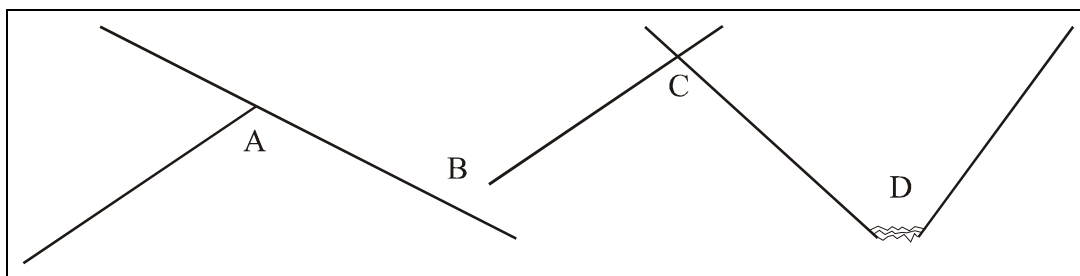


Figure 4.2 Fracture terminations: **A**butting, **B**lind, **C**rossing and **D**iffuse.

- Fracture aperture is the distance between the fracture walls and can be highly variable, between fractures and within the same fracture. To measure the aperture an automotive feeler gauge was used (Figure 4.3). This tool has different thin metal plates with a known thickness that can be inserted into a fracture to find the aperture.



Figure 4.3 Automotive feeler gauge designed to measure the gap of a spark-plug is used to measure fracture aperture.

- Infill of fractures. Fractures seldom stay open over geologic time. Minerals can precipitate, material can be deposited. The thickness can be recorded as well as the type of infill (calcite, quartz, iron hydroxides, breccia, etc.).
- Staining or fracture skins. These are mineral precipitations on the fracture walls, which can have a large influence on the contaminant transport through the rockmass and are the reason that at the Spain fieldwork site ancient flowpaths are visible. Again thickness and type can be recorded (adapted from Halihan, personal communication).
- Rockwall alterations. Rockwall alterations are located in the rockwall and are often proof for circulating fluids in the past and can greatly influence the transport properties as well. Again thickness and type can be recorded.
- Fracture roughness can be measured in different ways. For an extensive discussion on this topic the reader is referred to Grasselli (2001). In this research a descriptive method has been used in the field on different scales, first on the meter scale (wavy, curved, slightly curved, straight), than on a scale of about 20 cm (stepped, undulating, planar) and finally the roughness to the touch (rough, smooth, slickensided) as described in ITC/TUD (1996).

To record the shape of rockfaces or fracture channels, a carpenter's contour gauge has been used (Figure 4.4).



Figure 4.4 Carpenter's contour gauge.

The actual procedure for describing an outcrop in the field was to investigate the slope first and then make a detailed description and sketch of the slope including important features. The slope was then photographed as well as all interesting features. Then the data collection sheet was used. The data sheet is developed for scanlines and is very exhaustive in details. In the field, scanlines were not always practical and certain data were difficult if not impossible to obtain. In the field scanlines were mainly used to collect data on fracture densities. Due to the relatively small amount of fractures, all visible fractures were recorded.

4.2 Models

For modelling flow through a fractured medium a specific software CPA (**Critical Path Analysis**) has been developed at the EPFL. In section 4.2.1 this program is described in more detail.

In addition the Joint-OKY (**Joint** program of the **Ohnishi** laboratory at **Kyoto University**) program, which has been developed by Dr. Yu of the Kyoto University, has been used as well during this study. This program is described in section 4.2.2.

4.2.1 CPA

The CPA program in its original version has been developed in cooperation with the Department of Mathematics of the EPFL as part of this research project on flow in tubular networks.

The program was written in C++ to run on a Solaris system and extensively uses the CGAL (<http://www.cgal.org/>) and LEDA (<http://www.algorithmic-solutions.com/enleda.htm>) libraries. It has been developed with the idea in mind to test the hypothesis about strongly disordered systems (Cerny and Ben Arous *in* Bruines and Genske, 2001; Cerny, 2003) and has later been adapted by this author to realize groundwater flow models that assume flow through a network of tubes, located at the intersection of fractures for this thesis. The original program developed for a Solaris system has been made available on the Windows system and has since then undergone several adaptations and improvements. The program is built up out of the following modules (see also Figure 4.5):

- Development of the geometric model,
- Assignment of the conductivities to the channels,
- Calculation of percolation threshold and the fastest flowpath,
- Calculation of the total flow rate through the model,
- Graphical user interface that also includes visualization of the fracture network.

The CPA program includes different network models: a square two-dimensional grid, a regular three dimensional grid and a fracture generated network model. The two regular grids have been developed to investigate percolation and the fastest flowpath theory. Since in these regular grids the length of each tube is the same, the lengths of the tubes have not been taken into account in the original version of the program. This feature has been added later by the author for the fracture generated network model within the framework of the present thesis.

To generate a tubular network model that is more realistic it is however necessary to work with fractures. In the fracture intersection model different fracture sets can be constructed. To describe the orientation of the fracture sets different possibilities exist. In this research an eigenvector approach has been used since this is the easiest way to describe different distribution types.

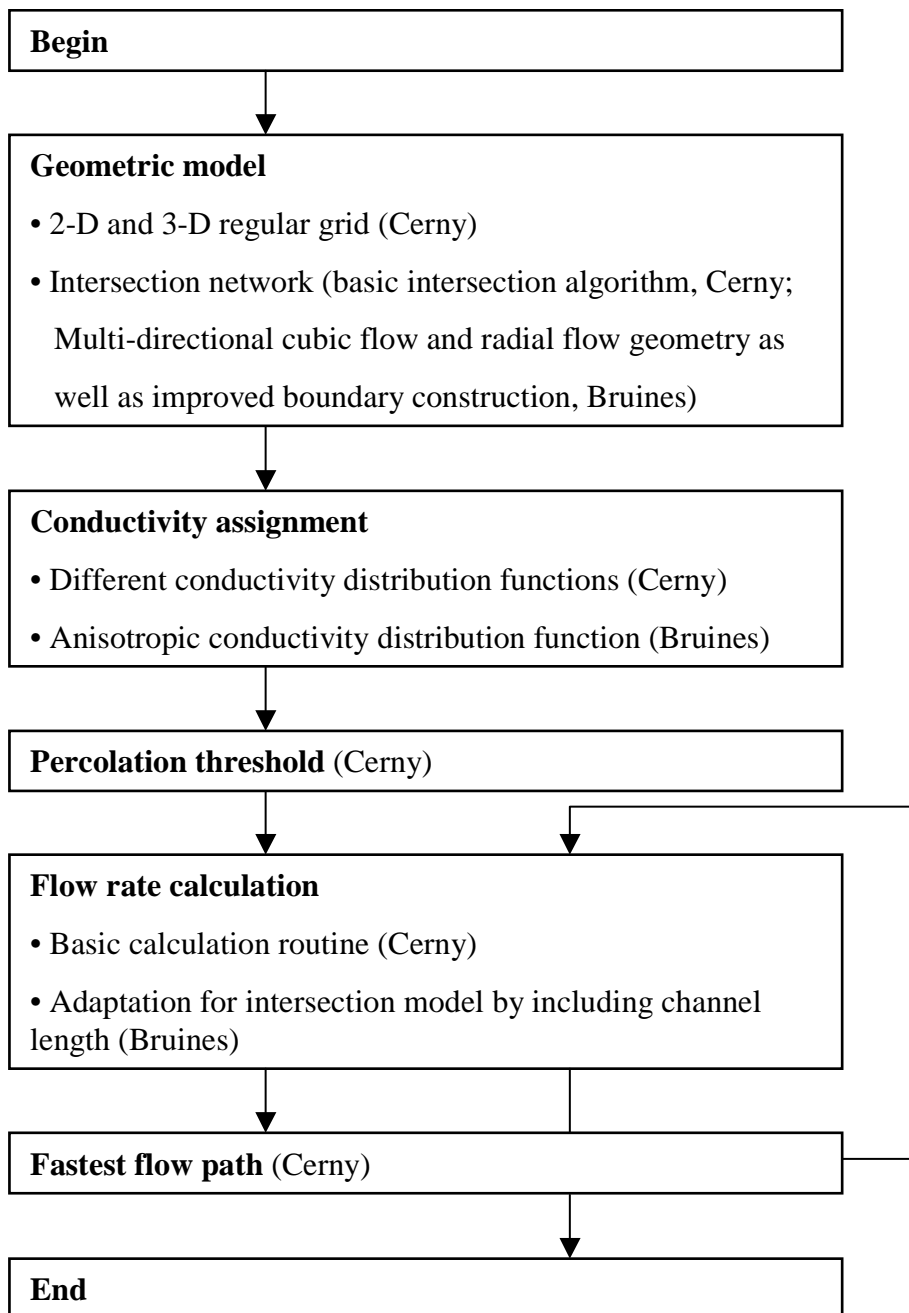


Figure 4.5 Flow chart of the CPA program. Behind each module the developer of that particular part of the code is mentioned between brackets.

To generate a certain density of fractures one can vary the number of fractures and the size of the fractures. In the CPA code the fracture sizes are assumed to be uniformly distributed between zero and a chosen maximum value. To obtain a correct density in the zone to be investigated, a larger zone has to be created for the generation of fractures. The investigation zone should then be a sub-zone of this creation zone to make sure that the densities in the middle and

at the edges of the zone are equal. The creation zone should be half the largest fracture diameter in the problem larger in each direction. This was not the case in the first version of the CPA program and has been corrected in the version used in this thesis. In the corrected CPA code the length of each side of the generation zone is twice that of the investigation zone. This means that the maximum fractures should not be larger than the area of investigation. An added problem is that in the new version 8 times (2^3) more fractures are generated than in the previous model, being an additional burden on computational efficiency. An alternative method could be to develop a fracture generation model that progressively enlarges the generation volume with increasing fracture size. This can dramatically reduce the number of fractures and allows the inclusion of larger discontinuities that, at least in the geologic reality, are of great importance.

In the CPA code the number of fracture centres in the investigation volume has to be provided as well. This is a rather difficult process since the fracture centre location cannot be determined in the field. For this, one has to decide upon a fracture shape and distribution function for the fracture radii. In this case circular fractures, along with a uniform distribution between zero and a given maximum radius are assumed (see Appendix C.7 for further explanation). The fracture lengths can be found in the field. The average area (A_{fr}) of fractures in a set of fractures with a maximum radius (r_{max}), can therefore be described in the following way:

$$A_{fr} = \frac{\int_0^{r_{max}} \pi r^2 dr}{r_{max}} = \frac{\pi}{3} r_{max}^2 \quad (4.1)$$

Assuming that the number of fractures per meter of scanline perpendicular to the fracture set is the same as the fracture area per volume, the number of fractures can then be calculated.

With this information the fractures and therefore the network can be generated. To generate a fracture, a fracture centre, a normal vector of the fracture plane as well as a fracture radius are generated. After all fractures are generated, all fractures are intersected twice. First, to find the fracture intersections, and then the fractures intersections with the fractures to find the nodes of the network. The calculation of the intersection of fractures can be computationally intense, to limit calculation time, two boxes that contain one fracture each are compared first. If the fractures are not located close to each other, the intersection algorithm is not started. (Figure 4.6)

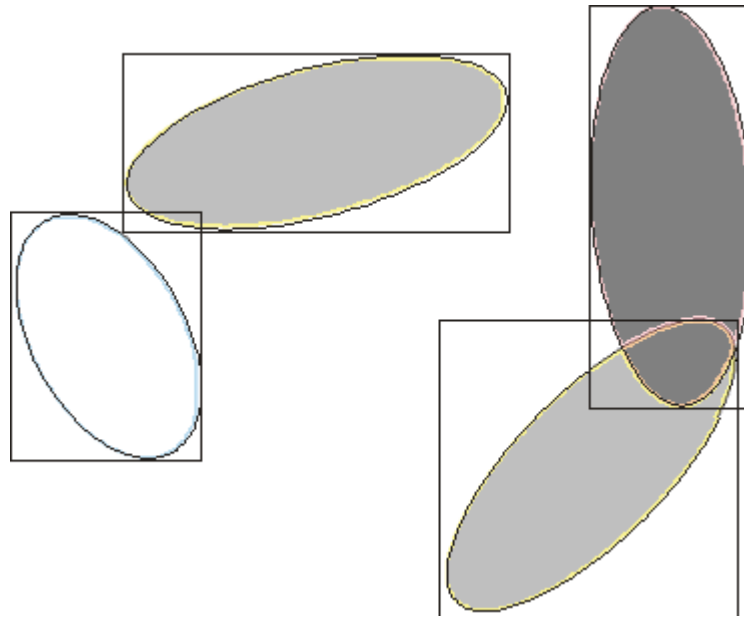


Figure 4.6 Before start of the intersection procedure a box will be placed around the fracture for easy comparison. In this case only for two intersection routine is started out of the six possible combinations.

In the original version of the CPA program, inflow and outflow points were defined as being all nodes located outside specified boundaries of the investigation volume. This meant that parts of the tubes located outside the investigation zone were also included in the flow rate calculations. To avoid this error nodes have to be constructed at the boundaries of the investigation region. To this end six additional fractures located at the faces of the unit cube are added to generate the nodes that are essential for the flow rate calculations (Figure 4.7).

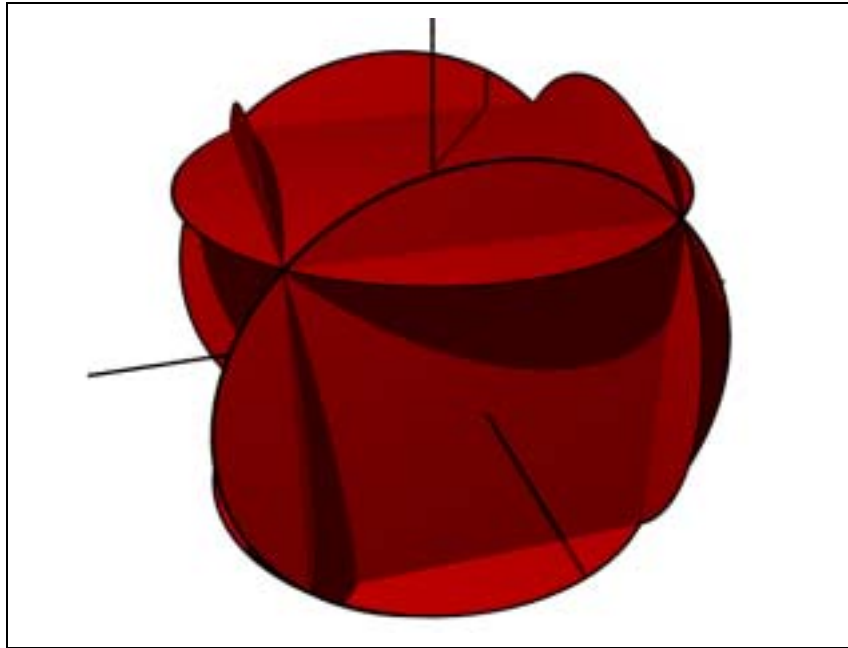


Figure 4.7 Artificial fractures used to generate boundary nodes necessary for flow rate calculations in three dimensions.

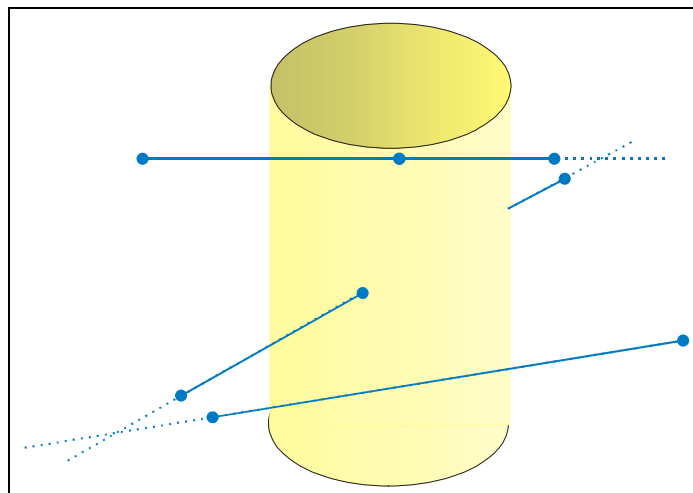


Figure 4.8 Possible intersection options for a channel intersecting a cylinder are no intersection, one intersection point, or two intersection points.

To investigate radial flow towards a borehole, a procedure to intersect cylinders with the tubular network has been added to the CPA program. Knowing the two endpoints of a tube, the associated line can be determined. By substituting the x and y coordinates in the equation for a cylinder ($x^2 + y^2 = r^2$) by the x and y coordinates of the line, described in terms of the two points, a

second order polynomial is obtained. The polynomial can be solved and gives one, two or no values that, after substitution in the equation of the line, will give the same number of points on the cylinder (Figure 4.8). Finally it has to be determined whether or not the points found are located between the two end points of the tube.

In the CPA code each of the fracture intersections has to be assigned a certain conductivity. In the first version of the CPA program the length of a section was not considered. In the current version the conductivity is independent of the length of the section, which enables it to distinguish between the properties of the intersection tube and its length. In the field the conductivity of such an intersection will depend on the geometry of the intersection. As with the aperture for fracture flow models, it is almost impossible to obtain reliable geometric data on fracture intersection from the field, so conductivities will be used instead. The assignment of conductivities to the network is performed after the generation of the network, using separate assignment functions. This allows the user to investigate the same fracture network using different distribution functions for the conductivity. In the CPA program uniform and exponential distributions are provided, user defined distributions can however be defined that use exponential, normal, Poisson, uniform, and binomial distributions. In the first version of the CPA program no distinction between the fractures can be made after they have been generated. This means that different fracture sets can no longer be distinguished and therefore no distinction can be made in fracture intersection conductivity for each set. In order to have the possibility to investigate the effect of different conductivities in different directions, an assignment function has been developed that can generate a weighted distribution for each direction in an orthogonal network. The CPA program also provides for the possibility to exclude a certain percentage of the network, by assigning conductivities of zero. This feature is important for investigating the percolation through a network.

After having constructed the network and the assignment of conductivities, calculations can be made. The CPA program first calculates the total flow rate through the model. It then deletes all fractures and restarts including the most conductive sections until percolation is reached in order to find the fastest flow path. A comparison of the flow rate in the fastest flow path with the flow rate through the entire system allows the user to see how large the influence is of the fastest flow path. In the first version of the CPA program only the conductivity was considered. In the improved version also the length of the tubes is considered, which is essential in case of flow through a network of the fracture intersection channels. By comparing the

number of channels in the system with the number that is necessary to reach percolation the program calculates a fraction that gives the user a measure of connectivity of the system.

For solving all equations for all the channels in the network a very large matrix has to be manipulated. Since many elements of the resulting matrix are zero, such a matrix is called sparse. Efficient routines are available to invert this type of matrix. For more detail on this subject the interested reader is referred to Press (2002).

The CPA program includes a graphical user interface which allows the user to change input and start routines interactively, and visualizes every step of the calculation. It allows the user to view the generated fractures, to make virtual cuts through the fracture network, visualize the channel network and every next step in the calculation of the channels network such as construction of boundary faces, the backbone and the fastest path. The CPA program can however also be used as a command line program where speed is required or with input files when for statistical purposes several stochastic realizations of a the same model are required. The different commands that can be used in the CPA program are further explained in Appendix B.

4.2.2 Joint-Okky

The Joint-Okky program has been designed by Yu (2000) and also models a fractured rock mass by means of a fracture network model. Contrarily to the fracture channel flow model considered in the CPA code, the basic assumption of the Joint-OKY program is that flow takes place through the fractures (see Figure 4.9).

The Joint-OKY program uses the centre of the fractures and the centre of the intersections of the fractures to construct its tubular network. A diameter is then assigned to each of the tubes using a distribution function. The mean and standard deviation of this function can be adjusted using an optimization algorithm. The width of the flow path through the fracture is not considered in the Joint-OKY code.

The special feature of the Joint-Okky program is that it uses optimization methods to fit the measured field data, like fracture densities and fracture permeabilities, with the model.

The basic structure of the model is as follows:

- fracture network generation,
- flow and transport calculations,
- 3D block analysis, which is of no importance for this research.

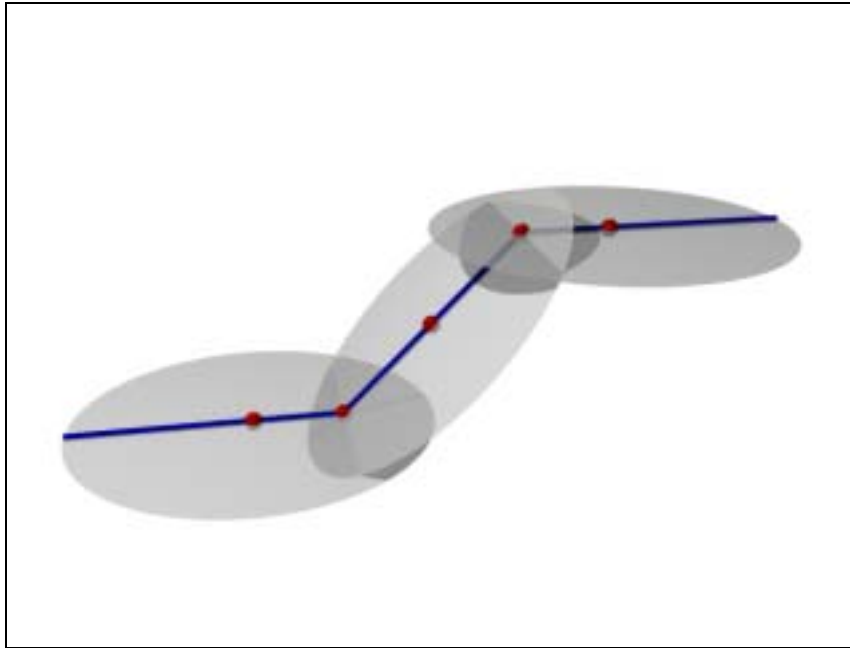


Figure 4.9 Idealization of in-fracture flow as modelled in Joint-OKY. The flowpaths connect the centres of the fractures to the centre of the fracture intersections.

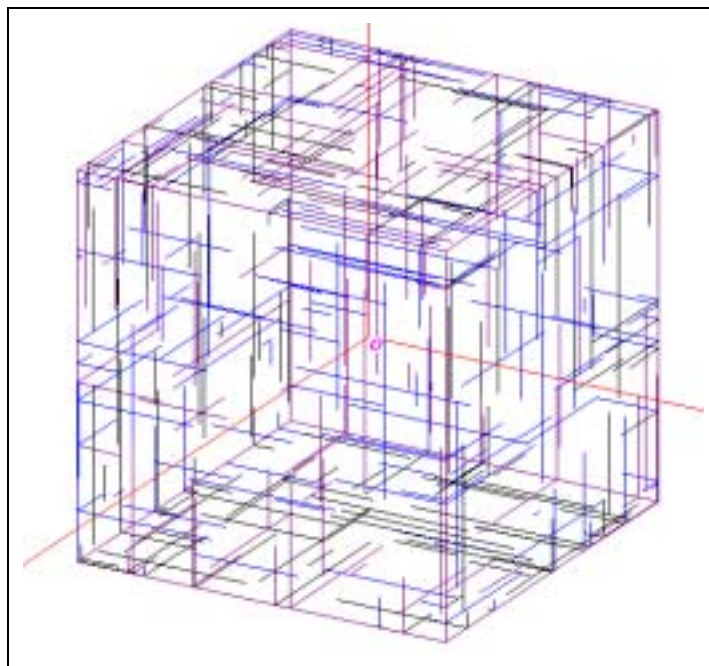


Figure 4.10 Intersections of fractures with the boundary faces in the Joint-OKY program.

To generate the fracture network different distributions of the fracture set characteristics have to be given. This includes fracture size, fracture aperture, fracture orientation, and the fracture

density. If one wants to optimise the model with field data, additional data on the area of the outcrop, the number of fractures in each fracture set mapped, orientation of the outcrop, bore-hole directions and fracture densities measured can be added so that an optimization algorithm can be used. Deterministic fractures can be added, to model for instance a large fault intersecting the problem domain. Within the fracture generation part it is possible to visualize the generated fracture network as well as the planes that delimit the problem domain.

In the flow and transport part of the program the unconnected fractures have to be removed. Fractures that have such a small diameter that they are unlikely to contribute to fracture flow can also be removed. The advantage of removing small and unconnected fractures from the problem is that calculations will be performed more efficiently. In the next step three different options are available:

- channel model,
- planar fracture model,
- channel-planar coupled model.

For this study only the channel model has been used. This channel model constructs a network model that connects the fracture centres with the centre points of the fracture intersections. The program will then calculate the flow rate through the network. The result of these calculations are saved for further investigation or use in a set of files.

4.2.3 Combination of models

To connect the two programs interfaces have been developed as part of this study. Within the CPA program a module has been made that automatically generates the file *randomfr.dat* which is the list of all the model fractures, an input file for the Joint Oky program. This makes fracture generation using the eigenvector / eigenvalue approach available to the Joint-Okky program.

It is also possible to import a network from the Joint-OKY program into the CPA code. For this purpose an auxiliary program has been written. The program needs the *head.dat*, *node_form.dat* and the *pipe_line.dat* files that are generated during the calculation of the flow rate using the channel model described in the previous section. From these data files the necessary data are extracted and a *graph* file is constructed. This file can be used in the CPA program using the “loadgraph” command and includes all the information to exactly reconstruct the geometry of the Joint-OKY model in the CPA program.

5

Application

In the previous chapter the different tools used have been introduced. In this chapter some applications of these tools will be shown. Section 5.1 describes the fieldwork performed. Section 5.2 shows the application of the CPA program. Section 5.3 shows the results of a comparison between the intersection network model and the in-fracture network model as generated by the Joint-OKY code.

5.1 Example of data gathering

Recent field observation in the Sierra Elvira, a small mountain range close to Granada, Spain, may help to explain certain flow and transport features. In this section a brief description of the most important findings are summarized. A more detailed account of the fieldwork has been included in Appendix C.

The outcrops show fossil flow channels associated with fracture intersections. The channels are clearly marked by discoloration along the fractures, which prove that at a certain time in the past fluids have circulated (Figure 5.1). Discolorations, which can attain tens of centimetres, mark the different episodes of flow. Due to the arid climate in the region the flow patterns have been preserved. Figure 5.2 shows a photo of one of the discolorations bands observed at the intersection of the bedding plane and a joint.

See Figure 5.1 on next page: View of one of the outcrops in the Sierra Elvira. The plane visible is the bedding. Fossilized flow paths are clearly visible at the intersection of joints with the bedding planes. The width of the section shown is approximately 15 meters.

See Figure 5.2 on next page: Discolorations at the intersection of bedding plane and fractures. Two episodes can be distinguished. First the brownish staining is followed by a second episode that seems to have leached minerals resulting in a much lighter colour. The width of the discoloured area is about 50cm.

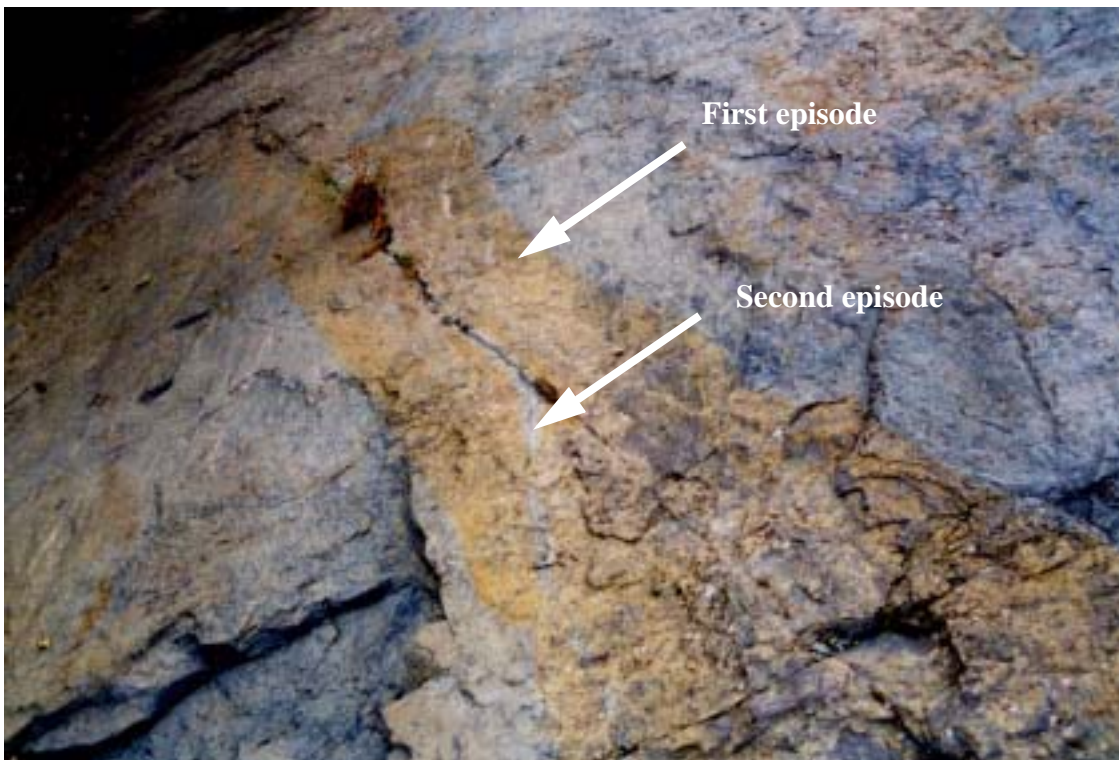


Figure 5.1 Upper photograph shows an outcrop at the Sierra Elvira.

Figure 5.2 Lower photograph show a close-up of a discoloration feature.

The calcareous formation in which the outcrops are situated is of Carixian age (upper Lias) and is a grainstone of crinoids and other bioclasts. This competent formation, which stands out in the topography, is approximately 25m thick. The primary structure is planar cross bedding, produced by the migration of mega-ripples (sandwaves).

It appears that a compressional tectonic regime in the direction SE-NW has created the AC fractures (vertical joint set with strike parallel to the main stress direction). This joint set lines up with translational faults in the area and is therefore possibly caused by shearing. Simultaneously, diagonal fractures might have developed. In a later stage of the compression, the extensional BC joints might have developed, due to the folding of the rock (joint set parallel to the fold plane). In a much later stage the area to the southeast subsided and a normal fault developed. Still ongoing subsidence is also observed in the SW, possibly causing new AC and BC joints smaller in size than the original ones. A reactivation of the original AC and BC joints is also likely. The stylolitic surfaces as seen at some of the bedding planes and joints are a proof that pressure solution and compression must have taken place. It is suspected that geothermal liquids circulated through the fracture network.

Joint surveys were carried out at four outcrops of the Sierra Elvira. The fieldwork focused on recording the channelled flow features along joint intersections. The orientations of the fracture sets were measured and are presented in a Schmidt net. Furthermore, an Eigenvector-analysis was carried to characterise the directional data of the fractures and the fracture intersections (Table 5.1).

		Eigenvectors and values (%) of poles		
	number of fractures	1	2	3
Bedding B	30	112/56; 99.6%	278/33; 0.3%	012/06; 0.1%
AC and Faults	43	190/10; 93.2%	055/76; 4.5%	282/10; 2.3%
BC	38	287/24; 94.4%	018/04; 4.3%	116/65; 1.3%
D1	11	255/03; 84.5%	001/79; 12%	164/10; 3.5%
AC/Bedding	37	285/32; 94.8%	017/02; 4.9%	110/58; 0.3%
BC/Bedding	16	018/06; 92.0%	283/35; 7.3%	116/54; 0.7%
D1/Bedding	20	353/18; 97.0%	257/16; 2.7%	128/65; 0.3%
D2/Bedding	6	220/12; 99.1%	314/21; 0.6%	102/66; 0.2%

Table 5.1 Directional statistics of the outcrops 1, 2 and 3.

Furthermore, the fracture spacing was recorded. Special attention has been given to fractures that are associated with channelled flow.

	No. of fractures (all / with channels)	Mean of all fractures	Standard devia- tion of all fractures	Mean of frac- tures with channel	Standard deviation of fractures with channel
AC joints	62 / 24	0.99	1.01	1.57	1.44
BC joints	93 / 34	0.44	0.73	1.05	1.62
D1 joints	28 / 20	1.41	2.06	1.82	2.32
D2 joints	10 / 10	0.88	1.14	0.88	1.14

Table 5.2 Statistics of the fracture spacing [m].

The length of the fracture traces are characteristically between 0.7 and 40-plus meters. About half the measured trace lengths extended beyond the borders of the outcrops. For these joints, a minimum length was recorded. The fact that half of the fractures extend beyond the borders of the outcrop and that there were a small number of fractures, made it impossible to obtain a correct trace-length distribution function. Due to the lack of better data the simplest distribution function, a uniform distribution function, has been used. Forty meters is about the distance between the faults that divide the outcrops in homogeneous areas and is thus a logical upper limit for the size of the fractures.

The recorded apertures of the discontinuities were up to 25 cm wide for the AC joints with large spacing (10-20 m), decreasing considerably with decreasing spacing. Most of the other fractures are either closed or show apertures smaller than 1 mm. The majority of the fractures are filled with calcite or residual soils.

In order to characterise the connectivity, the termination of fractures was recorded. Terminations are indicated with the letters A for abutting, B for blind, C for crossing, and D for diffuse. C fracture terminations are fracture-endings that extended beyond the boundaries of the outcrop and crossed other fractures. Characterising fracture-endings yields additional information on the fracturing history. Abutting fractures must have been developed later than the fracture on which they terminate. Active diffuse connections have not been found on the outcrops and blind fracture-endings are rare.

	AC (44)	BC (53)	D1 (12)
A	64%	38%	0%
B	2%	0%	33%
C	34%	62%	67%

Table 5.3 Termination statistics

The joint statistics from the fieldwork was used as input to model and simulate tubular migration paths, as discussed in the next chapter.

5.2 Application of the Critical Path Analysis program

To verify the CPA code a number of models have been generated to increase the confidence in the CPA code. The first tests were directed towards the modelling of a known fracture network to check the correct reconstruction.

In section 5.2.1 the CPA code has been fed with the data from the fieldwork in Granada and the results of the model were compared with field observations. The data from Spain only includes geometric data. No groundwater tests have been carried out.

To better understand how the tubular networks react, sensitivity analyses were conducted, which are covered in section 5.2.2 and following section. The sensitivity analyses focused on the following parameters in the CPA code: fracture density, problem domain size, randomness, fracture size and channel conductivity. The CPA program used for the sensitivity analyses, calculates the total flow rate through a standard cube in the x, y and z direction (Figure 5.3). This simulates flow similar to that observed in nature where groundwater flows in one direction due to a regional gradient or for instance underneath a large dam. Also a cylindrical model (Figure 5.4), where water flows radially towards the centre of the model, mimicking a pumping test, has been implemented. Additionally the flow rate of the fastest path was determined for each direction. In the case of the parallel flow through the cube, constant heads are applied to two opposing faces. All other faces are treated as no-flow boundaries. At the radial flow configuration constant heads are applied to the inner and outer cylindrical surfaces. No-flow boundaries are applied at the top and bottom. In both cases a unit head difference is assumed.

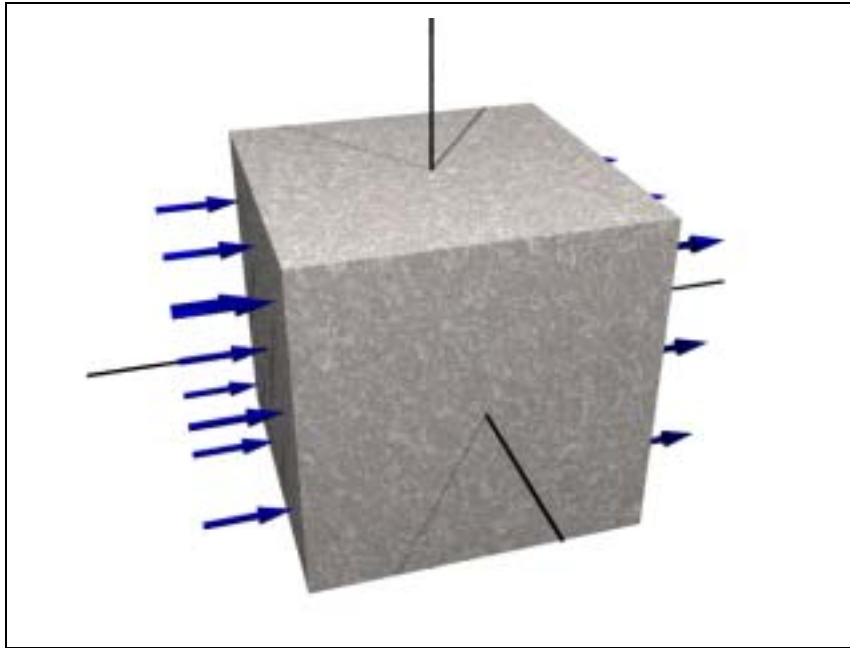


Figure 5.3 Flow rates through a cube are calculated using a fractured rockmass with unit dimensions (1x1x1). The flow rate is calculated in the three directions.

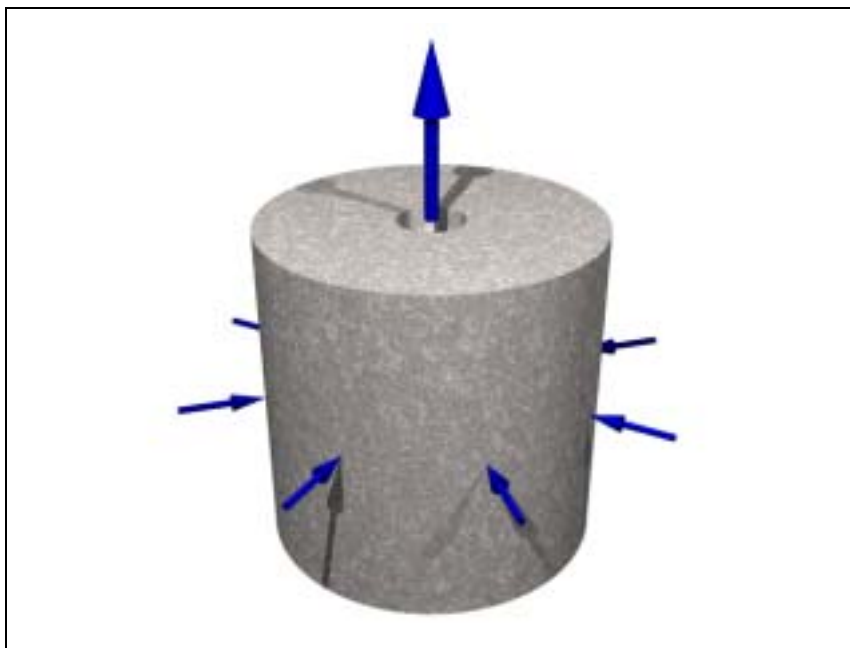


Figure 5.4 Radial flow rates are calculated by flow through a cylinder with an outer diameter of 1 and an inner diameter of 0.2 and simulates flow towards a borehole during groundwater testing or flow towards a shaft.

The CPA program uses normalized values for the size of the cube, the hydraulic head and the conductivities. To explain in more detail the variables in the CPA code a simple model with one single channel is presented here. The flow will be assumed to take place through a single channel with a diameter of 2 mm and a length of 1 m. The hydraulic head is 0.01 m, resulting in a gradient of 0.01 what in geological terms is very high. For laminar flow through a tube the Hagen-Poiseuille law applies.

$$Q_{tube} = \frac{\pi d^4 \gamma}{128 \mu} \cdot \frac{h_L}{l} = C_{tube} \cdot \frac{h_L}{l} \quad (5.1)$$

with Q_{tube} = volumetric flow rate through a single tube [m^3/s], d = tube diameter [m], γ = unit weight [N/m^3], μ = dynamic viscosity [Ns/m^2], h_L = hydraulic head [m], l = length of channel [m] and C_{tube} = tube (or channel) conductivity as used in CPA [m^3/s]. Inserting the values as mentioned above and assuming water at room temperature ($\mu = 1.00 \times 10^{-3} Ns/m^2$, $\gamma = 9.81 \times 10^3 N/m^3$) leads to a C_{tube} of $3.85 \times 10^{-5} m^3/s$. With a gradient of 0.01 this would lead to a flow rate of $3.85 \times 10^{-8} m^3/s$ (0.139 litre/hour). If a rock mass has one such channel per m^2 an equivalent hydraulic conductivity can be determined ($K = 3.85 \times 10^{-6} m/s$). The linear groundwater velocity through the channel would however be 0.0123 m/s. The linear groundwater velocity of a similar porous rock assuming for instance a 1% flow porosity, a reasonable assumption for igneous rock masses, would be $3.85 \times 10^{-6} m/s$. This simple calculation shows that channel flow therefore has a large influence on the fate of contaminant. Knowing the velocity through a channel, the Reynolds number (R) can be determined.

$$R = \frac{\rho v d}{\mu} \quad (5.2)$$

where ρ = the density of the fluid [kg/m^3] and v = velocity. The Reynolds number for this example is 24.6, which is well within the laminar flow region ($R < 2200$).

5.2.1 Network generation

The discrete fracture network generation model of the CPA program introduced in chapter 4 aims at realistically reproducing flow and transport channels, also called tubes, at the intersection of discontinuities, based on simple field measurements and joint surveys. After generating the fracture intersection network, conductivities are assigned and the flow rate calculations are

performed in the different directions. To obtain reliable results from the CPA program it is essential that the geometric model of the network generated corresponds with the fracture network observed in the field. Section 5.1 described the findings of the fieldwork in Granada, Spain. The data obtained during this fieldwork have been used to check whether or not a fracture network developed by the CPA program resembles that in the field.

The CPA program creates a three-dimensional network of discs. To accomplish this task the following data are needed for each fracture family: Number of fractures to be included in the standard box, dip direction and dip angle, the radii of the fractures. At the outcrops, five fracture sets were visible but since only four can be described statistically and the fifth fracture set (diagonal joints) is almost totally tight, only four fracture sets have been used. The input file used for generating the fracture network is given in table 4.1. An example of the fractures generated by the CPA code is given in Figure 5.5. The large discs coincide with the bedding planes at the site, the two perpendicular sets of discs with the BC and AC joints. As in the real outcrops there are rather few D1 joints (almost parallel to the BC joints).

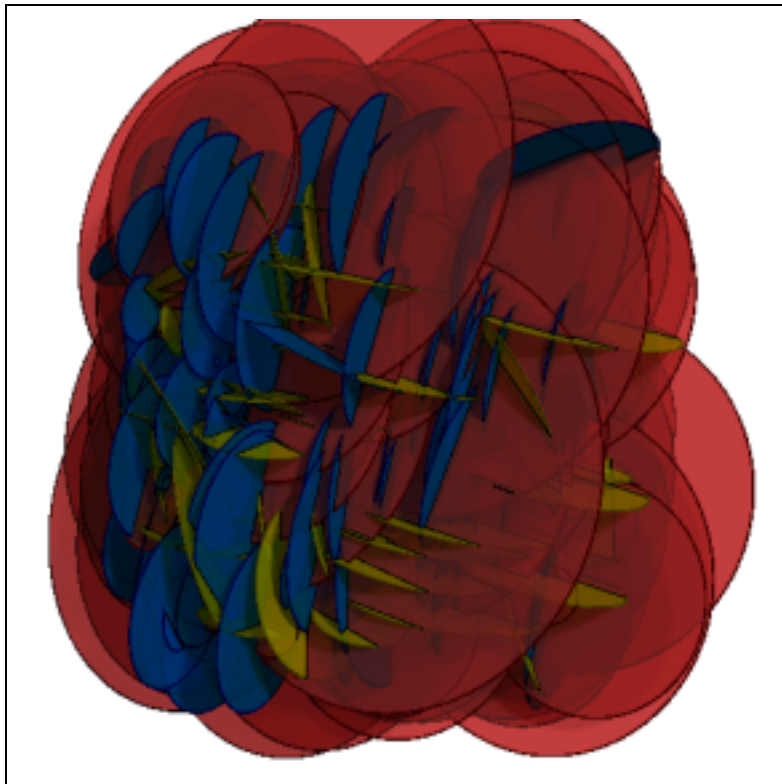


Figure 5.5 A realisation generated with CPA using the directional data from the Spain fieldwork. The view is from above. The different fracture sets can be distinguished.

From the fractures, the CPA program calculates the intersections of the discs, the fracture channels or tubes. The resulting tubular network can be visualized in the CPA program as well. Within this network many unconnected tubes are present. These unconnected tubes are deleted and the boundary nodes are determined (Figure 5.6). Two artificial nodes are added and connected with the boundary nodes. Tubes that are not connected to both the source and the goal node, i.e. inflow and outflow boundary, are deleted. The remaining network is called the backbone (Figure 5.7). Only through this part of the original network flow does take place. By “switching off” all tubes and later adding each of them starting with the most conductive, the fastest path is obtained, the moment percolation is reached (Figure 5.8).

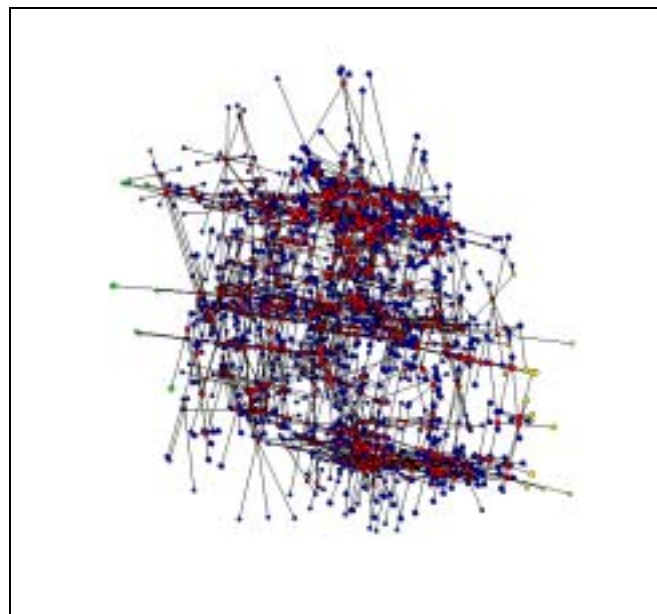


Figure 5.6 Model fracture intersections constructed with the data from Spain fieldwork. Only channels that are connected to other channels are shown.

the outcrops at the fieldwork location near Granada. This rock face, parallel to the AC joints in the area, was too steep to be investigated but the picture clearly shows the bedding planes and at least one perpendicular fracture set. Figure 5.10 shows a virtual cut through the modelled fractures.



Figure 5.9 Photo of an outcrop in the investigated area near Granada, Spain.

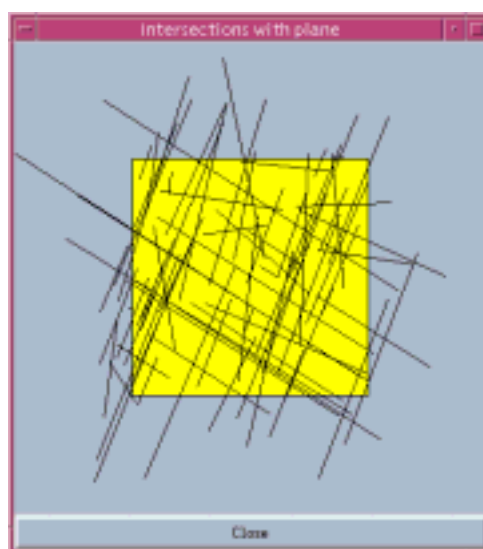


Figure 5.10 Virtual cut through model, parallel to the outcrop shown in previous Figure 5.9.

A stochastic realisation of fracture locations can never reproduce the locations of the fractures in the field exactly. Never the less a comparison of this and other virtual cuts with available photos of the fieldwork area gave similar good matches.

Finally one more tool for verifying the match between model and reality is available. The CPA program records the normal vectors of all generated fractures, which can be visualized in a Schmidt-net (Figure 5.11).

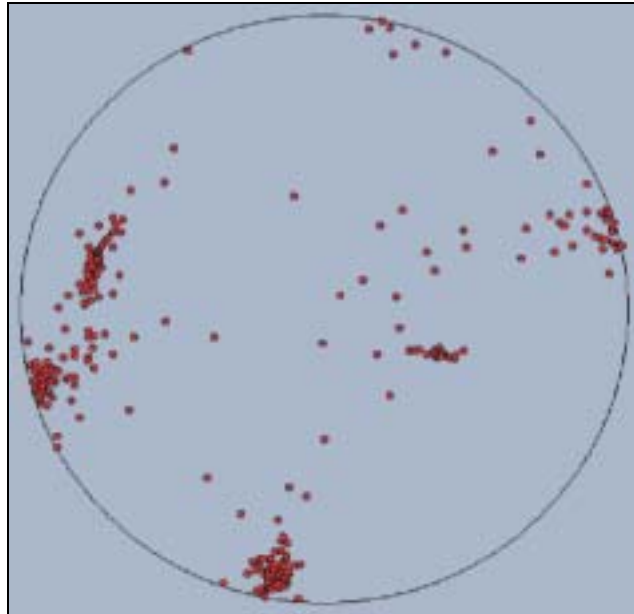


Figure 5.11 Stereo-graphic projection of all fractures generated of a realization using the orientational data from the Spain outcrops.

5.2.2 Sensitivity analysis with changing fracture density

Since the fracture density is likely to be of great importance for the total flow, this parameter has been varied for the calculation of the flow rate through a unit cube. Ten different model-realizations of eight models with different fracture densities have been generated and investigated. In these models the fractures are orientated at random. The fracture radii are assumed to be uniformly distributed between 0 and 0.5. The conductivities of the channels are uniformly distributed between 0 and 1. The eight different models have 25, 50, 75, 100, 125, 150, 175 and 200 fracture centres per unit volume. Including more fractures resulted in a model that was too large for the program to handle. This is not so surprising since the model with 200 fractures already generates networks with more than 100,000 nodes and almost 200,000 tubes (Table 5.4).

fractures	nodes	tubes	file size / kb
25	1200	1000	66
50	5100	5800	300
75	11200	14500	750
100	20300	29600	1470
125	34500	53500	2600
150	50400	93000	4400
175	74000	127800	6000
200	107200	194600	9000

Table 5.4 Average number of nodes, number of tubes and file size of ten model-realizations with different fracture densities.

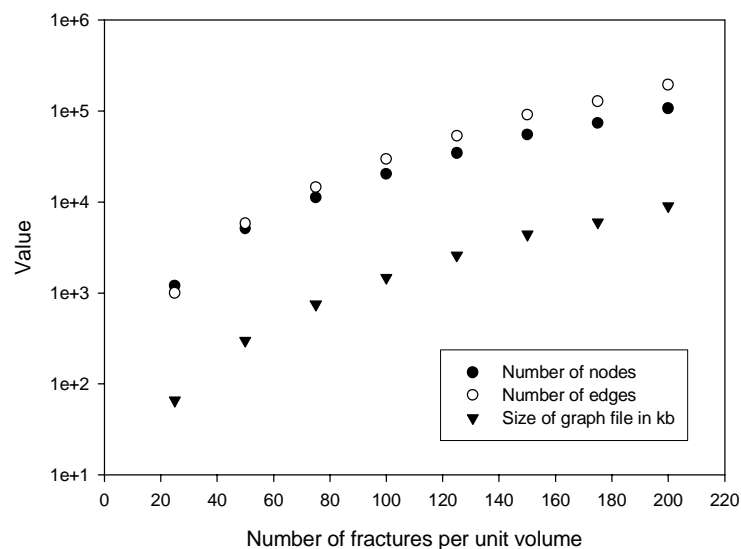


Figure 5.12 Semi-logarithmic plot of the number of nodes, number of tubes and the files sizes. An exponential increase of the tubular network can be observed.

In the *25 fracture model* only in one of the ten cases and then only in one direction, percolation is reached, which means that for 25 fractures the network is not percolating. In the *50 fracture model*, exactly half of the model-realizations reach percolation in parallel flow tests, which means that this model probably is at the percolation threshold. For the *75 fracture model* only 17% of the parallel flow rate calculations did not reach percolation. All other model-realizations

do reach percolation so that a flow rate can be determined. Figure 5.13 shows that with increasing number of fractures, the number of connected fractures increases, since the ratio between tubes and nodes increases.

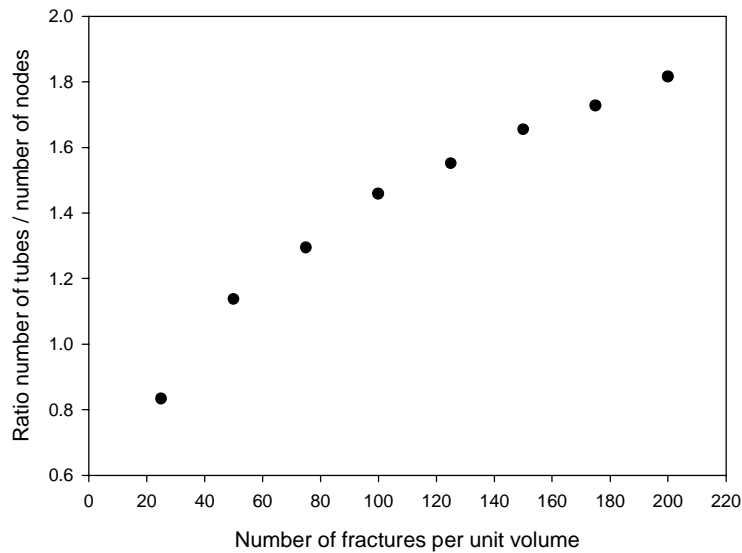


Figure 5.13 Ratio of the number of tubes and the number of nodes plotted against the number of fractures. An increase of fractures leads to a better connected systems with less nodes located at dead ends.

number of fractures	x-direction		y-direction		z-direction		radial	
	total flow rate	fastest path	total flow rate	fastest path	total flow rate	fastest path	total flow rate	fastest path
25	0	0	0	0	0.0513	0.0382	0.3114	0.0972
50	0.4921	0.1535	0.3455	0.1203	0.3970	0.1206	9.6000	1.1297
75	2.5801	0.2541	2.5680	0.2460	2.4294	0.2698	27.840	0.9442
100	9.5156	0.3034	9.8520	0.2553	8.7289	0.2879	78.315	0.8539
125	20.670	0.3176	18.369	0.2744	18.042	0.2973	120.23	0.8213
150	33.871	0.2820	34.115	0.2556	32.852	0.2668	201.02	1.3803
175	48.865	0.2827	48.329	0.2531	51.281	0.2770	286.28	0.8839
200	77.272	0.2458	76.088	0.2731	77.717	0.2761	452.51	1.1160

Table 5.5 The average results of the ten model-realizations for the different fracture density models. Recorded is the total flow rate and the flow rate of the fastest path.

The results of the calculations are summarized in Table 5.5, that shows the average flow rate of ten model-realizations for each direction and model.

Plotting the flow rate for each model against the number of fractures shows an ever increasing flow rate with an increasing number of fractures. On a semi-logarithmic plot, two distinct parts can be seen (Figure 5.14). In the part where the network does not always reach percolation, the curve is not straight. From the moment however that most networks reach percolation (100+ fractures) the flow rate follows a straight line. The parallel and radial flow rate curves show approximately the same gradient.

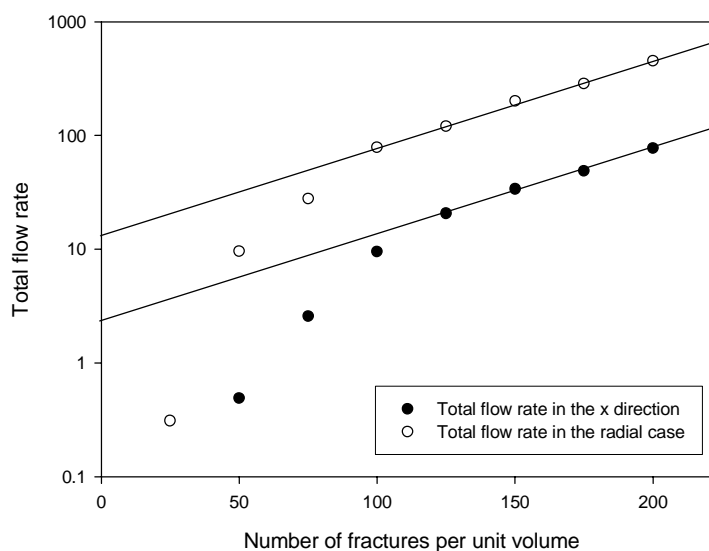


Figure 5.14 Semi-logarithmic plot of total flow rate against the number of fractures.

The total radial flow rate is about 6 times higher than the total flow rate in any of the x-, y- or z-directions (difference between the two lines in Figure 5.14). For the fastest path, the radial flow rate is about 3.7 times higher than in the case of parallel flow. From the Dupuit relation a ratio of 3.9 ($2\pi / (\ln 0.5 - \ln 0.1) = 3.9$) for the total flow case and 2.5 ($1.0 / 0.4$) in case of the fastest path flow rate is expected. The difference between the theoretical and the calculated values has to be explained.

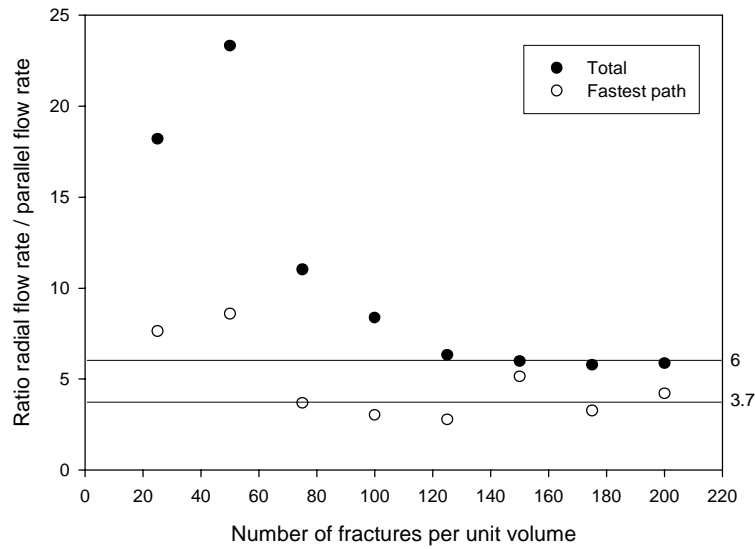


Figure 5.15 Ratio of radial flow rate and parallel flow rate for total flow rate (solid points) and the flow rate of the fastest path (open points).

One possible explanation could be the assumption of no flow boundaries on the faces parallel to the direction of the gradient. This means that the effective aquifer thickness is more reduced in the parallel flow case than in the radial flow case. But the most influential effect will be that of the dead end fracture channels. In the case of parallel flow, channels have to cross the entire unit cube whereas in the radial flow case a conductive feature needs to cross only 40% of the unit length.

The flow rates of the fastest paths are in the order of 0.25 to 0.30 for the parallel flow situation. To make a comparison, a model with only one channel is made. When assigning a random conductivity between 0 and 1 the average conductivity will be 0.5. The fastest path of the model with 200 fractures per unit area however, is built up of 95 single tubes on average. Splitting the single direct tube up in the same number of parts and assigning the same random conductivities results in an average conductivity of the system of approximately 0.160 whereas the average conductivity of the fastest path is 0.245. This means that the fastest path is at least 50% more conductive. The tortuosity of the flow paths however could not be considered in this case, since the total length of the fastest flowpath was not recorded. This would however only make the difference larger.

The following conclusions can be drawn:

- The model is very sensitive to the number of fractures per unit volume used. With a low number of fractures, in this case less than 100 fractures, the model can be either percolating or not.
- With increasing fracture density the amount of connected intersections will increase dramatically. On a semi-logarithmic plot this shows as a straight line, suggesting an exponential increase. However models with more fractures could not be generated with the available hardware so that the exact development is not known. To investigate models with higher densities, certain assumptions can be made to simplify the model. This can be achieved for instance by neglecting smaller fractures and low conductivity flow features.
- The Dupuit equation for the radial flow case shows that the total flow rate in a homogeneous porous medium is 3.9 times larger than for the parallel flow case. It can however be observed that in the modelled fissured medium the radial flow rate is in general much higher than expected. There are two causes likely to explain this phenomenon: First, in a network some tubes will not be connected or are dead-ends. With smaller distance between in- and outflow, such as in the case of radial flow, the effect will be reduced. With an increase of fractures, less dead-ends will exist also reducing the effect. Secondly, in defining the faces parallel to the direction of flow as no-flow boundaries, flow near these faces will be obstructed. This zone of artificially reduced flow will be of more influence in the parallel flow case for the same reasons as mentioned above. The investigated fracture system can therefore not be regarded as an equivalent porous medium.

5.2.3 Sensitivity analysis with changing modelling domain size

As has been pointed out in chapter 2, the availability and the size of a Representative Elementary Volume (REV) is of great importance in fractured rock mass flow modelling. A REV can however be difficult to determine. To study the influence of the size of the investigated region on the total flow rate through a tubular network calculated in one model-realization the following experiment has been conducted. The size of the fracture network has been gradually increased, starting with a model including 100 fracture centres within the unit cube, where each fracture is randomly orientated and a radius uniformly distributed between 0 and 0.5, and finishing with a model that has 800 fracture centres (Figure 5.16). The program does not easily allow for an increase of the model volume, so that the increase of the model volume has been

simulated by decreasing the fracture size while simultaneously increasing the number of fractures (Table 5.6).

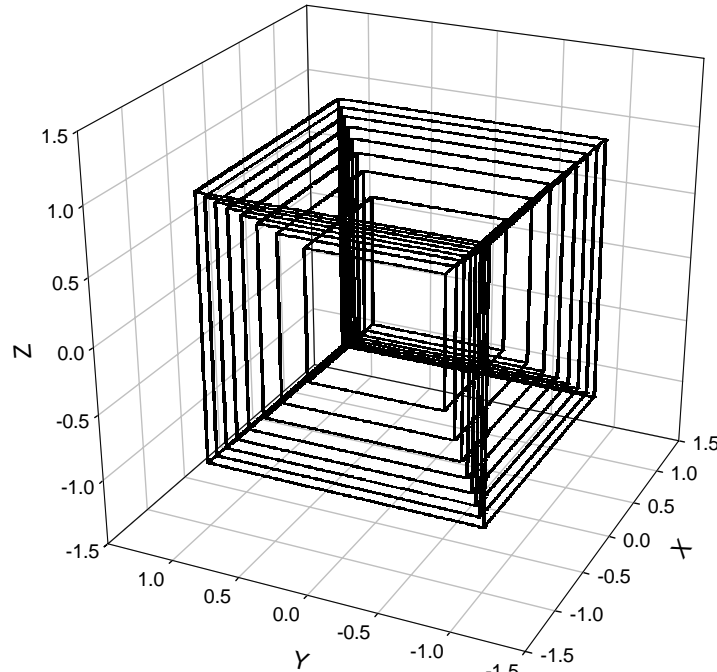


Figure 5.16 Showing the sizes of the different equivalent cubes used in the calculations.

number of fractures	equivalent fracture model size
100	1.000000
200	1.259921
300	1.442250
400	1.587401
500	1.709976
600	1.817121
700	1.912931
800	2.000000

Table 5.6 Conversion table showing the equivalent model length for the number of fractures added to the unit cube.

Of each of the eight models ten model-realizations were generated. Conductivities of the tubes are uniformly distributed between 0 and 1. The calculated flow rates were then divided by the

equivalent model size squared (flow through area) to make the results comparable. Of these ten model-realizations the average, the standard deviation and the coefficient of variation of the flow rate were determined. The results are plotted in Figures 5.17 and 5.18.

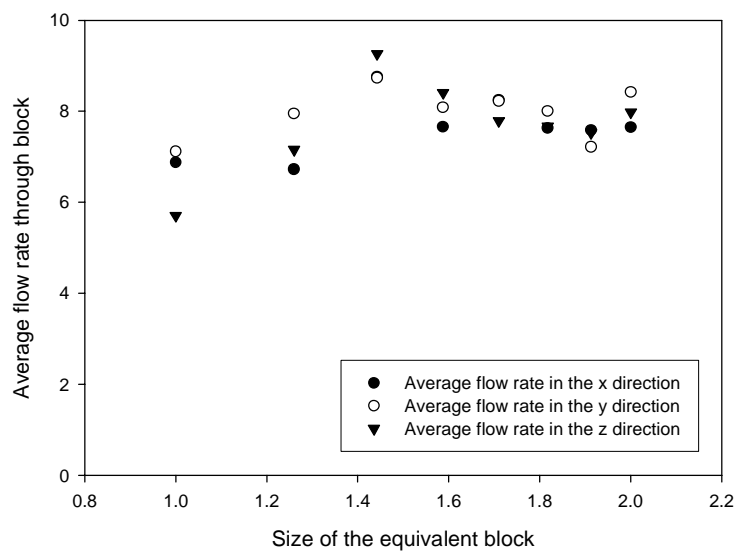


Figure 5.17 Average flow rates of the parallel flow simulations.

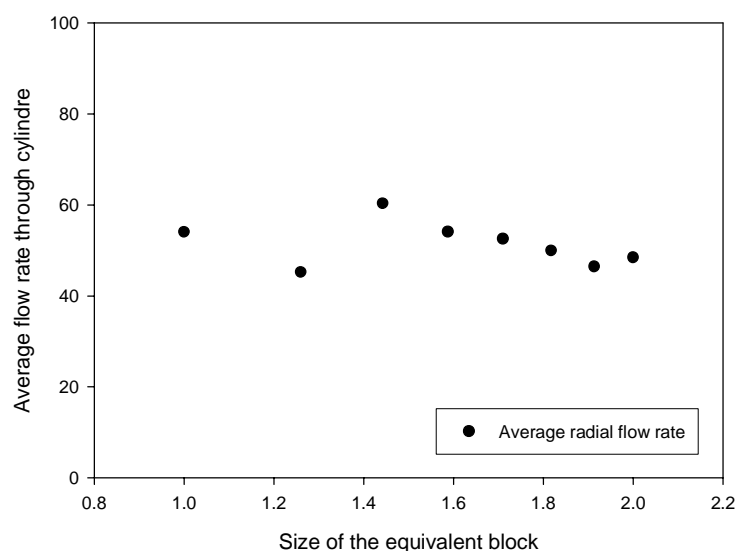


Figure 5.18 Average flow rates of the radial flow simulations.

The average conductivities of the different models seem to be relatively constant as expected (Figure 5.18). With reduced block size the fluctuation in the results should be higher. The fluctuation between the four smallest models seems indeed to be higher, but for a statistically significant statement the number of observations is too small.

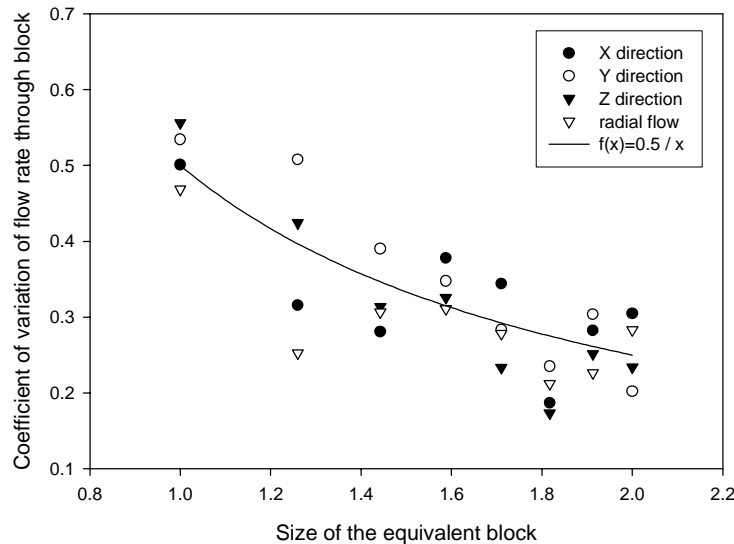


Figure 5.19 Coefficient of variation of flow rates against model size.

The plot of the coefficients of variation vs the model size (Figure 5.19) shows a clear decrease with increasing model size for flow rate in all directions. With a doubling of the block size the measured coefficient of variation is halved. The coefficient of variation seems to be inversely proportional to the size of the block under investigation. It is however difficult to further examine this relation, since a larger model can not be calculated with the available computer hardware and also a further reduction of the model is difficult because of issues related to the influence of fractures that are located with their centres outside the area of investigation.

The following conclusions can be drawn:

- The size of the problem domain has a clear influence on the spread of the calculated total flow rate through the system. How large a volume is needed to make sure flow rates calculated will be within a given error margin will depend on the fracture geometry. In the investigated system, the coefficient of variation of the resulting total flow rate was reduced by half by doubling the side-lengths of the investigated cube (8 times the vol-

ume). A significant change in the average flow rate per unit area with increasing domain size could not be observed.

- The use of a three-dimensional approach is more realistic when modelling a fractured rockmass, but these calculations show that with increasing model sizes, the limits of the computer used are soon reached. Other strategies are needed to reduce model size. It might be advantageous to disregard smaller fractures or to adapt the fracture generation procedure. A stepped generation algorithm would make it possible to reduce the generation volume for smaller fracture, greatly reducing the number of fractures within a model.

5.2.4 Sensitivity analysis to the randomness of geometry and conductivity distribution

An orthogonal fracture system will be the model of reference in the next few sections. Fractured rocks, especially those of sedimentary composition, often show three orthogonal fracture sets, where the first set is usually formed by the bedding planes. Two joint sets often develop in orthogonal directions to the bedding planes and to each other. The fieldwork area in Spain was of this type as well as the outcrop at the quarry for the second runway of Kansai International Airport.

For the following experiments three orthogonal fracture sets with each 100 fracture centres per unit cube and uniformly distributed fractures radii between 0 and 0.3 were generated. In total 10 different model-realizations of the geometry have been generated, which will form the basis for the investigations. This model will be used as a reference in the following section and will be referred to as model *orIII*. In four out of these ten models, percolation was not reached in one of the three directions (13.3%).

In a first test with these generations, new conductivities were generated using the “modgraph” command. The initial tests were carried out using constant conductivities. As expected, dividing the conductivities of all tubes by two, led to exactly half the total flow rate calculated by the CPA program. With a uniform distribution between 0 and 1 for the conductivities where the average conductivity of all channels is also 0.5, however, the results were different. If the total flow rate associated with such a distribution is compared with that of a constant conductivity of 1 for all channels, it shows that the total flow rate is only about 0.378 times the flow rate. This indicates that the flow through the least conductive channels in this model reduces the total flow rate. In the following sections *orIIIv* will be used to denote the model

with uniformly distributed conductivities between 0 and 1 and *orIIIc* for constant conductivities of 1.

In a next experiment, 5 model-realizations for each of the 10 orthogonal graphs have been generated, in order to investigate the spread in results due to the change in geometry and change in conductivities. The scatter, as a result of the network generation, is about 4 times larger than that due to an other model-realization of the same conductivity distribution function (Figure 5.20). Tests with exponential distribution functions on the same models gave similar results.

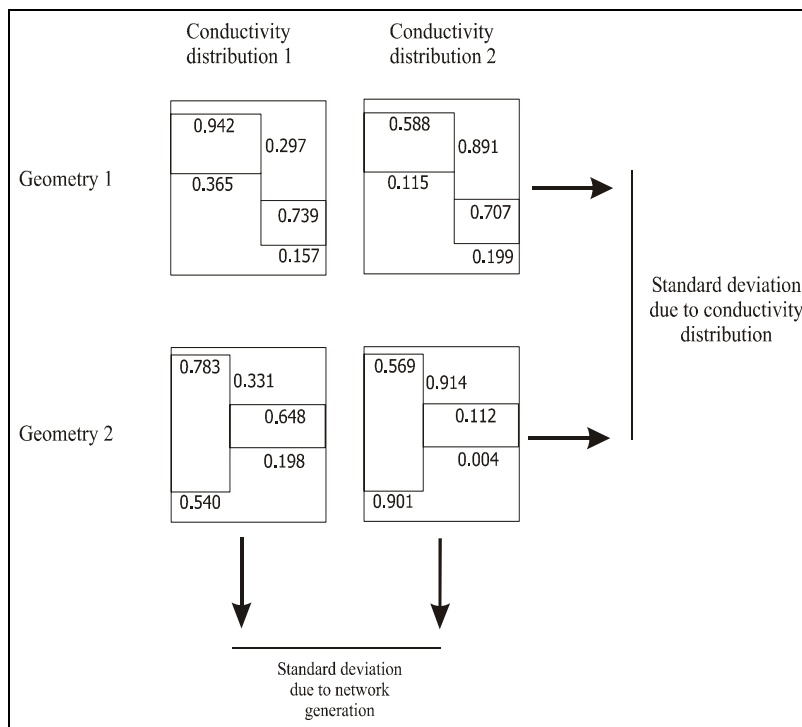


Figure 5.20 Flow rates calculated with the same networks but with different realizations of the same conductivity distribution function, as indicated by the random numbers, result in a certain amount of scatter (horizontal). Flow rates of different network geometries will however result in more scatter (vertical).

The following conclusion can be drawn:

- When generating a model using known statistical information of a rockmass, much of the variance will be intrinsic to the geometry of the model and not so much due to the generation of the conductivities. In the case of the generated models presented above, the variation due to the geometry variation was 4 times larger than that due to the variation within

the conductivities. This might change with a distribution function where a few large flow features might dominate flow.

- These results indicate that it would be beneficial to get deterministic data from the site under consideration and introduce these data into the model to reduce variation. The Joint-OKY program is one of the rare programs that can incorporate such knowledge.

5.2.5 Sensitivity analysis of an orthogonal system with changing fracture density

Although fracture systems are often orthogonal, the fractures will generally not be equally spaced in all directions. In certain geological situations one can imagine that the density of fractures in one or two directions is higher. To simulate this, different models have been generated, taking model *or111v* (see section 5.2.4) as reference. Fractures in all models have radii uniformly distributed between 0 and 0.3 and the conductivities are variable between 0 and 1. The models *or112* and *or121* have 200 instead of 100 fractures in the direction perpendicular to respectively the x- and the y-axis (Figure 5.21).

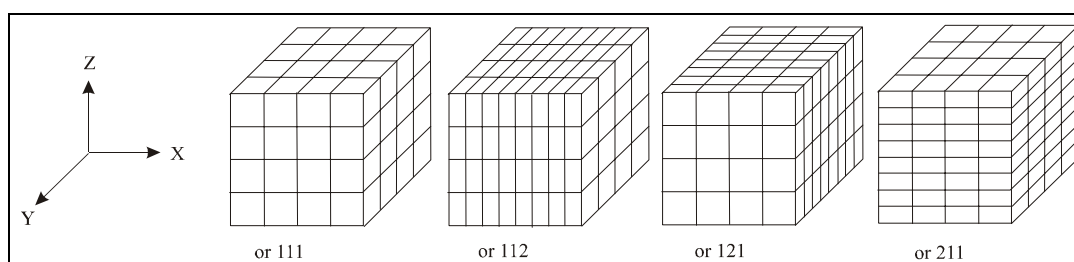


Figure 5.21 Schematic drawing of the models *or111*, *or112*, *or121*, *or211*.

This means that the network includes about twice as much tube length in the y and z direction in the case of model *or112*, and in the x and z direction for *or121*. These models would correspond with a geological situation where a vertical joint set shows significantly more fractures. Model *or211* has twice the number of horizontal fractures. This could correspond for instance with a sedimentary formation with closely spaced bedding planes. Model *or221* corresponds with a formation where a vertical fracture set shows a lower fracture density. In this case the blocks formed at such a site would be elongated. Finally *or222* has been developed to see how twice as many fractures would influence the total flow rate. As with previous tests, ten model-realizations of each model have been produced and the results averaged. The results are summarized in Table 5.7.

Model	x	y	z	radial
or111v	1.216534	1.198744	1.264027	21.34862
or112	4.417078	<u>6.567733</u>	<u>6.310681</u>	53.00559
or121	<u>4.990917</u>	5.417522	<u>4.650242</u>	51.15156
or211	<u>6.425033</u>	<u>8.026893</u>	7.536683	68.00469
or221	14.09789	13.442228	14.87693	100.17447
or222	40.51982	51.74959	56.66479	292.5078

Table 5.7 Average flow rate calculations of ten model-realizations for models with different fracture densities in orthogonal fracture sets.

It can be clearly seen that the increase of the number of fractures in only one direction has a large influence on the flow rate in all directions. In the case of model *or112*, for instance, we can see that the total flow rate in the x-direction has almost quadrupled even though the number of fractures with their plane parallel to that direction has not increased. It is possible, that due to the increased number of orthogonal fractures, previously dead-end channels, can become connected. The flow rate in the other two directions has even increased by a factor six. The radial flow rate has increased by only 2.5 times. Model *or121* shows the same behaviour as *or112* with the difference that the y-direction, which should show the lowest flow rate, actually shows the highest value. However, the radial flow rate is the same as in model *or112*. Model *or211* shows a behaviour similar to that of model *or121*, with the difference that in this case the radial flow rate is higher. This is because the increase of conductive features are orientated in the direction of flow of the radial flow simulation. The somewhat higher value of the z-direction flow rate suggests that this might be due to the random generation of geometries and conductivities.

With most tubes orientated in the x-direction, model *or221* should have a preference for the x-direction but no significant differences in the calculated flow rates are apparent. The values are about twice as high as the previous models.

Model *or222* should be symmetric in behaviour, but the flow rate in the x-direction is 20% lower than in the y- and z-directions. The parallel flow rate values are approximately 40 times larger than those of the *or111* model, whereas the radial flow rate increased only with a factor 14.

The following conclusions can be drawn:

- What influence has a fracture set with a considerably larger fracture density? The results show that, as has been shown in section 5.2.2 with the random fracture models, the system is sensitive to the amount of fractures. The direction of the increase of the number of fractures however seems to be of less or no importance in the investigated fracture geometries.
- The ratio between radial flow rate and parallel flow rate seems to decrease considerably with the amount of flow features included in the model as could be seen before in Figure 5.15.
- Both previous statements have important implications for the validity of borehole tests that are essentially radial in character.

5.2.6 Sensitivity analysis of an orthogonal system with changing fracture sizes

So far the distribution of the fracture size has been held constant. Often however different fracture sets have different distributions. In this step, the influence of fracture size will be investigated. Larger fractures will result in longer tubes, and more direct flow paths. The previous tests have shown that a higher density leads to more flow. Therefore, taking *or111c* as a reference model, the size of one of the fracture sets has been doubled (radii uniformly distributed between 0 and 0.6 instead of 0.3). To maintain the same fracture density the number of fractures have been reduced to a fourth (25 fracture centres per unit cube). The conductivities of all tubes were set at 1.

Three models were investigated and compared with the standard model *or111c*. In each case the direction perpendicular to the enlarged fracture set shows the lowest total flow rate, in general slightly lower than the reference model, whereas the flow rate in the two other directions is slightly higher than in the reference model. The first model *or02511* has enlarged horizontal fractures, as can be observed in for instance a sedimentary formation with bedding planes. Only in this model (*or02511*) the radial flow rate is similar to the reference model. In the two other models, the radial flow rate is reduced.

	x	y	z	radial
or111c	3.556009	3.666253	3.555933	49.64694
or02511	4.863049	5.923031	<u>2.979337</u>	51.12814
or10251	5.100033	<u>3.745409</u>	4.39077	41.54192
or11025	<u>2.106077</u>	5.321588	4.305955	40.78326

Table 5.8 Average flow rate calculation results of ten model-realizations with a single fracture set with enlarged fractures. The underlined flow rates are directed perpendicular to the enlarged fracture set.

In this test series 30 instead of 10 model-realizations of each model have been calculated. There are therefore 120 results that correspond with parallel flow perpendicular to the enlarged fractures. Figure 5.22 shows the flow rate distribution obtained by these calculations. The distribution seems to follow a log normal. Using SigmaPlot equation 5.1 was obtained. The adjusted Rsqr value of 86% suggest a good fit of this function.

$$f(x) = 0.165 e^{-\left[-0.5 \frac{\left(\ln\left(\frac{x}{1.6593}\right) \right)^2}{0.9282} \right]} \quad (5.3)$$

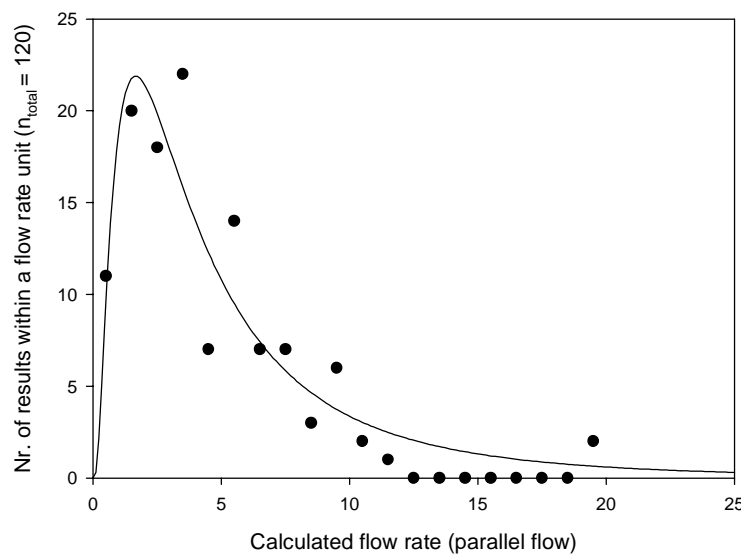


Figure 5.22 Histogram of the calculated flow rate frequency in a direction perpendicular to the enlarged fracture set and distribution curve fitted through the data.

The following conclusions can be drawn:

- An increase of the fracture size, without changing the fracture density, will lead to a decrease of flow rate perpendicular to these fractures and an increase in the plane of the fracture. The radial flow rate will remain the same if the well axis is perpendicular to the enlarged fractures, but will otherwise decrease.
- The results of 120 model-realizations shows a log normal distribution of the flow rate, which corresponds with observations made by other researchers that investigated channel networks, such as for instance Yu (2000).

5.2.7 Sensitivity analysis of an orthogonal system with changing conductivities

In the previous calculations, a single distribution function has been used for all channels. At the development of fracture channels in nature, however, one direction will generally be developed preferentially. The basis for this sensitivity study are ten generations of the *orIIIc* model, where the conductivity of all channels is fixed at 1. These ten model-realizations are then calculated again with reassigned conductivities for each of the directions. The conductivities used are 1, 10 and 100. The average flow rates calculated for ten model-realizations with fracture radii between 0 and 0.3 are listed in Table 5.9.

The *orIII* model has been designed in such a way that no direct connections from the inflow face to the outflow face exist. An increase of conductivity in one direction will therefore be “smoothed”, the flow rate in that direction will increase, but not with the same factor as the related conductivity. Flow rates in the other directions will increase as well. The table above shows that with the geometry used in the model 100, 10, 1 for instance, an increase of channel conductivities by a factor of 100 in the x-direction, leads to an actual overall conductivity increase by a factor of approximately 7.3 for this direction. However, the flow rate in the unchanged z-direction doubles.

Conductivities for x, y and z directions	x	y	z	radial
1, 1, 1	3.556009	3.666253	3.555933	49.64694
10, 1, 1	<u>9.071677</u>	4.751746	4.538114	126.6735
1, 10, 1	4.594649	<u>9.75755</u>	4.951127	108.1325
1, 1, 10	4.452974	4.831926	<u>8.65338</u>	60.62088
10, 10, 1	16.3707	16.69884	<u>6.725609</u>	312.8561
10, 1, 10	16.17929	<u>6.793823</u>	14.22933	188.0956
1, 10, 10	<u>6.046711</u>	16.90091	17.74317	157.7888
1, 10, 100	6.350733	19.59951	<u>30.01243</u>	180.6638
1, 100, 10	6.424853	<u>28.85357</u>	21.78609	323.6748
10, 100, 1	19.01461	<u>29.64692</u>	7.342518	593.0543
10, 1, 100	18.78723	7.306403	<u>22.97781</u>	215.8573
100, 1, 10	<u>26.88667</u>	7.339303	16.3897	404.2258
100, 10, 1	<u>25.88857</u>	19.29112	7.172218	672.6527

Table 5.9 Average total flow rate calculation results of ten model-realizations with variable channel conductivities. The underlined flow rates point to similar result in the same set of models. The bold flow rates indicate similar values for the radial flow, but widely varying values of the flow rate in the x-direction.

The set-up of the radial flow test simulates the behaviour of a steady state borehole pumping test, such as the often used Lugeon test. The radial flow towards a well, and therefore the flow rate in the simulations is mainly influenced by the flow in the x and y direction. For many practical applications however only one flow direction is of importance. An example would be one-dimensional flow underneath a dam. The model-realizations show that different configurations of the conductivities can lead to approximately the same radial conductivities. E.g., the models 1, 100, 10 and 100, 1, 10 should yield approximately the same values for the radial flow rate. Regarding the conductivities in the x and y directions, it can be seen that the flow rate in one direction is approximately 4 times higher than the other. In the example case of flow underneath a hydraulic dam, a four-times higher flow rate might pose a considerable problem for the profitability and safety of a dam. In such situations multiple borehole pumping tests would have to be performed to find the direction of the anisotropy.

The conductivities of the channels can be represented in the form of a directional tensor. Also the resulting overall conductivities can be presented in that way. It might also be possible to include additional tensors for connectivity, fracture lengths and densities. It might be possible to define transform functions to link these tensors together, in order to determine the anisotropy of a fractured rockmass. A similar approach in 2-D has already be proposed by Sharp (1993), for instance.

The following conclusions can be drawn:

- When introducing widely varying distribution functions for each direction in a channel network model, the resulting effect on the overall conductivity will be greatly reduced.
- There is however still a remarkable effect of conductivity changes on the overall conductivity. The radial flow rate observations, as they can be obtained for example by Lugeon tests, can therefore be misleading. The direction of the anisotropy can not be determined with such single hole pumping tests. Multiple borehole test would be needed to obtain such information. Some transient pumping tests can give an indication whether flow is one-dimensional (tubes), two-dimensional (fractures perpendicular to borehole), three-dimensional (porous media) or something in between.
- Using tensors it might be possible to describe the overall conductivity tensor in terms of the channel conductivity tensor.

5.3 Combination of the CPA and the Joint-OKY programs

The CPA program is based on the assumption that flow in a fractured rock mass takes place through the intersections of fractures, whereas the Joint-OKY code assumes flow through the fractures only. These approaches are different and the results of a direct comparison have to be interpreted with caution. Nevertheless a comparison has been made.

In order to compare the approach of channels at fracture intersections with that which uses in-fracture channelling, the *orIIIc* model has been used in the Joint-OkY program to generate in-fracture channel model-realizations. Using a special interface program, the model generated in Joint-OkY can be translated into a file that can be used in the CPA program. Ten model-realizations of the *orIII* model have been produced in the Joint-OkY program. The resulting networks were then used in the CPA program (Figure 5.23). Since no data about conductivities of

fracture channels or fractures are known, all channels have been assigned the conductivity 1. The choice of the same, constant conductivity in both models means that the resulting flow rates should be seen as a measure of the geometry and conductivity resulting from the two approaches.

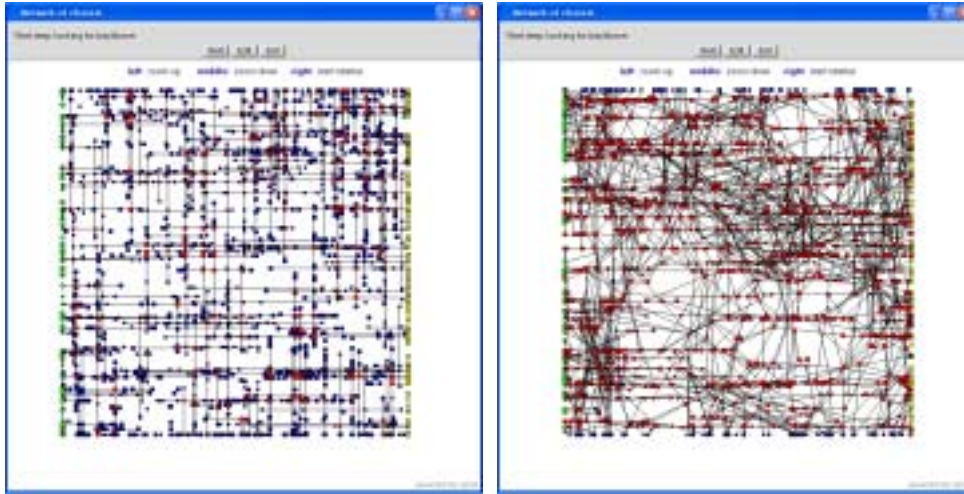


Figure 5.23 Comparison of networks generated by CPA (left) and Joint-OKY (right) using the same fracture model parameters (*or111*) as an input.

	x	y	z	radial
Fracture intersection model average	3.200408	2.933001	3.20034	49.64694
In-fracture model average	73.30775	73.39752	74.34777	328.492
Fracture intersection model coefficient of variation	0.737187	0.921815	0.808281	0.396248
In-fracture model coefficient of variation	0.087418	0.141727	0.108894	0.185745

Table 5.10 Comparison of the average and the coefficient of variation of the flow rates of ten model-realizations of the *or111c* model using the fracture intersection and the in-fracture approach.

The calculated flow rate results, as summarized in Table 5.10, show that the in-fracture model displays a much higher flow rate, which is due to the higher number of connections as can be clearly seen in Figure 5.23. The in-fracture models also have a significantly lower percolation threshold. The ratio between radial and parallel flow rate is greatly reduced, which is due to the larger number of connections and indicates that the behaviour of the in-fracture is closer to that of an equivalent porous media. The coefficient of variation shows that the coefficient of varia-

tion of the intersection model is 7.5 times higher than that of the in-fracture model for parallel flow, but just 2 times for the radial flow case. The variation in case of radial flow is larger than that of parallel flow with the in-fracture assumption, which is not the case with the fracture intersection assumption. These results show that the choice of the tubular network generation has a large impact on the connectivity and channel density. The assumption of in-fracture flow will lead to a network that can be approximated with an equivalent porous media approach, much smaller than when assuming fracture channel flow. In other words, assuming flow through fracture intersections means larger variations in the flow rate and therefore also in contaminant transport calculations.

In the field it is observed that fracture channels are usually much more conductive than single fractures. For these analyses a conductivity of 1 was assumed for all tubes in both models. It would be more realistic to assign larger conductivities to the fracture intersection model in such a way that the flow rate results of both models are comparable. By performing some of the previously described sensitivity analyses, (investigation of the influence of fracture density, for example), a more detailed comparison of the two approaches could be performed.

The following conclusions can be drawn:

- The in-fracture flow model has more connections, resulting in significantly higher flow rates when the same conductivity is assumed for each tube.
- The ratio between radial and parallel flow rates in the in-fracture model situation is considerably lower than that of the fracture intersection model, suggesting that the model behaves more like an equivalent porous media.
- More sensitivity analyses should be performed by using variations of a standard model that will result in the flow rates for both approaches.

6

Conclusions

The research presented in this thesis includes four major parts.

- Literature study
- Fieldwork
- Model development
- Model application

Literature study. The literature study showed that flow through intersections of fractures exists and may play a major role in flow through a fractured rockmass (Abelin et al., 1988; Neretnieks, 1994). Some researchers have included fracture intersections in their fracture flow models (i.e. Sugimura et al., 1999; Gylling, 1997), which makes it difficult to distinguish between the effects on the flow system.

Fieldwork. Fieldwork has been conducted at outcrops close to Granada, Spain. At the outcrops fossilized flow paths have been observed at the intersections of fractures. During the fieldwork fracture data has been gathered, with which the fracture geometry could be reconstructed. The fieldwork also showed that it is almost impossible to obtain reliable values in the field for fracture aperture or the cross section of fracture channels.

Model development. As major part of this research a mathematical model has been developed to simulate flow purely at the intersections of fractures, neglecting flow within the fractures or through the rock matrix. The CPA computer code that models a tubular network of fracture intersections has been developed initially in cooperation with the department of mathematics at the EPFL for a different purpose. The original CPA code therefore also includes tools to investigate the behaviour of strongly disordered systems, of which a naturally fractured rockmass is

an example. It is the subject of the PhD thesis of Cerny (2003). Parts of this work have been published in Bruines and Genske (2001) and is currently under review (Cerny, under review).

The initial program has been further developed by the author to accommodate more realistic fracture networks, in particular randomly orientated fractures, and flow configurations. Flow rates of parallel flow through a cube as well as radial flow through a cylinder can be modelled with the improved code. Due to lack of time, transport has however, not been addressed specifically.

Model application. The CPA code developed has been applied to a number of problems to test the correctness of the model and investigate the effects of the different input parameters. This section can be roughly divided in three parts:

- Network generation
- Sensitivity analysis
- Comparison with the Joint-OKY program

The data gathered during fieldwork in Spain has been used to confirm the geometric modelling capabilities of the CPA program. A comparison between the network model generated by CPA and the observations in the field show good agreement. The use of an eigenvectors approach to represent fracture orientation distribution has proven to be a good and simple method.

The CPA code calculates flow rates through a tubular network using fracture data input. During fieldwork in Spain, however, no hydrogeological data could be obtained. It has been attempted in the framework of this research to obtain data bases of sites that included fracture and hydrogeologic data. Data were obtained from the Stripa mine in Sweden, the Yucca Mountain Project in the US, Kuji underground petroleum storage site, Kamaishi mine, and the Tohno geoscience center all located in Japan. The data of the underground petroleum storage facility at Kuji seems to be most promising since many permeability tests are available, as well as fracture maps of the caverns. Still extensive processing of the data would have been required, but no time was available.

It was therefore decided to perform sensitivity analyses of the models generated by the CPA code, in order to better understand the influence of each input parameter in the CPA model.

The first analysis regarding the *fracture density* shows that it has an important influence on the total flow rate. Too low densities result in an unconnected system. An increase of fracture

density above the percolation threshold results in an exponential increase of the flow rate through the model. For the geometrical conditions of the test calculations, the Dupuit relation predicts that flow rate in the case of radial flow in a homogeneous medium should be 3.9 times higher than the flow rate of the parallel flow model. The network models created by the CPA code with randomly orientated fractures however show a factor of approximately 6 for the well connected networks with a high fracture density, and up to 20 for the less connected networks. These differences can be explained by the influence of dead-end features in the cubic model, that might however still provide a pathway in the radial flow case where the distance between in- and outflow boundary is significantly smaller (40%). The conductivity of the tubular network models therefore depends also on the definition of the problem domain.

The second sensitivity analysis with randomly orientated fractures has been conducted to determine the influence of the *size of the model volume* chosen (scale effect). The standard network model domain has been gradually enlarged up to a factor of two in all directions (eight times larger volume). These tests show that the flow rates, scaled back to that of the standard model, do not change significantly. On the contrary, the coefficient of variation of the ten model-realizations shows to be inversely proportional to the model size. Doubling the size of the sides of the cube resulted in a halving of the variation. A further increase of the model size was not possible because of computational power limits.

A third sensitivity analysis carried out with orthogonal fractures showed clearly that the variation due to the *stochastic nature of the location of the fractures* has a larger influence on the flow rate than that of the *stochastic nature of the conductivities* assigned to each of the tubes in the network.

Tests to evaluate the influence of the *anisotropy of fracture density* in orthogonal systems show that the increase of fracture density is, as in the randomly orientated fracture models, of great influence on the total flow rate. The orientation of the fracture sets with higher densities seems however to be of less importance in the models investigated.

In addition, an analysis of the influence of *fracture size* (with constant fracture density) in orthogonal systems has been carried out. The fracture radii of selected fracture sets were doubled. The number of fractures was reduced accordingly to keep the density constant. An increase in the fracture size of one fracture set, without changing the fracture density, leads to a decrease of the flow rate perpendicular to these fractures, and an increase in flow in the plane of the fractures. The radial flow rate will remain the same if the well is perpendicular to the

enlarged fractures, but will otherwise decrease. A large number of model-realizations have been run for this particular model configuration. It was therefore possible to investigate the distribution of flow rates for the same configuration. The results of 120 model-realizations showed a log normal distribution of the flow rate. These results agree with previous studies such as by Yu (2000) for his contribution to the “Inter-comparison of flow calculation for H-12 reference fractured rock”, carried out with the Joint-OKY program.

Finally the influence of *anisotropic conductivity* in orthogonal systems has been studied by assigning different conductivities in different directions. When introducing a high anisotropy on the local scale for the conductivity of single tubes, the calculations show that the resulting effect on the overall anisotropy of the conductivity is greatly reduced. However there still remains, a remarkable effect on the directional total flow rates. The results of radial flow rate calculations and also single hole pumping tests can be misleading. No information on anisotropy can be extracted. Multiple borehole pumping tests can yield such information. Outcrop information can help to better describe anisotropy (see also Appendix C)

Within the CPA program a procedure has been added that generates a file containing generated fractures which is readable by the Joint-OKY program. Fractures generated using the eigenvector approach can therefore also be used in the Joint-OKY program. An additional program has been made to make networks, generated in the Joint-OKY program, that assumes flow through fractures, available to the CPA program, which assumes flow at the intersection of fractures. This made it possible to investigate the networks generated with both assumptions for the same fracture models. These investigations showed that the model, which assumes in-fracture flow presents a considerably higher number of flow features resulting in much higher conductivity and reaches percolation earlier than the intersection model.

7

Recommendations

During this study some questions have remained unanswered and some new questions have arisen that seem to be of interest for further investigation.

For describing the spread of fracture orientation an Eigenvalue approach has been used in this study. Equivalent porous media model approaches need to quantify the anisotropy of the rock mass under investigation. Both the fracture orientation and the anisotropy can be described as tensors. In fact, fracture spacing, fracture length, connectivity and conductivity of single features can be described in this manner. The relations between the different tensors should be investigated, in order to develop a method that can estimate the anisotropy of a tubular or fracture network using outcrop data.

In the current version of the CPA program the tube conductivities are independent of neighbouring tubes, which is not the case in geology. Tubes resulting from the intersection of the same fractures of fracture sets often have similar conductivities. Connected tubes can be enlarged by circulating fluids, so that preferential flow paths are formed. The LEDA library used in the CPA code, has possibilities to address these issues. The CPA program would be improved by implementing such a conductivity assignment methodology.

The flow distance from input face to output face of the radial flow models used, was smaller than that of the parallel flow model. Although this clearly showed the effects of shorter flow distances, it made the comparison of parallel and radial flow difficult. It is therefore suggested to investigate radial models using a cylinder with a radius of 1 to allow a direct comparison between parallel and radial flow rate results.

The CPA code uses normalized data. The size of the model is a cube with a unit length, conductivities are distributed between 0 and 1, etc. It is recommended to improve the CPA code such that non-normalized values can be used. The H-12 flow calculation experiment could then be realized and results compared with other mathematical models.

The data available from the Kuji underground petroleum storage facility include fracture and hydrogeologic data, and seem to show promise for checking the CPA code using field data. By realizing different models, calculated and measured conductivity distributions could be compared. In a next step some improvements to the CPA could be made. At the Kuji site extensive research is being made to the clustering of fractures (Choi, 1999 et al.). As part of the research stay at Kyoto University preliminary studies have been performed to modelling clustered fracture networks (Chiba, 2002). This methodology could then be integrated in the CPA code.

To eliminate some of the effects of randomness, deterministic data, if available, should be included in the models. The Joint-OKY program has some of those capabilities. It is recommended to improve exchange between Joint-OKY and CPA possible. The Joint-OKY program also has more options to describe contaminant transport that would then be available. The optimization algorithm in Joint-OKY, however, can be improved. Computational intelligent methods such as artificial neural networks, fuzzy logic and genetic algorithms seem promising options.

References

- Abelin, H., L. Birgersson, J. Gidlund, L. Moreno, T. Gren, H. Widén and I. Neretnieks (1988). 3-D Migration experiment in sparsely fractured crystalline rock. Stockholm, Sweden, Royal Institute of Technology, Department of Chemical Engineering: 199-207.
- Barenblatt, G. I., I. Zheltov and I. N. Kocina (1960). "Basic concepts in the theory of seepage of homogeneous fluids in fissured rock (strata) (English translation)." *Journal of applied math. mech.* 24: 1286-1303.
- Barton, C. C. and P. A. Hsieh (1989). *Physical and hydrological flow properties of fractures: American geophysical union, Field guide book T385, 28th International Geological Congress.*
- Bear, J., and B. Berkowitz (1987). "Groundwater flow and pollution in fractured rock aquifers." *Developments in Hydraulic Engineering*, 4: 175-238.
- Bear, J. (1988). *Dynamics of fluids in porous media*, Dover Publishing.
- Bear, J., C.-F. Tsang and G. de Marsily (1993). *Flow and contaminant transport in fractured rock*. San Diego, Academic Press..
- Billiaux, D. (1990). *Hydrogéologie des milieux fracturés: géométrie, connectivité, et comportement hydraulique*. Paris, Ecole National Supérieure des Mines de Paris.
- Bruel, T. (1998). *Caractérisation des circulations de fluides dans un réseau fracturé et rôle des contraintes "in situ"*. Montpellier, Université de Montpellier II: 402.
- Bruines, P. A. and D. D. Genske, Eds. (2001). *Proceedings of the international workshop on "Migration of contaminants in fractured media" in Lausanne*. Bern, Leylakitap.
- Bruines, P.A. and T. Halihan (1999). *Filling the field data gap in fractured aquifer interpretation. Proceedings of Envirowater99: Emerging Technologies for Sustainable Land use and Water Management, Sept 1-4, 1999, 10 pp., CD format publication.*
- Cacas, M. C. (1989). *Développement d'un modèle tridimensionnel stochastique discret pour la simulation de l'écoulement et des transports de masse et de chaleur en milieu fracturé*. Fontainebleau, Ecole des Mines de Paris.

-
- Cacas, M. C., E. Ledoux, G. DeMarsily, A. Barbreau, P. Calmels, B. Gaillard and R. Margritta (1990). "Modeling fracture flow with a stochastic discrete fracture network: 2. The transport." *Water Resources Research* 26(3): 491-500.
- Cacas, M. C., E. Ledoux, G. DeMarsily, B. Tillie, A. Barbreau, E. Durand, B. Fuega and P. Peaudecerf (1990). "Modeling fracture flow with a stochastic discrete fracture network: 1. The flow model." *Water Resources Research* 26(3): 479-489.
- Cerny, J. (under review). Critical Path Analysis for Continuum Percolation. *Annales de l'institut Henri Poincare (B) Probability and Statistics*.
- Cerny, J. (in preparation). On two properties of strongly disordered systems, Aging and critical path analysis. PhD thesis, Lausanne, EPFL.
- Choi, H., H. Tosaka and K. Kojima (1999). "Estimation of the segmented structure of fracture zone based on morphological characteristics." *Journal of the Japan Society for Engineering Geology* 40(4): 207-219.
- Cloos, H. (1936). *Einführung in die Geologie*. Berlin, Borntraeger : 504.
- Darcy, H. P. G. (1856). *Les fontaines publiques de la Ville de Dijon*. Paris, Victor Dalmont.
- Dershowitz, W. S. and H. H. Einstein (1988). "Characterizing rock joint geometry with joint system models." *Rock Mechanics and Rock Engineering* 21: 21-51.
- Domenico, P. A. and F. W. Schwartz (1990). *Physical and chemical hydrogeology*. New York, John Wiley & Sons.
- Drogue, C. and J. C. Grillot (1976). "Structure géologique et premières observations piézométriques à la limite de sous système karstique de Terrieu." *Geologie* 25, 3e série.
- FracMan Technology Group (2002). <http://fracman.golden.com>.
- Freeze, R. A. and J. A. Cherry (1979). *Groundwater*, Prentice Hall.
- Grasselli, G. (2001). Shear strength of rock joints based on quantified surface descriptions. *Civil Engineering*. Lausanne, Ecole Polytechnique Federal de Lausanne: 117.
- Grindrod, P. (1993). "The impact of colloids on the migration and dispersal of radionuclides within fractured rock." *Journal of contaminant hydrology*(13): 167-181.
- Gylling, B. (1997). Development and applications of the channel network model for simulations of flow and solute transport in fractured rock. Department of chemical engineering and technology. Stockholm, Royal Institute of Technology: 61 and papers.
- ITC/TUD (1996). Fieldwork procedures, part II. Delft.

- Jourde, H. (1999). Simulation d'essais de puits en milieu fracturé à partir d'un modèle discret basé sur des lois mécaniques de fracturation. Validation sur sites expérimentaux. Montpellier, Université de Montpellier II : 183.
- Kolditz, O. (1997). Strömung, Stoff- und Wärmetransport in Kluftgestein. Stuttgart, Borntraeger.
- LaPointe, P. R. and J. A. Hudson (1985). Characterization and interpretation of rock mass joint patterns, The Geological Society of America.
- Lomize, G. M. (1951). Seepage in fissured rocks, Moskow-Leningrad, State Press.
- Long, J. C. S. and D. M. Billaux (1987). "From field data to fracture network modeling: An example incorporating spatial structure." *Water resources research* 23(7): 120-1216.
- Long, J. C. S. and Committee on Fracture Characterization and Fluid Flow (1996). Rock fractures and fluid flow: contemporary understanding and applications. Washington, National Academy Press.
- Louis, C. (1974). "Introduction à l'hydraulique des roches." *Bulletin du BRGM (deuxième série) Section III(4)*: 283-356.
- Moench, A.F. (1984). "Double-porosity models for a fissured groundwater reservoir with fracture skin." *Water Resources Research*, 20: 831-846.
- Moreno, L., C.-F. Tsang, Y. Tsang and I. Neretnieks (1990). "Some anomalous features of flow and solute transport arising from fracture aperture variability." *Water Resources Research*, 26(10): 2377-2391.
- Moreno, L. and I. Neretnieks (1993). "Fluid flow and solute transport in a network of channels." *Journal of contaminant hydrology*(14): 163-192.
- NAGRA (1985). Kristallin-I Safety assessment report. Baden, Switzerland, NTB 93-22.
- NAGRA (1994). Projekt Gewähr: Endlagerung für hochaktive Abfälle: Das System der Sicherheitsbarrieren. Baden, Switzerland, NAGRA.
- Neretnieks, I. (1994). Nuclear waste repositories in crytalline rock - An overview of nuclide transport mechanisms. MRS Meeting on scientific basis for nuclear waste management, Mater. Res. Soc., Kyoto, Japan, : 24-26.
- Pollard, D. D. and A. Aydin (1988). "Progress in understanding jointing over the past century." *Geological Society of America Bulletin* 100: 1181-1204.
- Press, W. H. (2002). Numerical recipes in C++: The art of scientific computing, Cambridge University Press.

-
- Priest, S. D. (1993). *Discontinuity analysis for rock engineering*. London, Chapman & Hall.
- Robinson, N. I., J. M. Sharp and I. Kreisel (1998). "Contaminant transport in sets of finite fractures with fracture skins." *Journal of contaminant hydrology* 31(1-2): 83-109.
- Sharp, J. M. (1993). *Fractured aquifers/reservoirs: Approaches, problems and opportunities*. XXIVth congress of IAH, Oslo, Norway.
- Shimo, M. and S. Iihoshi (1995). *Experimental and numerical study on fluid and mass transport through fractured rocks*. 8. International congress on rock mechanics, Tokyo, Balkema.
- Snow (1968). "Rock fracture spacings, openings and porosity." *Journal Soil Mechanics* 94: 195-201.
- Streltsova, T. D. (1976). "Hydrodynamics of groundwater flow in a fractured formation." *Water resources research* 12(3): 405-413.
- Sugimura, Y., I. Matsuda, S. Tomimori, K. Masumoto and K. Watanabe (1999). "Numerical inversion method of seepage flow using channel network model. (in Japanese)." *Proceedings of the Japan Society of Civil Engineers* 638/III-49: 41-50.
- Tang, D. H., E. O. Frind and E. A. Sudicky (1981). "Contaminant transport in fractured porous media: Analytical solution for a single fracture." *Water resources research* 17(3): 555-564.
- Taylor, G. (1953). "Dispersion of soluble matter in solvent flowing slowly through a tube." 186-202.
- Tsang, C. F. and I. Neretnieks (1998). "Flow channeling in heterogeneous fractured rocks." *Review of geophysics* 36(2): 275-298.
- Tsang, C. F., Y. W. Tsang and F. V. Hale (1991). "Tracer transport in fractures: Analysis of field data based on a variable-aperture channel model." *Water resources research* 27(12): 3095-3106.
- Wallbrecher, E. (1986). *Tektonische und gefügegenalytische Arbeitsweisen*. Stuttgart, Ferdinand Enke Verlag.
- Warren, J. E. and P. J. Root (1963). "The behavior of naturally fractured reservoirs." *Journal of the Society of Petroleum Engineering* : 245-255.
- Watanabe, K. (1995). "Recent Progress in groundwater flow modeling - channelling flow and fracture geometry- (in Japanese)." *Soils and foundations* 43-9(452): 1-5.

- Witherspoon, P. A., J. S. Y. Wang, K. Iwai and J. E. Gale. (1980). "Validity of cubic law for fluid flow in a deformable rock fracture." *Water Resources Research* 16(6): 1016-1024.
- Yu, Q. (2000). *Analyses for fluid flow and solute transport in discrete fracture network*. Department of civil engineering. Kyoto, Kyoto University: 161.



Appendix A

Filling the field data gap in fractured aquifer interpretation

Patrick Bruines, currently ENAC-ICARE-LMR, EPFL, 1015 Lausanne, Switzerland

Todd Halihan, currently Oklahoma State University, School of Geology, 105 Noble Research Center, Stillwater OK 74078, USA

Previously published in: Proceedings of Envirowater99: Emerging Technologies for Sustainable Land use and Water Management, Sept. 1-4, 1999, 10 pp., CD format publication.

Abstract: This paper establishes a framework for developing conceptual models for fractured aquifers using outcrop data. In this framework, we illustrate how outcrop data can be applied to interpret other forms of data that may be available in these settings (i.e. hydraulic tests, tracer tests, etc.). With outcrop data, hydraulic conductivity distributions, retardation effects, and anisotropy will be easier to quantify.

A.1 Introduction

Fractured aquifers present many challenges to hydrogeologists. Their variability and complexity make assessment of these aquifers with standard well testing techniques difficult. Drilling additional wells to interpret the flow and transport in these aquifers does not generally provide significant new information. Other techniques that can provide quantitative information to interpret these aquifers are needed to advance our understanding and ability to characterise flow and transport in fractured aquifers.

Outcrop information can add valuable knowledge to interpreting fractured aquifers that is unavailable with most other methods. However, efficient methods of interpreting outcrop data

have not been fully developed with fluid flow questions in mind. Outcrop data has generally been utilised from structural or engineering perspectives, and techniques and analysis suited to hydrogeology are lacking.

This paper establishes a framework for characterising fractured aquifers using outcrop data to determine the necessary parameters needed to calculate flow and transport. In this framework, we illustrate how outcrop data can be utilised to interpret and constrain additional available data that on its own may not yield a satisfactory or appropriate solution. Outcrop data can do much to eliminate incorrect conceptual models and lend support to more appropriate ones.

In the next sections we show some of the data requirements for characterising and modelling flow and contaminant transport through fractured rock. We demonstrate which of these data can be obtained from outcrop, illustrating the advantages and limitations of outcrop data. Where possible, we present some examples from recent fractures studies.

A.2 Data requirements

A.2.1 Flow

Flow in a simple homogeneous, isotropic model aquifer can be modelled using a hydraulic conductivity and a porosity or some other storage parameter depending on the aquifer type. When evaluating fractured aquifers, the hydraulic conductivity can vary with scale covering many orders of magnitude [1-3]. At a single scale, the variation can still be orders of magnitude. In fractured aquifers, storage occurs in the matrix, the fracture network, and over the millimeter-scale damaged region near the fractures (fracture skins).

Quantifying conductivity from permeameter tests conducted on core can yield results that are three orders of magnitude too low or more [3]. Using only a limited number of pump tests yields only a tiny picture of the variability of conductivity. Installation of a statistically significant number of wells is prohibitive, and not recommended for waste disposal applications.

Outcrop data can overcome some of these difficulties by providing estimates of permeability variability. It can also yield the information at a cost far below most other techniques. Conductivity measurements on core pieces when combined with measurements of fracture orientation, aperture, length, connectivity, and density can yield valuable insight into aquifer function. These measurements can also provide information on storage properties of the aquifer.

A.2.2 Transport

Obtaining parameters for transport calculations can be difficult in fractured aquifers. The heterogeneous flow field combined with the multiple levels of diffusion and retardation require a better understanding of the aquifer than a single tracer test can provide. In order to better evaluate tracer experiments, constraint on transport mechanisms obtained from the outcrop are key in understanding aquifer function.

Outcrop data on fracture roughness, diffusion coefficients of the rock matrix and the fracture skin can provide valuable information regarding transport between the fracture network and the matrix storage. Data on roughness, skin chemistry, and aperture variation provide some of the information needed to understand flow in the fracture network.

A.3 Outcrop data application

A.3.1 Fracture orientation

Fractures can usually be approximated as occurring along a plane, which has an orientation. The dip direction and angle can describe the orientation. Large amounts of orientation data as gathered with a geological compass on outcrops can be best depicted by stereonet and rose diagrams (Figure A.1). In a naturally fractured rock, fractures commonly occur in sets. Fractures in the same set have approximately the same orientation and often also have other properties in common. Depending on the scale, fracture orientation data can be collected from satellite and aerial photographs, boreholes, thin sections and different geophysical methods.

None of these methods are as efficient or reliable as data obtained from outcrops, be it natural or manmade. For statistical interpretations around 150 to 350 fractures should be mapped [4]. The orientation of fractures will influence the direction of flow and transport, and can impart a strong anisotropy to the flow field (Figure A.1). The strength of this influence will depend on the hydraulic diffusivity of the rock matrix and the properties of additional fracture sets. Each site requires an assessment of structure to determine how well outcrop orientation data will correspond to depth, but good correlations at some sites have already been established [5, 6].

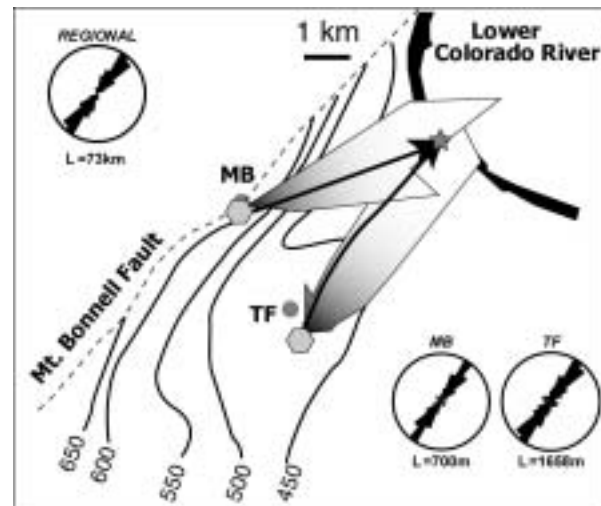


Figure A.1 Anisotropy of the Edwards aquifer [adapted from 7]. Rose diagrams of length weighted orientation are illustrated from regional scale lineament map as well as fracture mapping at two location with exposed creek beds. Using anisotropy predicted from the outcrop, predictions of flow direction correspond well to dye trace experiments (solid line). Without the fracture data, the predicted dye direction would be east to Southeast instead of to the Northeast. (Groundwater elevation in feet)

A.3.2 Fracture density / spacing

The density of fractures can be measured in many different ways: number of fractures per area or volume, length per area, area per volume, RQD, fracture spacing. The most convenient way is to measure the spacing of the fractures in each set individually. For individual fracture sets the spacing can be treated as a lognormal distribution [6, pg. 111, 8]. If the different sets are not separated, the discontinuity spacing can be distributed as a negative exponential function [4]. Typical spacings for joint sets are in the order of tens of centimetres to metres, but spacings might vary depending on the scale of the fractures [8]. Spacing data is valuable for interpreting tracer data using dual porosity models where fracture spacing is required. It is also useful for calculating equivalent well permeabilities using aperture distributions [3]. Fieldwork in Colorado, USA has indicated that spacings observed at outcrop can be correlated for some depth [5, 6].

A.3.3 Fracture aperture

Aperture is the distance between the fracture walls. The aperture is the most sensitive parameter for determining flow rate through a fracture. This is evident from examining the cubic law [9]:

$$Q = \frac{\rho_w g b^3}{12\mu} \cdot wi \tag{A.1}$$

ρ_w = density of the fluid; g = gravitational constant; b = aperture; μ = fluid viscosity; w = width of the fracture

The flow is proportional to the third power of the aperture. For the distribution of the apertures we have to make a distinction between distribution among multiple fractures and along a single fracture.

Measuring fracture apertures is complicated by the presence of multiple aperture values for the same fracture. The mechanical aperture is average distance between the fracture walls, while the hydraulic aperture represents the aperture that agrees with the cubic law. Additionally, the fracture can have a transport aperture for solutes of interest. Mechanical apertures can be measured with automotive feeler gages or comparators (thin lines of known width). Hydraulic apertures can be measured with an outcrop permeameter. Typically the aperture of fractures at outcrop is in the order of micrometers to millimetres, but are scale dependent [10].

Among a fracture set, the distribution of apertures is not simple. Various authors have proposed different distributions. Lognormal, fractal, or Levy stable distributions all provide approximation to measured aperture distributions [3, 10, 11]. It should be noted that most dual porosity models assume a constant aperture distribution, when field evidence suggests otherwise, and laboratory evidence suggest that this approximation is inappropriate [12]. The distribution of apertures is the primary cause of variability in flow measurements of fractures [13]. When estimating transport rates, the properties of the distribution are required to make appropriate predictions [12].

In a single fracture, walls have irregularities termed roughness. The arithmetic mean of the apertures in a single fracture is called the mechanical aperture [14]. This mechanical aperture however does not well represent the flow in fracture [12, 14, 15]. A better measure is the geometric mean, which is much closer to the hydraulic aperture [14]. A varying aperture leads to channelling.

A.3.4 Roughness

Fractures are in reality rarely smooth parallel plates. Usually they are rough. This is a simple consequence of the process of fracturing [16, 17]. An often-used measure of roughness is the surface roughness index, which is the mean fracture aperture divided by twice the mean asperity size. For different Reynolds numbers and roughness indices, fracture flow models were developed by Poiseuille, Blasius, Nikuradse, Lomize and Louis [see i.e. 18, pg. 86]. In general roughness will result in less flow and will increase the in-fracture dispersion.

Roughness can be measured at the outcrop using a carpenter's contour gauge, or with a profilometer. However, the roughness in a fracture is scale dependent, and more work need to be done to determine how roughness varies with the formation of fractures to determine how to best apply outcrop information to fluid flow problems.

A.3.5 Channelling

The fracture characterisation group [6] makes a distinction between fracture channels and channellised transport. A fracture channel is a long narrow region of enlarged aperture formed at the intersection of two fractures or by processes such as shearing and is fixed in orientation and position. Channellised transport arises from nonuniform velocity of fluid and solute transport in a variable-aperture fracture and varies according to the flow direction [6]. Channelling includes both these definitions.

In the Stripa 3D experiment an experimental drift was covered with more than 375 plastic sheets. The natural flow rate onto each of these sheets was recorded. It showed that 70% of the sheets were dry and 50% of the total inflow occurred at 3% of the sheets. Observation at the SFR drifts and tunnels shows that most water entered at distinct points, be it from a single fracture or intersection of fractures [19].

A.3.6 Fracture length

The shape of a fracture is often assumed disc shaped. Whether this is actually the case is a big question. When one makes this assumption, one will, on the outcrop scale, almost never be able to measure maximal size of this disc. There is also the problem of the limits of an outcrop. What to do if the size of the fracture exceeds the size of the outcrop? Priest [4] gives some statistical tools to deal with this problem.

Cladouhos and Marrett [20] show that the length of faults can be approximated, in a certain region, with a power-law distribution. Outcrops, aerial photograph, and lineament maps provide the only way to get length data. Sampling difficulties have not been fully resolved, but the data is important for flow rates and determining connectivity.

A.3.7 Fracture connectivity

The geometric connectivity depends on the length, orientation and density of the fractures. Crossing and abutting fractures will increase the connectivity, blind or dead-end fractures won't. The number of crossings, abutting and blind fractures can be presented in a ternary diagram [21].

Connectivity can be quantified in terms of percolation theory. Network percolation is the conductance of random networks of conductors. Each of the conductors in the network can be open or closed depending on a probability. There exists a critical probability at which an infinite system of conductors will allow for percolation. At probabilities just over the percolation threshold many physical properties can be related to the probability:

$$M \propto (p - p_c)^\tau \tag{A.2}$$

M = a physical property, $(p - p_c)$ = the difference between density and the critical density and τ = universal scaling exponent, which may only depend on the percolation model which is two or three dimensional [6, pg. 394].

In continuum percolation a random fracture is labelled as the first order fracture. Each fracture connected with this fracture is labelled as a second order fracture. The non-labelled fractures connected to the second level fractures are labelled third order, and so on. The number of fractures at each level is a measure for the connectivity, more conducting networks show increasing numbers, whereas decreasing numbers indicate less conducting networks.

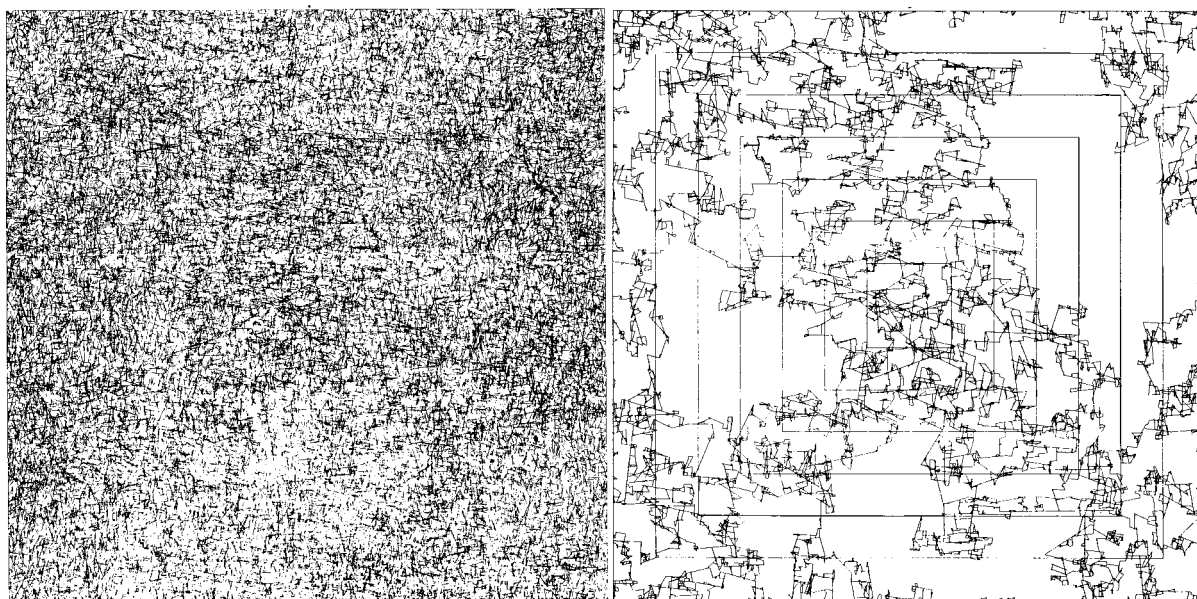


Figure A.2 Left - Fractures generated in a 100-m by 100-m region from the Fanay-Augères. Right - A 70-m by 70-m section of the generated fracture network, only the connecting fractures are shown [from 27].

At the outcrop other measures of the connectivity of the network have been utilised. The number of intersection is a measure of the connectivity used by Robinson [22]. The ratio of connected fractures to total number of the fractures is used by Zhang [23]. Flow in a purely fractured rock will only occur at fracture densities over the percolation threshold. Berkowitz [24] states that the percolation properties are valid also far from the threshold and gives some tests to determine if a 2-D network is connected.

Field testing of connectivity was conducted at the Fanay-Augères mine in France (Figure A.2). Fractures were extensively mapped and a fracture network was constructed with these data. It showed that only 0.1% of the generated fractures actually contributed to the flow [25-27], with the remaining fractures acting as storage for the aquifer. They also showed that the connectivity of the networks is a function of the fracture density and the fracture length.

A.3.8 State of stress

Effective stress is the total stress minus the fluid pressure. Deformation of a rockmass is related to changes of the effective stress. An increased stress level results in closure of fractures. The effective stress increases with depth, so that fracture permeability decreases with depth. Hori-

zontal fractures will usually close sooner than vertical fractures. A sufficient increase in fluid pressure can open fractures.

Outcrop investigation of fractures can yield information about stress history in an area, but it is very difficult to obtain information about the current state of stress from an outcrop. One somewhat promising technique is the use of high precision GPS monitoring to make observations, which may allow the state of stress to be defined for a small region.

A.3.9 Fracture skin

Fracture skins are the millimeter-scale regions along a fracture surface, which comprise coatings on the matrix or altered zones within the matrix [28]. These regions are especially important in flow and transport in fractured rock aquifers. They provide the primary mechanism for allowing moving between fractures and the matrix.

Moench [29] developed a double porosity model that takes the fracture skin properties into consideration for hydraulic testing. For the contaminant transport properties a fracture skin can be even more influential [30], causing increase sorption along fracture surfaces. Skin surfaces can have higher or lower permeability and porosity than the surrounding matrix and therefore need to be tested for each aquifer.



Figure A.3 Shale from a quarry near Mintaro, South Australia showing fracture skin. This iron-rich fracture skin occurred along a bedding plane fracture and indicates that flow occurred between asperities in the bedding plane in a combination "pillar" flow. Fractures occurring perpendicular to bedding demonstrated a planar flow with highly uniform iron coatings.

Outcrops allow these features to be assessed visually and quantitatively. Laboratory analysis of these zones can determine if their porosity and permeability are higher or lower than the rock matrix [31]. Additionally, diffusion measurements allow the interactions between the fracture network and matrix to be estimated. Outcrops are therefore essential to get an idea of these influence properties. On the outcrop the coatings and staining can also give us some clear indications on the type of flow. The outcrop evidence can suggest linear or channelled flow, planar flow, or as a combination "pillar" flow (Figure A.3).

A.4 Conclusions

In this paper we presented data requirements for fractured rock aquifer assessment and showed how these data can be gathered from outcrops. Outcrop study is the only method that can yield data on fracture length, distribution, intersections, and connectivity. Theoretically other methods can provide us with fracture orientation, roughness, mineralization, aperture and tectonic features. In practice only outcrops can yield these data in statistically significant amounts. Methods for outcrop data collection have not been fully developed with fracture flow problems in mind, so that much work has to be done to improve data gathering techniques.

A.5 References

- [1] Kiraly, L., "Rapport sur l'état actuel des connaissances dans le domaine des caractères physiques des roches karstiques", *Hydrogeology of karstic terrains*, 53-67, 1975.
- [2] Clauser, C., "Permeability of crystalline rocks", *EOS, Transactions American Geophysical Union*, vol 73, 233-238, 1992.
- [3] Halihan, T., R. E. Mace and J. M. Sharp, "Flow in the San Antonio segment of the Edwards aquifer: Matrix, fractures or conduits?", *Groundwater flow and contaminant transport in carbonate aquifers*, in press.
- [4] Priest, S. D., *Discontinuity analysis for rock engineering*, Chapman & Hall, London, 1993.
- [5] Lorenz, J. C. and S. J. Finley, "Regional fractures II: Fracturing of Mesaverde reservoirs in the Piceance basin, Colorado", *AAPG bulletin*, vol 75, 1738-1757, 1991.

- [6] Long, J. C. S. and Committee on fracture characterization and fluid flow, *Rock fractures and fluid flow: contemporary understanding and applications*, National Academy Press, Washington, 1996.
- [7] Zahm, C. K., "Use of outcrop fracture data to estimate regional groundwater flow: Barton Spring segment of Edwards aquifer, Central Texas", M.Sc. Thesis, Dept. of Geological Sciences, University of Texas, 1998.
- [8] Narr and Suppe, "Joint spacing in sedimentary rocks", *Journal of sedimentary geology*, vol 13, 1037-1048, 1991.
- [9] Hele-Shaw, H. S., "Investigation of the nature of surface resistance of water and of streamline motion under certain experimental conditions", *Transactions of the Institute of Naval Architects*, vol 40, 21-46, 1898.
- [10] Marrett, R., "Permeability, porosity, and shear-wave anisotropy from scaling of open fracture populations, in fractured reservoirs", *Characterization and modeling guidebook*, 217-226, 1997.
- [11] Belfield, W. C., "Incorporating spatial distribution into stochastic modelling of fractures: Multifractals and Levy-Stable statistics", *Journal of structural geology*, vol 20, 473-486, 1998.
- [12] Sonnenborg, T. O., M. B. Butts and K. H. Jensen, "Aqueous flow and transport in analog systems of fractures embedded in permeable matrix", *Water resources research*, vol 35, 719-729, 1999.
- [13] Hsieh, P. A. and A. M. Shapiro, "Hydraulic characteristics of fractured bedrock underlying the FSE well field at the Mirror Lake site, Grafton County, New Hampshire U.S. Geological Survey Toxic Substances Hydrology Program; proceedings of the technical meeting", U.S. Geological Survey Toxic Substances Hydrology Program technical meeting, 127-130, 1996.
- [14] Renshaw, C. E., "On the relationship between mechanical and hydraulic aperture in rough-walled fractures", *Journal of geophysical research*, vol 100, 24629-24636, 1995.
- [15] Brown, S. R., "Transport of fluid and electric current through a single fracture", *Journal of geophysical research*, vol 94, 9429-9438, 1989.
- [16] Marder, M. and J. Fineberg, "How things break", *Physics today*, vol 49, 24-29, 1996.
- [17] Sharon, E., S. P. Gross and J. Fineberg, "Energy dissipation in dynamic fracture", *Physical review letters*, vol 76, 2117-2120, 1996.

- [18] Kolditz, O., *Strömung, Stoff- und Wärmetransport in Kluftgestein*, Borntraeger, Stuttgart, 1997.
- [19] Neretnieks, I., H. Abelin and L. Birgersson, "Some recent observations of channeling in fractured rocks: Its potential impact on radionuclide migration", *Geostatistical, sensitivity and uncertainty methods for ground-water flow and radionuclide transport modeling*, 387-410, 1987.
- [20] Cladouhos, T. T. and R. Marrett, "Are fault growth and linkage models consistent with power-law distributions of fault lengths?", *Journal of structural geology*, vol 18, 281-293, 1996.
- [21] Barton, C. C. and P. A. Hsieh, *Physical and hydrological flow properties of fractures: American geophysical union, Field guide book T385, 28th International Geological Congress*, 1989.
- [22] Robinson, P. C., "Connectivity, flow and transport in network models of fractured media", St. Cathrine's College, 1984.
- [23] Zhang, X., R. M. Harkness and N. C. Last, "Evaluation of connectivity characteristics of naturally jointed rock masses", *Engineering geology*, 11-30, 1992.
- [24] Berkowitz, B., "Analysis of fracture network connectivity using percolation theory", *Mathematical geology*, vol 27, 467-483, 1995.
- [25] Cacas, M. C., E. Ledoux, G. DeMarsily, B. Tillie, A. Barbreau, E. Durand, B. Fueva and P. Peaudecerf, "Modeling fracture flow with a stochastic discrete fracture network: 1. The flow model", *Water resources research*, vol 26, 491-500, 1990.
- [26] Cacas, M. C., E. Ledoux, G. DeMarsily, A. Barbreau, P. Calmels, B. Gaillard and R. Margritta, "Modeling fracture flow with a stochastic discrete fracture network: 2. The transport", *Water resources research*, vol 26, 491-500, 1990.
- [27] Long, J. C. S. and D. M. Billaux, "From field data to fracture network modeling: An example incorporating spatial structure", *Water resources research*, vol 23, 120-1216, 1987.
- [28] Sharp, J. M., I. Kreisel, K. L. Milliken, R. E. Mace and N. I. Robinson, "Fracture skin properties and effects on solute transport: Geotechnical and environmental implications", *Rock mechanics: Tools and techniques*, vol 2, 1329-1335, 1996.
- [29] Moench, A. F., "Convergent radial dispersion in a double-porosity aquifer with fracture skin: Analytical solution and application to a field experiment in fractured chalk", *Water resources research*, vol 31, 1823-1835, 1995.

- [30] Zimmerman, M. D., P. C. Bennett and J. M. Sharp, "Experimental determination of sorption in a fractured rock flow system", *Journal of Contaminant Hydrology*, in preparation.
- [31] Fu, L., K. L. Milliken and J. M. Sharp, "Porosity and permeability variations in fractured and Liesegang-banded Breathit sandstones (Middle Pennsylvanian), eastern Kentucky: Diagenetic controls and implications for modeling dual-porosity systems", *Journal of Hydrology*, 351-381, 1994.

Appendix B

Description and manual of the CPA program

Basic features:

- Name of the program: Critical path analysis (CPA)
- Platforms: Solaris (original program) and Microsoft Windows (improved program)
- Language: C++
- Libraries used: CGAL (<http://www.cgal.org>) and LEDA (<http://www.algorithmic-solutions.com/enleda.htm>)
- Development: GNU project C++ compiler (<http://gcc.gnu.org/>) for the Solaris version of the program and Microsoft Visual C++ 6.0 (<http://msdn.microsoft.com/visualc/>) for the improved version.
- Graphical User Interface: written in Tcl/Tk

Although the program includes a graphical user interface, the program can be also be used as a command line program when visualization of the tubular network is not required or if batch files need to be executed. The following commands are available:

- genZ2
- genZ3
- sit_disku
- modgraph
- savegraph
- loadgraph
- cpa
- quit

The commands `genZ2` and `genZ3` generate two- and three-dimensional lattices. Its usage is as follows: `genZ2 [n]` and `genZ3 [n]` where `n` is the number of nodes in each direction. If no argument is given, the default size of 20 is used.

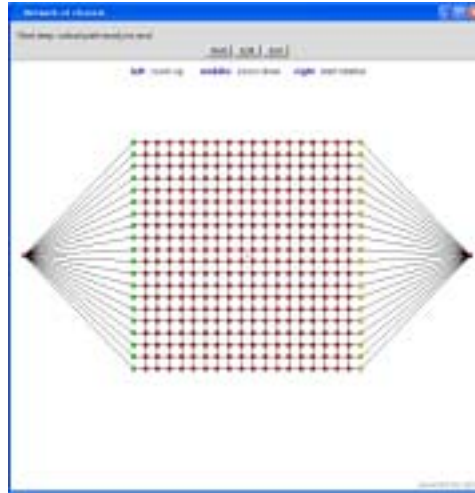


Figure B.1 Two dimensional regular lattice generated within the CPA program

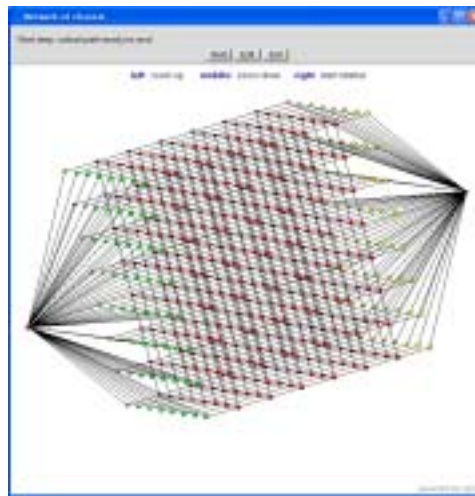


Figure B.2 Three dimensional regular lattice generated within the CPA program

The `sit_disku` command generates fractures, intersect these fractures and so generates the fracture intersection network. Its usage is `sit_disku [option] [values]` where the options are preceded by a dash followed by the values necessary for the option to complete. More than one option can be given in the same statement. This command will also work without options, in

which case the default values are taken for the construction of the fracture network. The following options are available:

- -f [name_of_parameter_file], will construct a fracture network from a parameter file. -n and -r arguments will be ignored.
- -r [maximum_radius_of_discs], the radius value is uniformly distributed between zero and the maximum, the default value is 0.5.
- -n [number_of_discs], the number of discs that are to be distributed inside the unit cube as a Poissonian cloud, the default value is 100.
- -o [name_of_output_graph_file], the default output is to "../graf.gr".
- -p [name_of_pov_file], the default output is to "obr.pov". This file is an input file for the POV-ray program, which allows the user to visualize the fracture network model.
- -m [name_of_file], creates a file with the spherical coordinates of discs normals. The default output will be to "norm.sph".
- -i px,py,pz,dipangle,dipdirection (without spaces), creates a file with the coordinates of intersections with the specified plane to the file "inter.entr".
- -I name of output file for intersections is to be used if the output of the previous option has to be saved under a different name.

The most convenient way to construct a network is by using a parameter file option. The parameter file has the format as shown in table 4.1.

(1)	(2)	(3)	(4)	(5)	(6)	(7)	(8)	(9)	(10)	(11)	(12)
4											
20	a	1	34	338	99.6	57	172	0.3	84	78	0.1
30	a	0.5	80	200	93.2	14	35	4.5	80	168	2.3
80	a	0.5	66	168	94.4	86	72	4.3	25	334	1.3
20	a	0.5	8.7	195	84.5	11	89	12	80	286	3.5

Table B.1 Format of the parameter file with explanation

The first number shows the number of fracture sets, followed by a line for each set. The first number in that line (1) gives the number of fractures in the unit cube, (2) followed by a switch s or a, triggering the simple or advanced option. The next number (3) is the maximum radius of

that set. For the simple option only three values will follow (4-6): The average dip angle at the site, the average dip direction and a multiplication factor for main Eigenvector direction. In the advanced case the two other eigenvectors with eigenvalues have to be given (7-9, 10-12).

Once the model has been constructed the conductivities can be modified. The general usage is `modgraph [-option] [value]`. Here more than one option can be given in the same statement. The following statements are available:

- `-u [minimum maximum]`, generates a uniform distribution of conductivities.
- `-w [minimum maximum weightx weighty weightz]`, generates a uniform distribution and introduces an anisotropy in the x, y and z direction.
- `-e [lambda (λ)]`, generates a exponential distribution where λ is $p(x) = \lambda e^{-\lambda x}$
- `-p [fraction_of_conduits_permeable]`, allows the user to switch off a certain percentage of conduits.
- `-s [equation]`, allows the user to make own distributions, using exponential, uniform, binomial, normal and Poissonian distribution functions.

With the `savegraph [file_name]` command a generated graph can be saved and later retrieved with `loadgraph [file_name]`. Especially for larger fracture networks, the time to generate a model can be quite long. It is therefore practical to save generated networks.

The `cpa [option]` command starts the `cpa` routine as described before. If the option 0 is chosen in the current version the total flow rate is calculated in the x, y, and z direction as well as the flow rate for a radial flow problem. Without an argument an interactive session will be started in which the model and each step in the process, from network generation, determination of in- and outflow nodes, elimination of unconnected tubes to the determination of the fastest flow path, is visualized.

To facilitate the use of the program a graphical user interface has been produced in Tcl code, a platform independent language. The graphical user interface is self explaining and has the added advantage that projects can be saved in project files. To be easily accessible for later use.

Appendix C

Spain field work

The fieldwork was conducted from the 10th to the 28th of June 1999 at the Sierra Elvira, a mountainous area, located about 10 kilometres Northwest of the town of Granada, Andalusia, Spain. The aim of the fieldwork was to find and record field evidence of linear groundwater flow in fractured media. The data gathered will be used to make a three-dimensional model of the fractured subsurface needed for the flow and transport modelling of tubular network flow.

C.1 Geography of the area

The Sierra Elvira (37N 14' 15" 3W 41' 00") is a small mountain range which covers about 20 km². The elevations range from 650 to 1102 metres. The largest towns in the area are Atarfe, south of the Sierra and Pinos Puente in the west. South-west of the Sierra lies the national road (N432) from Granada to Cordoba (see Figure C.1). The annual rainfall at the Granada Airport is 350 mm. Average temperatures range from 6.5 degrees Celcius in January to 25 degrees Celcius in July. During the fieldwork the temperature in the morning was pleasant, becoming almost unbearable in the afternoon.



Figure C.1 Location of the fieldwork area.



Figure C.2 Excerpt of the geological map of the Granada area.

C.2 Terms of reference

The fieldwork presented here was intended to gather data for modelling a fractured rockmass. The data needed for a good description of the rockmass for groundwater flow problems are summarised in Bruines and Halihan (1999).

For measuring directional data a geological compass was used. The aperture was measured with an automotive feeler gauge. A carpenters profile gauge was used for the measurement

of the channels as well as a simple measuring tape for determination of the fracture spacing. For the description of the rockmass BS 5930 (1981) was used. Thin sections of rock samples were made and investigated.

C.3 Available information

Before the start of the fieldwork only a few notes and pictures from a previous fieldwork conducted by Genske were available. The geological information is for a large part from the Mapa Geologico de Espana, No. 1009, 19-41, Granada and the accompanying explanatory booklet.

Prof. Chacon-Montero, head of the Environmental, Geological Risks and Land Engineering research group of the University of Granada has helped during the field campaign with his extensive knowledge on the geology of the Granada area.

C.4 Landscape and general geology

C.4.1 Landscape

Geomorphology. The geomorphology is related to the underlying geology. Competent rock formations create the highest peaks and steepest slopes, whereas weaker rockmasses have flatter slopes. This general phenomena can be clearly observed in the Sierra Elvira, where the highest peaks mainly consist of limestone and the lower parts of shale and marl.

In the Sierra Elvira all structures line-up in the direction of approximately 030. At the east and the west there are two mountain chains, both consisting of lime and dolostones. In the middle, where the elevations are considerably lower, the main constituent is shale. At the south and west of the Sierra, colluvial is present. The Sierra Elvira is bordered by the fluvial deposits of the Rio Genil to the south and to the north by different rocks of mainly Tertiary age.

Hydrogeology and drainage systems. Except for a single ephemeral stream in the central part of the Sierra, no streams are present. Due to the relatively high permeability of the rockmass, the dry climate and high elevation of the Sierra, in comparison with the surrounding area, the groundwater level will be found at a relatively great depth.

At Banos de la Sierra, hydrothermal water is pumped out and used in a pool. This hydrothermal water might originate from great depths since the well is located at an active fault (An

earthquake with a magnitude of 3.8 on the Richter scale has been recorded at this exact location three days before arrival at the site).

Land use and vegetation. The Sierra Elvira is not used agriculturally, except for some olive trees. The Ermita de los tres Juanes is exploited as a tourist attraction, since it gives a beautiful view over Granada and the Sierra Nevada. The limestone is quarried as dimension stone, as construction material and for cement production, which is produced on-site. The pine forest in the Northeast part of the Sierra is also used recreationally. The lower part in the centre of the Sierra is used as waste dump. The other parts of the Sierra are only sparsely vegetated.

Dwelling and industrialisation. On the Sierra there are no dwellings. Only at the foot some villages can be found. Atarfe, on the west of the Sierra, has a respectable size and is developing into a suburb of Granada. Pinos Puente, to the east, is an impoverished village, which seems to lack even the most basic infrastructure expected in a European village. A few dwellings and military barracks can be found along the road N-432, south of the Sierra.

The quarries and the cement plant are the only industrial activity in the area.

C.4.2 General geology of the area

Geological history. The area is mainly shaped by the collision of the African and the European continents during parts of the Mesozoic and the Tertiary periods. The Cordilleras Béticas are the most western part of the Alpine chains in Europe. In the collision area, two major zones are distinguished, called the interior and the exterior zones. The interior part is heavily deformed and metamorphosed, the exterior to a much smaller degree. From the north to the south, four subzones are distinguished. Classified in increasing degree of deformation and metamorphosis these are Prebetica and Subbetica in the exterior, and Circumbetica and Betica in the interior.

The layers in the Sierra Elvira are mostly calcareous deposits of the middle Subbetica domain in the upper Lias which developed at relatively great water depths as indicated by the presence of radiolaria and submarine volcanic deposits.

Stratigraphy. The geological history of the fieldwork area started in the Trias. The oldest sediments, from the Keuper formation, consist mainly of marly and clayey sediments of red, green, yellow and purple colours. These deposits must have been deposited in a quiet environment

with a continental flux. The latest deposits of the Keuper are dolomites and carneol. In the marls and clays igneous intrusions of doleritic composition are found as well as proof of a very low grade metamorphosis. On top of the Keuper an approximately 200 m thick dolomite deposit, intruded by subaqueous volcanic rocks (pillow lava), is present. This is followed by a limestone layer of about 80m (packstone) with chert layers. The exact border between dolomite and limestone is not constant due to changes in dolomitisation. The limestone is a packstone consisting of pelagic biomicrite. The overlaying formation is of Carixian age and is a grainstone of crinoids and other bioclasts. It is in this layer of approximately 25m, that the studied outcrops are situated. The top of this formation is karstified and infilled with a pelagic biomicrite and has developed a hard-ground. On top of this layer we find a formation of the upper Lias, mainly consisting of marls and marly limestones with occasional chert nodules and sandy limestones. The following formation contains slightly less marl, contains radiolaria and is part of the Dogger. The Malm that is topping the series at the Sierra Elvira consists mainly of limestone and marly limestones with chert nodules and lenses.

Since the Middle Lias (Carixian) is the layer in which the outcrops are situated, a more detailed description has to be given. The detritic limestone consists mainly of crinoid particles (grainstone), is 25 metres thick and is mainly characterized by cross bedding and sand waves. Because of its strength, this formation protrudes in the topography and is well recognisable in the field. The composition of the rock corresponds with a grainstone (crinoidal) and contains small amounts of biomicrite. The entire composition is held by a syntaxial cement, where the crystals are in optical continuity to monocrystalline skeletal fragments. An array of internal structures can be found. The primary structure at the base of the formation is planar cross bedding that is produced by the migration of mega ripples (sandwaves). Planar cross bedding means that the lower bounding surfaces are planar surfaces of erosion (Visser, 1980). In the upper part of the formation the cross bedding is "surcos", produced by the wave action in the direction NE-SW (herringbone crossbedding). Parallel lamination follows the ripples. At the top of the formation some karstification is present and infill with a gray limestone of biomicritic and pelagic character. The top of this formation has developed a hard-ground.

Structural geology of the field work area. The layers in the Sierra Elvira are mostly calcareous deposits of the middle Subbetic domain in the upper Lias which developed at relatively great water depths as indicated by the presence of radiolaria and submarine volcanic deposits.

At the field work area the slopes are dipping to the west. East of the area is a large normal fault, which borders to the Granada basin. The displacement along this fault is not reported but is most likely in the order of kilometres. To the west lies a synclinal structure, followed by an anticlinal structure. The Sierra Elvira is entirely surrounded by quaternary deposits and forms an isolated mountain range.

The Sierra Nevada as it exists today, was formed during the Alpine orogeny which is still ongoing in the region. The Alpine orogeny started in the middle Miocene period, and even in Holocene deposits, extensive and compressive features have been observed. The Alpine orogeny resulted in folding, faulting and metamorphism. The most likely sequence of events in the Sierra Elvira is a compressive phase, resulting in folding of the area, followed by an extensional phase, forming the normal faults to the east and the south of the area.

C.5 Survey techniques

C.5.1 Fracture survey techniques

For the fracture survey a form was developed on the basis of the ITC/TUD data sheet used for stability of rock slopes (ITC/TUD, 1997). It was then adapted using the data collection sheet of Halihan (personal communication) and Priest (1980). This data sheet was developed for a scanline survey. At the outcrops however the sheet turned out to be too detailed. Due to the limited amount of fractures, a scanline approach was impractical. Each measurable fracture had to be included in the data base. The final approach followed, was to first make a general description of the outcrop, also pointing out interesting geological features. The location of these features was then indicated in a sketch. The outcrop was then photographed. Subsequently the fractures were measured and described with the aid of the data sheet.

C.5.2 Channels survey techniques

In the next step the channels at the intersections of fractures were recorded. Measured was type of intersection, length, terminations, possible mineralisation, size, and the type of the channel they were connected to.

C.5.3 Laboratory work

Rock samples were collected and thin sections prepared and investigated with the help of the Centre d'Analyse Minerale at the University of Lausanne.

C.6 Fracture survey

Outcrop 1. The first outcrop is situated in the small abandoned quarry, about 100 m north of the hermitage. The outcrop, as all the other outcrops in this study, is a dip slope. The bottom of the quarry is filled with sand and levelled. The smell of fuel oil can be intense. The outcrop is bound to the left by a large open joint and a steep, slightly overhanging wall. The wall at the back of the outcrop is overhanging as well and also represents a joint. The right side is also bound by a joint with a considerable aperture and forms a step downward to a stratigraphic, lower lying dip slope. The bedding dips to the west and has a dip angle of about 35 degrees. The outcrop is about 15 by 10 meters.

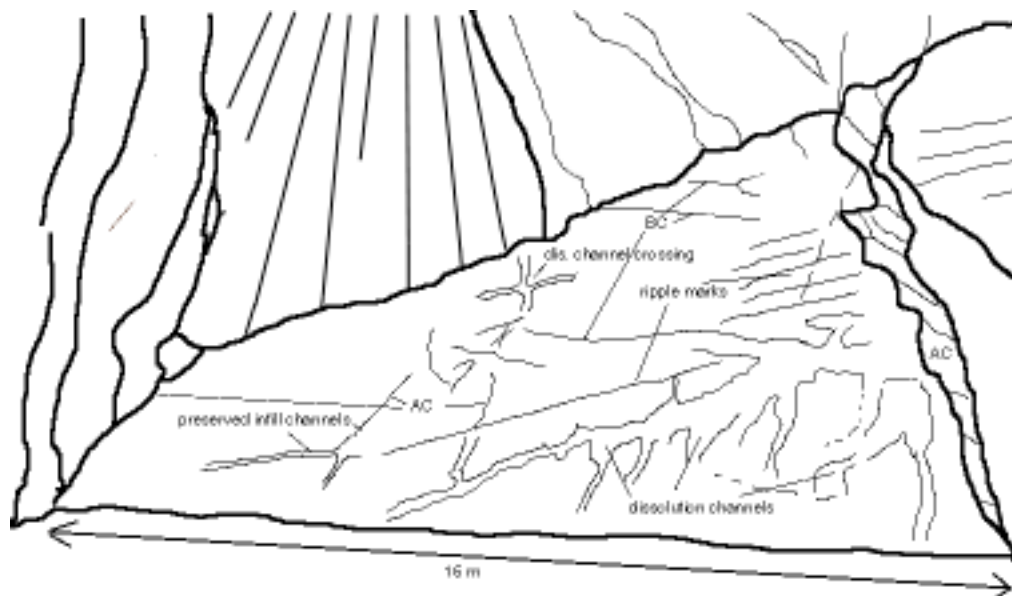


Figure C.3 Sketch of outcrop 1

The geological map indicates a detritic limestone of crinoid particles of the Caraxian period (see description of stratigraphy). The outcrop shows indeed a grainstone, the size of the grains might also indicate that of rudstone.

The colour of the outcrop is light grey. On the bedding surfaces, ripple marks are present. The spacing of these ripples is approximately 15 cm. The planar cross bedding is visible in weathered and dissolved sections because the different layers have slightly different compositions. At the bedding planes the material seems to be very fine in composition. Most likely the

finest fraction is usually found at the tip of foresets. This fine material has a greenish appearance. Especially around the channels and fractures the colour changes to red. This is most likely due to oxidation of ferric to ferrous iron, but in some cases is due to influx from above. In the thin sections the material is studied in more detail. At the outcrop four joint sets are found. Following the classification of Cloos (1936) they were called the AC, BC, D1 and D2 joints. At the intersections of the joints with the bedding plane, sometimes channels develop, although channels also develop within the bedding plane. Some of these channels can be up to 15 cm wide and a few cm deep. A few channels have been filled in partially with calcite. These fills are exact copies of the channels at the time of the precipitation. Of both the open and filled channels, cross-sections have been taken using a contour gage.

The bedding surface is straight, undulating and rough, on respectively the meter and the decimetre scale and to the touch.

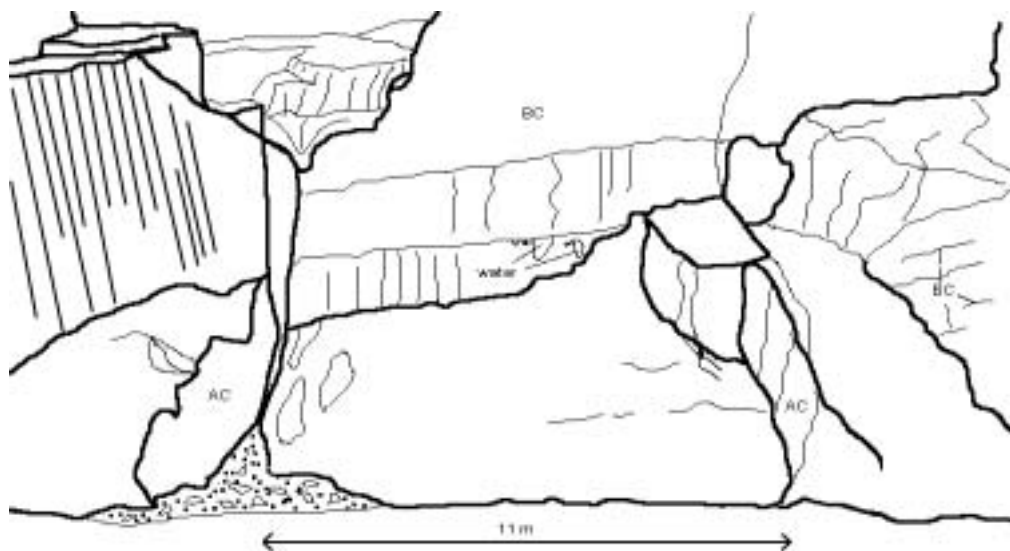


Figure C.4 Sketch of outcrop 2

Outcrop 2. The second outcrop is situated in the same abandoned quarry as outcrop 1. This outcrop is a dipslope. Stratigraphically, it is situated about 9 meters deeper and has had a larger depth to the ground surface before being quarried. This is most likely the reason why the alteration features on this slope are less developed than in the first outcrop. The outcrop is 11 m wide and 6.5 m deep and is limited by three major fractures, each of these fractures can conduct large amounts of fluids. The AC joints to the left and right have relatively large, irregular apertures (up to 25 cm). This is because the fractures are filled in with mainly amorphous calcite. Part of

the fractures developed large tubular features due to dissolution, as can be seen in the BC joint forming the back of the outcrop (Figure C.5).



Figure C.5 Photo of tube. This tube is located south of outcrop 2, the diameter of the tube is about 20 cm. The rough surface (popcorn) indicates precipitation of calcite in the unsaturated zone.

The back face, hanging wall, does show some water discharging. This is due to the artificial waterfall to the west of the outcrop. The discharge is at distinct points along a single bedding plane.



Figure C.6 Photo of wet spots. Water seeps from a bedding plane and from some spots where the fractures are not directly visible.

At the right border of the face water seems to follow the intersection of the bedding plane and the AC joint.

The bedding plane is wavy, undulating and rough. Although the colour of the rock is light grey, the fracture surface is greenish and at some places it is reddish, most likely due to oxidation. The bedding plane seems to be stylolitic, which would account for the undulating surface and the accumulation of the greenish minerals that, upon oxidation, turn red, marking previous flow paths. Stylolitic surfaces can be clearly identified in the adjacent walls, which give a cross-section of stratification.



Figure C.7 Photo of a stylolitic surface, which indicates the direction of stress.

On this face only a few channels are visible which are located near the limiting fractures, which are most likely the major conductors at this site.

Outcrop 3. The third outcrop is situated just west of the hermitage. It is about 20 metres wide, 15 metres deep and dips approximately 35 degrees west. The slope is limited by a larger fault to the left. Left of this fault an ostrich pen is located. Although the outcrop to the left of outcrop 3 was promising, the ostriches did not allow any investigation. To the right the outcrop is limited

by a steep descending slope. The back of the outcrop is limited by the hermitage area. The stratigraphical unit is of the same limestone as seen at the previous outcrops: a light grey grainstone situated on a dipslope. Also this slope is man-made as the blasting holes proved. The upper part must have had the least coverage, the lower part the most. On this slope there are many different types of fluid flow features visible. In the upper part of the slope some larger openings along a BC joint exist. The flow will be vertical following in-plane channels. At the lower part there are clear indications of fracture intersection related flow, as well as, in-plane channellized transport. The roughness of the slope is straight, undulating and rough.



Figure C.8 Sketch of outcrop 3

Outcrop 4. The fourth outcrop is interpreted from photo data together with some basic directional data (dip of slope, direction of pictures taken). This is partly due to the steep dipslope which made working on the slope dangerous. It also allowed to test whether it is possible to perform a joint survey with stereographic photos. Using the stereo pairs, the fractures were identified. Fractures and dissolution features were then marked on a composite photo (Figure C.8). The joints (green lines) were then measured. Using the angle at which the photos were taken and the angle of the slope, the lineaments could be determined after rotation of the data, using a Schmidt net.



Figure C.9 Composite photo of outcrop 4

This data is lacking information about the three dimensional spread of the discontinuities. It will be necessary to look at the eigenvalues of the joint sets of the outcrops 1, 2, and 3 to make an estimate of the spread of the outcrop 4 data.

C.7 Data processing

Directional data. By comparing the data, it soon became clear that the outcrops 1, 2, and 3 can be treated as one unit, whereas the fourth outcrop is distinctly different, since it lies on the other side of a major fault. For the interpretation of the directional data the program NETPROG for Windows version 2.2 by Allison was used (<http://www.usouthal.edu/geography/allison/w-net-prg.htm>). This program allows the user to generate Schmidt projections and to determine the mean directional vector for a set of discontinuities, as well as the eigenvectors and values of the set and calculates a standard deviation of fit when assuming a vector, girdle or conic distribution. Although the standard deviation for the different geometries and their confidence values, obtained with a chi test, have in the author's opinion, little or no use. Eigenvectors provide the only method to describe distributions that are in between, for instance, vector and girdle distributions in a simple and consistent way. The eigenvalues of a distribution of fractures can be visualized in the following manner: If a unit mass is assumed at every point at which a directional vector or normal cuts through a unit sphere, a physical equivalent of the Eigenvector approach develops. If the sphere is to be rotated around a random axis, a specific energy is needed to start the rotation. This energy requirement is proportional to the inertia of the sphere. In most cases there will be one axis with maximal inertia, one with the smallest inertia and an axis perpendic-

ular to both. These axes are orthogonal. The directions of these axes are identical with the eigenvectors of the inertia tensor matrix t_{ij} .

$$t_{ij} = \begin{bmatrix} \sum x_i^2 & 0 & 0 \\ \sum x_i y_i & \sum y_i^2 & 0 \\ \sum x_i z_i & \sum y_i z_i & \sum z_i^2 \end{bmatrix} \quad (\text{C.1})$$

Where x, y and z are normal coordinates of the unit vector of each measurement. The eigenvalues are developed by solving the following equation.

$$\det(t_{ij} - \lambda \delta_{ij}) = \begin{bmatrix} t_{11} - \lambda & 0 & 0 \\ t_{21} & t_{22} - \lambda & 0 \\ t_{31} & t_{32} & t_{33} - \lambda \end{bmatrix} \quad (\text{C.2})$$

By inserting the so found eigenvalues λ_1 , λ_2 and λ_3 into the equation $t_{ij} - \lambda \delta_{ij}$, the eigenvectors can be found. The eigenvectors orientate the tensor in three-dimensional space and the eigenvalues give the shape of the tensor. From the eigenvalues and their ratios conclusions can be drawn about the type of distribution. Further explanations of the concept and detailed calculation procedures of eigenvectors and eigenvalues, can be found in Wallbrecher (1986).

Orientation. Here follows a summary of the statistics of the outcrops 1, 2, and 3. The data of these three outcrops can be combined into one data set.

Eigenvectors and values (%) of poles								
	N	1	2	3	SD	X ²	X ² ($\alpha=0.01$; $v=5$)	
Bedding	30	112/56; 99.6%	278/33; 0.3%	012/06; 0.1%	3.89	24.18	15.1	
AC & Faults	43	190/10; 93.2%	055/76; 4.5%	282/10; 2.3%	15.54	14.36	15.1	
BC	38	287/24; 94.4%	018/04; 4.3%	116/65; 1.3%	14.06	21.57	15.1	
D1	11	255/03; 84.5%	001/79; 12%	164/10; 3.5%	24.61	59.68	15.1	
AC/Bedding	37	285/32; 94.8%	017/02; 4.9%	110/58; 0.3%	13.67	25.18	15.1	
BC/Bedding	16	018/06; 92.0%	283/35; 7.3%	116/54; 0.7%	17.26	25.59	15.1	
D1/Bedding	20	353/18; 97.0%	257/16; 2.7%	128/65; 0.3%	10.37	14.71	15.1	
D2/Bedding	6	220/12; 99.1%	314/21; 0.6%	102/66; 0.2%	5.83	51.15	15.1	

Table C.1 Directional statistics of the outcrops 1, 2, and 3.

Fracture spacing. The fracture spacing data are summarized in Table C.2. A distinction is made between the spacing of all fractures and of those fractures that have developed channels.

	Nr of fractures (all/w. channel)	Mean of all fractures	Standard deviation of all fractures	Mean of fractures w. channel	Standard deviation of fractures with channel
AC joints	62 / 24	0.99	1.01	1.57	1.44
BC joints	93 / 34	0.44	0.73	1.05	1.62
D1 joints	28 / 20	1.41	2.06	1.82	2.32
D2 joints	10 / 10	0.88	1.14	0.88	1.14

Table C.2 Fracture spacing distribution data (in metres)

Aperture. The aperture data are biased, since small fractures could not be measured. Also the aperture distribution along a fracture has not been recorded. In the flow through fractured media however, the largest fractures are most important so that the data are still relevant. The AC joints display the largest apertures. Two scales of jointing in the AC direction can be distinguished. The larger joints have a spacing of 10 to 20 meters and show apertures between 0 and 25 cm. The closer spaced set has much smaller apertures. Most fractures are closed or have a small aperture 0-1 mm. The largest aperture is about 5 cm. Most of the fractures of the AC group have some kind of infill.

With the exception of some joints, the AB joints are totally filled with mainly calcite. The open AB joints opened probably later due to dissolution or due to tectonic reactivation. The open AB joints are partly filled with amorphous calcite and residual soils.

The D1 joints show apertures reaching from 0 to 5cm, most however have apertures smaller than 1mm. The D1 joints have an infill that has a "metallic" shimmer and has an iron oxide aura where flow seems to have taken place.

The D2 joints do not have an important aperture. A lognormal distribution might be appropriate.

Length. The length of the fracture traces as measured from the outcrop reached from 0.7 to over 40 meters. About half the measured trace lengths extended beyond the borders of the outcrops. For these joints a minimum length was recorded. The average of all the data is 8.56 and the standard deviation is 8.58. The fact that the mean and the standard deviation of the fractures are

of approximately the same suggest that the distribution function is either lognormal or exponential. The data however were not sufficient to prove one way or the other. In order to easily determine the relation between fracture density and fracture size, given the lack of more conclusive data, a uniform distribution is assumed. This choice can be justified by the fact that a large number of fractures were beyond the cut-off limit, imposed by the size of the outcrops, suggesting a long and fat tail of the distribution and the relatively small importance of small fractures.

Connectivity. To measure connectivity, the termination of the fractures was recorded. In the data base they are indicated with the letters A for abutting, B for blind, C for crossing, and D for diffuse. C fracture terminations are fracture endings that extend beyond the boundaries of the outcrop and cross other fractures. This method allows to tell something about the fracturing history. Abutting fractures have developed later than the fracture on which it terminates. Active diffuse connection have not been found on the outcrops and blind fracture endings were rare.

	AC (44)	BC (53)	D1 (12)
A	64%	38%	0%
B	2%	0%	33%
C	34%	62%	67%

Table C.3 Termination statistics.

Since the AC fracture set has the most abutting fracture endings, it is most likely the most recent set. The D1 set might be the oldest set of joints. The appearance of both abutting and crossing fractures in the AC and BC sets might indicate that fractures have developed at different times or that older joints have been reactivated. The larger fractures of the AC set seem to be continuous, whereas the smaller AC fractures of the same set seem to terminate on other fractures.

Stress. A possible tectonic history that could explain the fractures in the outcrops is as follows. A compressional tectonic regime resulted in a shortening of the area in the direction SE-NW. This might have created the larger AC fractures. Simultaneously the diagonal fractures might have developed. In a further stage of the compression, extensional BC joints might have developed, due to the folding of the rock. In a much later stage the area to the south-east subsided, a normal fault developed. Also to the south-west the area subsided. Both these events, which are still ongoing, might have resulted in the development of new AC and BC joints (the smaller

fractures) or reactivation of some of the old joints. These subsidence features might also be responsible for over-pressured hydrothermal fluids.

Different fractures have developed. The Large AC fractures line up with the translational faults and might have developed by shearing. At the third outcrop a D1 feather fracture shows clear marks of shear. It is even suspected that geothermal liquids have circulated through this fracture. The stylolitic surfaces as seen at some of the bedding planes and on one of the fractures at the third outcrops are a proof that pressure solution and compression must have taken place.

Roughness. Since most of the data is from fracture traces the roughness of the fractures could not be measured. For most fractures only a visible rough estimate could be made using the method previously described. Only on the large scale roughness, the fractures differ. The larger AC joints have the most roughness (wavy multi-directional), followed by the smaller AC joints (curved). The BC and D1 joints are mainly slightly curved.

Channelling. Most channels are observed at the intersection of joints with the bedding plane. In-fracture channels were not found on the bedding plane of the first three outcrops. In the fourth outcrop some of the channels do not seem to follow the fracture intersections. Unfortunately only one side of the channels could be seen. Some profiles of the half-channels were taken. It showed that the cross-sectional area is in general not changing along a single half-channel, except in some cases. Because only half of the tube is visible, the exact dimensions of the channels are not known. Not all channels are so large that they can be measured, but discoloration of the surrounding rock shows that at a certain time in the past fluids must have circulated. These discolorations can attain several tens of centimetres. Sometimes different episodes can be distinguished.

Some thin sections of the rock have been made. Analyses of the thin sections showed that composition of the rock corresponded with the description from the geologic map. Not mentioned on the geological map was the presence of glauconite and the discolorations on the fracture faces and at the fracture intersections. Glauconite is generally associated with green sands that develop at relatively shallow conditions. Glauconite can however also be a secondary mineral that has formed due to a light form of metamorphism. Since the thin sections often show replacement of fossilised particles the later seems to apply. The syntaxial cement and stylolitic surfaces observed in the thin sections further support this assumption. The relative abundant

amounts of echinoid particles indicate a high-energy environment, (at least for the grainstones) The porosity of the rock is very low. No significant amount of pores can be observed (fine material, pressure dissolution, cementation). The main porosity in the rock will therefore be secondary, i.e. through the fractures. The stains as seen on the outcrop that show the fossilised flowpaths, are most likely a form of iron hydroxide that stem from opaque minerals in the rock mass and fracture fill. It is shown that this transformation takes place preferably around fractures. It is unfortunately not possible to determine the types of mineral of the discolorations and the opaque mineral.

C.8 Conclusions

This fieldwork showed the existence of flow at the fracture intersection. Some of the flow features however correspond to in-fracture flow. The channels in this area are mainly developed due to dissolution. The distinct discolorations along the fractures and fracture intersections are an interesting feature that allows us to prove fracture of channelled flow.

During this fieldwork enough data has been gathered to stochastically reconstruct the fracture network. However, no qualitative hydraulic data of the site could be obtained.

Curriculum vitae

Surname	BRUINES	
Given names	Patrick Arnoldus	
Date and place of birth	16.11.1973 Purmerend, NL	
Nationality	Dutch	
School education	1990-1993	St. Viti Gymnasium, Zeven, D
Higher education	1993-1998	Studies in mijnbouwkunde en petroleumwinning, Technische Universiteit Delft, NL
	1996-1997	University of Texas, Austin, USA
Doctoral studies	1999-2003	Swiss Federal Institute of Technology Lausanne, CH
	2001-2002	Kyoto University, JP

